

**IDENTIFICATION, DESIGN AND SYNTHESIS OF OXYGENATED HYDROCARBON-
BASED CO₂-SOLUBLE POLYMERS FOR CHEMICAL AND PETROLEUM
ENGINEERING APPLICATIONS**

by

Lei Hong

B.S., East China University of Science and Technology, 1996

M.S., East China University of Science and Technology, 1999

Submitted to the Graduate Faculty of
School of Engineering in partial fulfillment
of the requirements for the degree of
Doctor of Philosophy

University of Pittsburgh

2006

UNIVERSITY OF PITTSBURGH

SCHOOL OF ENGINEERING

This dissertation was presented

by

It was defended on

March 29, 2006

and approved by

Dr. Eric J. Beckman, Professor, Chemical and Petroleum Engineering Department

Dr. J. Karl Johnson, Professor, Chemical and Petroleum Engineering Department

Dr. Toby Chapman, Associate Professor, Department of Chemistry

Dissertation Director: Dr. Robert M. Enick, Chairman and Professor, Chemical and Petroleum
Engineering Department

Copyright © by Lei Hong

2006

ABSTRACT

IDENTIFICATION, DESIGN AND SYNTHESIS OF OXYGENATED HYDROCARBON-BASED CO₂-SOLUBLE POLYMERS FOR CHEMICAL AND PETROLEUM ENGINEERING APPLICATIONS

Lei Hong, Ph.D.

University of Pittsburgh, 2006

Over the past two decades the use of sub/supercritical CO₂ has received much attention as a green alternative to organic solvents for chemical processes because of its pressure-tunable physicochemical properties and economic advantages. However the advantages are diminished because of a relative narrow range of CO₂-soluble materials. The goal of this work is to identify, design and synthesize oxygenated hydrocarbon-based CO₂-soluble polymers that are able to serve as construction blocks for copolymers, dispersants, surfactants, and thickeners. Without concerning on the cost and the environmental persistence like fluorinated materials, the inexpensive and environmentally benign materials would significantly enhance the viability of sub/supercritical CO₂-based technology. Based on both experimental heuristics and *ab initio* simulation of molecular modeling (performed by Dr. Johnson's group), we proposed specific new polymer structures: poly (3-acetoxy oxetane) (PAO), poly (vinyl methoxymethyl ether) (PVMME), poly (vinyl 1-methoxyethyl ether) (PVMEE), and cellulose triacetate (CTA) oligomers. Phase behavior studies were also performed with novel CO₂-philic compounds containing vinyl acetate, propylene glycol, or multiple tert-butyl groups.

PAO, PVMME and PVMME were soluble in CO₂, but not as soluble as poly (vinyl acetate). Oligomers of cellulose triacetate with as many as four repeat units solubilized into dense CO₂ less than 14 MPa in the concentration range of 1-5 wt%. Phase behaviors of more than twenty compounds in dense CO₂ were studied in this project. A new type of phase behavior for solid CO₂-philes that melt and dissolve in CO₂ was detailed using a model binary mixture of β -D-maltose octaacetate and CO₂. Copolymers of tetrafluoroethylene (TFE) and vinyl acetate (VAc) exhibited lower miscibility pressures than either of the homopolymers, probably due to quadridentate binding configurations with CO₂. Phase behavior investigation of poly (propylene glycol) (PPG) monobutyl ether in CO₂ demonstrated ether-CO₂ interactions should receive as much attention as carbonyl-CO₂ interactions when designing CO₂-philic functional groups. 1,3,5-tri-tert-butylbenzene and 2,4,6-tri-tert-butylphenol were both extraordinarily soluble in CO₂, and are excellent candidates for CO₂-soluble sand binders.

In summary, although a new CO₂ thickener was not identified, new non-fluorous CO₂-soluble materials were identified, which were, in general, acetate-rich with flexible chains, weak self-interactions, and multidentate interaction between CO₂ and solute functional groups.

TABLE OF CONTENTS

TABLE OF CONTENTS	VI
LIST OF TABLES	X
LIST OF FIGURES	XII
ACKNOWLEDGEMENT	XVII
1.0 INTRODUCTION.....	1
1.1 PROPERTIES OF SUPERCRITICAL CARBON DIOXIDE	2
1.2 SUPERCRITICAL-CARBON DIOXIDE-BASED MATERIAL SCIENCE APPLICATIONS.....	5
1.2.1 Polymerization.....	5
1.2.2 Formation of Polymer Blends	8
1.2.3 Encapsulation of Pharmaceuticals	9
1.2.4 Scaffolds for Tissue Engineering Applications.....	10
1.3 CO ₂ THICKENING AGENTS.....	11
1.3.1 Exploratory Research on Decreasing the Mobility of CO ₂	16
1.3.2 Success of Fluorinated Copolymers as CO ₂ Thickeners	19
1.4 RESEARCH OBJECTIVES.....	27

2.0	BACKGROUND	29
2.1	SOLVENT PROPERTIES OF CO₂.....	29
2.2	THERMODYNAMIC FUNDAMENTALS OF SUB/SUPERCRITICAL CO₂ SOLUTION.....	31
2.3	PROGRESS IN IDENTIFICATION OF NON-FLUOROUS/SILICONE CO₂ SOLUBLE FUNCTIONAL GROUPS	35
	2.3.1 Experimental Study	35
	2.3.2 Empirical Heuristics of Designing Oxygenated Hydrocarbon-Based CO₂-Soluble Functional Groups	42
2.4	MODELING AIDED DESIGN ¹³¹	44
2.5	PHASE BEHAVIOR MEASUREMENTS	47
2.6	VISCOSITY MEASUREMENT	51
2.7	SYNTHESIS CHARACTERIZATIONS.....	54
3.0	POLYMERS DESIGNED BY MODELING COMPUTATION	55
3.1	POLY(VINYL ACETATE)	55
3.2	POLY(3-ACEOXY OXETANE)	58
	3.2.1 Modeling Design.....	58
	3.2.2 Preparation.....	60
	3.2.3 Phase Behavior Study	64
3.3	POLY(VINYL ETHER)S WITH ACETAL GROUPS.....	65
	3.3.1 Modeling Design.....	65
	3.3.2 Preparation.....	66

3.3.3	Phase Behavior Study	70
3.4	CONCLUSIONS	71
4.0	PERACEYLATED CELLULOSE TRIACETATE OLIGOMERS.....	72
4.1	LITERATURE REVIEW	72
4.2	CELLULOSE TRIACETATE OLIGOMERS	75
4.2.1	Design of Cellulose Triacetate Oligomers.....	75
4.2.2	Synthesis.....	77
4.2.3	Phase Behavior Study	79
4.3	CONCLUSIONS	84
5.0	PHASE BEHAVIOR STUDY	86
5.1	GLOBAL PHASE BEHAVIOR FOR CO ₂ -PHILIC SOLIDS	86
5.1.1	Introduction.....	86
5.1.2	Results and Discussion.....	88
5.1.3	Conclusions.....	94
5.2	SOLUBILITY OF LINEAR POLY(TETRAFLUOROETHYLENE-CO-VINYL ACETATE) IN DENSE CARBON DIOXIDE	95
5.2.1	Introduction.....	95
5.2.2	Results and Discussion.....	97
5.2.3	Conclusions.....	104
5.3	PHASE BEHAVIOR OF POLYPROPYLENE GLYCOL IN DENSE CARBON DIOXIDE	105
5.3.1	Introduction.....	105

5.3.2	Results and Discussion.....	109
5.3.3	Conclusions.....	112
5.4	SOLUBILITY OF TERT-BUTYLATED AROMATICS IN DENSE CARBON DIOXIDE	113
5.4.1	Introduction.....	113
5.4.2	Results and Discussion.....	116
5.4.3	Conclusions.....	122
6.0	VISCOSITY STUDY	124
6.1	SAMPLES FROM AIR PRODUCTS AND CHEMICALS.....	124
6.2	VISCOSITY OF SUGAR ACETATE IN CO ₂	126
7.0	SUMMARY	129
8.0	FUTURE WORK.....	133
	APPENDIX A.....	137
	APPENDIX B	157
	BIBLIOGRAPHY.....	160

LIST OF TABLES

Table 1.1 Physical properties of a gas, liquid, and supercritical fluid (SCF) ^{4,5}	3
Table 1.2 Critical properties of various solvents ^{5,6}	4
Table 1.3 Formulas of fluorinated CO ₂ thickeners	21
Table 2.1 Summary of prospective CO ₂ -philic functionalities	35
Table 3.1 Binding configurations and energies for IPA/ CO ₂ ¹³⁶	56
Table 3.2 T _g of PVA, PVMME, and PVMEE	69
Table 4.1 Parameters of wet-column separation	79
Table 5.1 Bulk Analysis of TFE-VAc copolymers	98
Table 5.2 Physical properties of butylated compounds and linear compound (Aldrich)	115
Table 6.1* Comparison of neat CO ₂ viscosity obtained by falling cylinder viscometer with reference data ¹⁸⁰	125
Table 6.2* Viscosities of neat CO ₂ and S1, S2, and S3 in CO ₂ at 298 K and 10 wt%	125
Table 6.3* Viscosity of neat CO ₂ and galactose pentaacetate solutions at 313 K and 17.24 MPa (2500 psi)	127
Table 8.1 Thickening candidates with phenyl groups	135
Table 8.2 Proposed amino groups for CO ₂ thickening groups	136
Table B.1 Falling cylinder viscometer experimental data for neat CO ₂ at 298 K with a fixed falling distance of 0.05 m	158

Table B.2 Experimental data of Air Products and Chemicals' samples at 298 K and 10 wt% with a fixed falling distance of 0.02 m..... 159

Table B.3 Experimental data of β -D-galactose pentaacetate at 313K and 17.24 MPa with a fixed falling distance of 0.05 m..... 159

LIST OF FIGURES

Figure 1.1 Phase behavior of supercritical CO ₂ and H ₂ O	3
Figure 1.2 Viscosity of CO ₂ as a function of temperature and pressure ⁷³	14
Figure 1.3 CO ₂ flooding in a typical reservoir: (a) “fingering” phenomena without mobility control, (b) CO ₂ flows with thickeners	15
Figure 1.4 Viscosity of PFOA in CO ₂ at 323K under different concentrations. ^{88,89}	20
Figure 1.5 CO ₂ solubility of PHFDA-xPSt copolymers at 298K ⁹¹	23
Figure 1.6 CO ₂ viscosity enhancement achieved with the fluoroacrylate-styrene copolymers ⁹¹	23
Figure 1.7 π - π stacking of the aromatic phenyl groups, (a) an overview structure; (b) a close view structure ⁸⁷	25
Figure 1.8 Effect of shear rate and concentration on the viscosity of fluoroacrylate-styrene copolymer solution in CO ₂ ; Glass tube inside radius=1.588 cm; copolymer of 29mol% Styrene-71mol% fluoroacrylate; T=298K; P=34 MPa. ^{92,98}	26
Figure 2.1 Comparison of the partial charges on the individual atoms of H ₂ O (A) and CO ₂ (B) with the charges derived by fitting the electrostatic potentials (CHELPG charges) in electrons calculated at the MP2/aug-cc-pVDZ level. ¹⁰⁹	30
Figure 2.2 Schematic diagram of interactions between CO ₂ and CO ₂ -philic group, (a) CO ₂ as a Lewis acid (C=O···C); (b) CO ₂ acts as a Lewis base (C–H···O)	31
Figure 2.3 Cloud point pressures at ~5% polymer concentration and 298 K for binary mixtures of CO ₂ with polymers as a function of number of repeat units based on Mw, where PFA, PDMS, PVAc, PLA, PMA and PACD represent poly(fluoroalkyl acrylate), poly(dimethyl siloxane), poly(vinyl acetate), poly(lactic acid), poly(methyl acrylate) and per-acetylated cyclodextrin, respectively. ^{119,123}	41

Figure 2.4 Schematic of experimental apparatus for phase behavior study with a high pressure, variable volume, windowed cell (D.B. Robinson Cell).....	48
Figure 2.5 Detailed drawing of a high pressure, windowed, stirred, variable-volume view cell .	49
Figure 2.6 Schematic diagram for a falling cylinder viscometer.....	52
Figure 3.1 Structure of poly(3-acetoxy oxetane), PAO	58
Figure 3.2 Three dimensional view of methoxy-isopropyl acetate, MIA.....	59
Figure 3.3 Three multiple binding geometry of CO ₂ with methoxy isopropyl acetate.....	60
Figure 3.4 Synthesis scheme for monomer 3-acetoxyoxetane ^{140,141}	61
Figure 3.5 Synthesis scheme for poly(3-acetoxy oxetane) (PAO, Polymerization II)	62
Figure 3.6 Synthesis scheme for poly(3-acetoxy oxetane) (PAO, Polymerization II)	63
Figure 3.7 Pressure-composition diagram for CO ₂ + poly(3-acetoxy oxetane) system at 298 K. 64	
Figure 3.8 Structure of poly(vinyl methoxymethyl ether) (PVMME).....	65
Figure 3.9 Optimized binding geometry of CO ₂ with acetal group.....	66
Figure 3.10 Synthesis scheme for poly(vinyl methoxymethyl ether) and poly(vinyl 1-methoxyethyl ether)	67
Figure 3.11 Pressure-composition diagram for CO ₂ + poly(vinyl ether) systems at 298 K.....	70
Figure 4.1 Pressure-composition phase diagram for the CO ₂ +AGLU/BGLU/BGAL at 313K ¹¹²	73
Figure 4.2 Pivaloylysis of cellulose triacetate ¹⁵²	76
Figure 4.3 Composition tracking of every CTA oligomer during pivaloylysis ¹⁵²	77
Figure 4.4 Pressure-composition diagram for CO ₂ + CTA oligomer system at 298 K	81
Figure 4.5 General pressure-composition (P-x) phase diagram for classic sub/supercritical CO ₂ + heavy solid system ⁷	82

Figure 4.6 General pressure-composition (P-x) phase diagram for the novel sub/supercritical CO ₂ + heavy solid system ¹¹³	83
Figure 4.7 General pressure-composition (P-x) phase diagram for the novel sub/supercritical CO ₂ + heavy solid system ¹¹³	84
Figure 5.1 Structure of β -D-maltose octaacetate	88
Figure 5.2 Pressure-composition diagram for the carbon dioxide (1) + maltose octaacetate (2) system at 283 K.....	89
Figure 5.3 Pressure-composition diagram for the carbon dioxide (1) + maltose octaacetate (2) system at 298 K.....	89
Figure 5.4 Pressure-composition diagram for the carbon dioxide (1) + maltose octaacetate (2) system at 323 K.....	90
Figure 5.5 P-T Projection for the carbon dioxide (1) + maltose octaacetate (2) system. Solid lines represent pure-component saturation curves, dashed lines represent critical curves, and dotted-dashed lines represent three-phase lines. \square is the triple point and \diamond is the critical point of CO ₂ ; \star is the triple point and \circ is the critical point of MOA.	92
Figure 5.6 General pressure-composition (P-x) phase diagram for CO ₂ and solid CO ₂ -philic compounds or polymers.....	99
Figure 5.7 Pressure-composition phase diagram for CO ₂ + TFE-VAc copolymer system at 25 °C	101
Figure 5.8 Cloud-point curve for ~5 wt% CO ₂ + TFE _{46.7} -co-VAc system ¹⁷⁰	102
Figure 5.9 Quadrantate binding configuration for CO ₂ + TFE-VAc dyad using MP2/6-31+g(d) level of theory	102
Figure 5.10 Structure of poly(propylene glycol) monobutyl ethers	109
Figure 5.11 The comparison of the cloud point pressures with the published data ¹²¹	110
Figure 5.12 Pressure-composition isotherm at 298 K for binary mixture of carbon dioxide with Poly(propylene glycol) monobutyl ethers.....	111
Figure 5.13 The comparison of the phase behavior of PPGMBE with the PPGMBE surfactants ¹⁰⁰	112

Figure 5.14 Structures of 1,3,5-tri-tert-butylbenzene, 2,4,6-tri-tert-butylphenol, and n-octadecane	115
Figure 5.15 Phase behaviors of n-octadecane ¹⁸⁰ and 1,3,5-tri-tert-butylbenzene in CO ₂	117
Figure 5.16 Pressure –composition diagram for CO ₂ +TTBP system at 301K, (a) a overall view, (b) a close view for low concentration.....	119
Figure 5.17 Pressure –composition diagram for CO ₂ +TTBP system at 328K	120
Figure 5.18 Pressure –composition diagram for CO ₂ +TTBP system at 343K	121
Figure 5.19 P-T diagram for CO ₂ +TTBP system; C ₁ and C ₂ represent critical points of CO ₂ and TTBP, respectively; M is melting point of TTBP; AC ₁ is CO ₂ vapor pressure curve; MN and DM are TTBP melting curve and sublimation curve, respectively; BM is three-phase solid-liquid-vapor line; C ₁ C ₂ is the mixture critical curve.	122
Figure 6.1 Structure of β-D-galactose pentaacetate.....	127
Figure 6.2 Relative viscosity of β-D-galactose pentaacetate solution in CO ₂ at 313 K and 17.24 MPa	128
Figure 7.1 Upgraded Figure 2.3	132
Figure 8.1 Structure of a new poly(vinyl ether) for future work	134
Figure 8.2 Structure of poly(1-O-(vinyloxy)ethyl-2,3,4,6-tetra-O-acetyl-β-D-glucopyranoside) (poly(AcGlcVE)).....	134
Figure A. 1 ¹ H NMR (300 MHz, CDCl ₃) spectrum of 3-acetoxy oxetane	138
Figure A. 2 ¹ H NMR (300 MHz, CDCl ₃) spectrum of poly(3-acetoxy oxetane) (polymerization I)	139
Figure A. 3 MALDI spectrum of poly(3-acetoxy oxetane) (polymerization I).....	140
Figure A. 4 ¹ H NMR (300 MHz, CDCl ₃) spectrum of poly(3-acetoxy oxetane) (polymerization II).....	141
Figure A. 5 MALDI spectrum of poly(3-acetoxy oxetane) (polymerization II).....	142

Figure A. 6 ^1H NMR (300 MHz, CDCl_3) spectrum of 1-chloroethyl methyl ether.....	143
Figure A. 7 ^1H NMR (300 MHz, DMSO-d_6) spectrum of poly(vinyl ether).....	144
Figure A. 8 ^1H NMR (300 MHz, DMSO-d_6) spectrum of poly(vinyl methoxy methyl ether)...	145
Figure A. 9 ^1H NMR (300 MHz, DMSO-d_6) spectrum of poly(vinyl 1-methoxyethyl ether) ...	146
Figure A. 10 IR spectra of PVA, PVMME, and PVMEE.....	147
Figure A. 11 DSC for poly(vinyl alcohol).....	148
Figure A. 12 DSC for poly(vinyl methoxymethyl ether).....	149
Figure A. 13 DSC for poly(vinyl 1-methoxyethyl ether)	150
Figure A. 14 ^1H NMR (300 MHz, CDCl_3) spectrum of acetylated cellulose acetate.....	151
Figure A. 15 MALDI spectrum of pivaloylysis products of CTA after 24 hours	152
Figure A. 16 Mass spectrum of CTA monomer by ESI	153
Figure A. 17 Mass spectrum of CTA dimer by ESI	154
Figure A. 18 Mass spectrum of CTA trimer by ESI.....	155
Figure A. 19 Mass spectrum of CTA tetramer by ESI	156

ACKNOWLEDGEMENT

In my long list of names, the first person I would like to thank is Dr. Robert Enick, my Ph.D. advisor, for his resourceful suggestions, endless encouragement, and enormous patience throughout my studies. He allowed me to think, study, and work independently while offering me advice and respecting my opinions. Meanwhile, I would like to thank Dr. Eric Beckman and Dr. Karl Johnson for their constructive suggestions, brilliant ideas and random interruptions in the group meetings. I would also like to thank Dr. Beckman, Dr. Johnson and Dr. Chapman for taking time out of their tight schedule to serve on my committee.

I would like to thank Dr. Inchul Kim and Dr. Andrew Hamilton at Yale University, and Dr. Jutta Pyplo-Schnieders in Germany for their assistance of the synthesis. Many thanks are also in order for Dr. Jacob Crosthwaite and Dr. Mark Thies for their generosity, support and patience when I was visiting Clemson University.

I would like to thank Jianying Zhang, Xin Fan, Yannick Heintz, Xiaoqian Shen, Deepak Tapriyal, Chris Karnikas, Liz Fidler, Matthew Fisher, and Charles Everhart for their discussion and assistance. Particularly I would like to thank Yang Wang for the *ab initio* modeling results. I also appreciate the faculty and staff of the chemical engineering department: Dr. Sachin Velankar, Rob Toplak, Bob Maniet, Ron Bartlett, Allison Crick, Adrian Starke, and Kelly Radocay for their assistance and cooperation. Additionally, I appreciate all my friends for the pleased time we ever shared.

Finally, I would like to express my most sincere gratitude to my parents for their endless support and unconditional love throughout not only my Ph.D. study but also my entire life. Without them this work would not have been possible.

1.0 INTRODUCTION

In the past two decades, supercritical fluid (SCF) technologies, such as extraction, polymerization, chromatography, and organic synthesis, have attracted considerable attention from chemists and engineers for its potential applications as an sustainable solvent for chemical engineering.^{1,2} Carbon dioxide is one of the most widely used gases for SCF applications because of its moderate critical constants ($T_c=31.1\text{ }^\circ\text{C}$, $P_c=73.8\text{ bar}$), nontoxic, nonflammable and abundantly available from natural sources. Moreover, many of the physical and chemical properties of supercritical CO_2 , such as density, polarizability and quadrupole moment, can be finely tuned by adjusting system's temperature and pressure.

However, a critical factor in limiting the use of supercritical CO_2 is its weak solvent strength relative to that of conventional organic solvents. One strategy for enhancing the capabilities of CO_2 as a green solvent is to identify the additives, such as surfactants, dispersants, chelating agents, thickeners, and polymers, which are designed to exhibit favorable thermodynamic interactions with CO_2 .

1.1 PROPERTIES OF SUPERCRITICAL CARBON DIOXIDE

A SCF is defined as a substance above its critical temperature (T_c) and critical pressure (P_c). The critical point represents the highest temperature and pressure at which the substance can exist as a vapor and liquid in equilibrium. The range of pressures and temperatures that define the supercritical fluid region of the diagram are shown in the phase diagram for pure compound (Figure 1.1).³ A supercritical fluid exhibits physico-chemical properties intermediate between those of liquids and gases. Mass transfer is rapid with supercritical fluids. Their dynamic viscosities are nearer to those found in normal gaseous states. The diffusion coefficient is (in the vicinity of critical point) more than ten times that of a liquid. Hence, a supercritical fluid is able to penetrate anything, such as polymers and solid matrix. At the same time, a supercritical fluid maintains a liquid's ability to dissolve substances that are soluble in the compound, which a gas cannot do. In addition, it offers the advantage of being able to change the physico-chemical properties to a great extent in a continuous manner. As was the case for density, values and subsequent changes for viscosity and diffusivity are dependent on temperature and pressure. The viscosity and diffusivity of the supercritical fluid approach that of a liquid as pressure is increased. Diffusivity will increase with an increase in temperature, whereas, viscosity decreases (unlike gases) with a temperature increase. Changes in viscosity and diffusivity are more pronounced in the region of the critical point. Even at high pressures (300-400 atm) viscosity and diffusivity are 1-2 orders of magnitude different from liquids. Therefore, the properties of gas-like diffusivity, gas-like viscosity, and liquid-like density combined with the pressure-dependent solvating power have provided the impetus for applying supercritical fluid technology to various problems (Table 1.1).^{4,5}

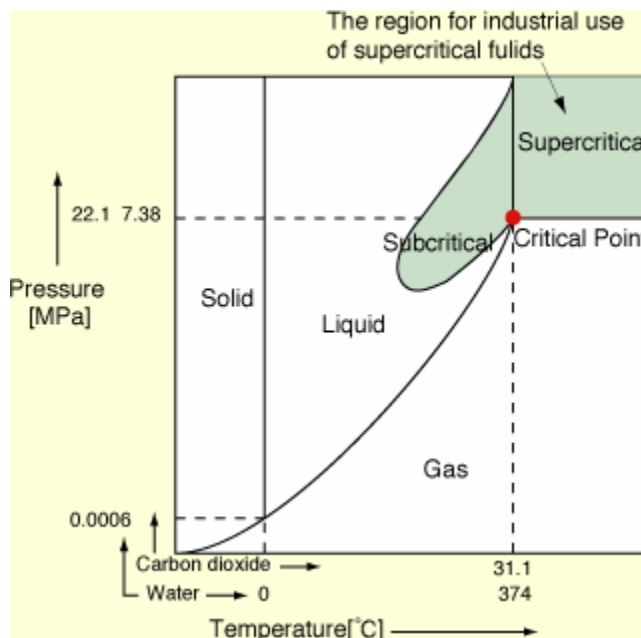


Figure 1.1 Phase behavior of supercritical CO₂ and H₂O

Table 1.1 Physical properties of a gas, liquid, and supercritical fluid (SCF)^{4,5}

Mobile phase	Density (g/mL)	Viscosity (poise)	Diffusivity (cm ² /sec)	Dynamic Viscosity (g/cm sec)
Gas	~10 ⁻³	0.5-3.5(×10 ⁻⁴)	0.01-1.0	1×10 ⁻⁴
SCF	0.2-0.9	0.2-1.0(×10 ⁻³)	0.1-3.3 (×10 ⁻⁴)	1×10 ⁻⁴
Liquid	0.8-1.0	0.3-2.4(×10 ⁻²)	0.5-2.0(×10 ⁻⁵)	1×10 ⁻²

Although many SCFs are available, the most widely used SCF is carbon dioxide because it is non-flammable, non-toxic, and its use does not contribute to the net global warming effect. It is easy to achieve its supercritical state because of its moderate T_c and P_c values (see Table 1.2). Further, CO₂ is available in large amounts and inexpensive. Because the solubility of CO₂ drops to essentially zero under atmospheric conditions, depressurization of a CO₂-based solution

results in complete precipitation of any solutes or suspended materials, substantially easing downstream product recovery. One more advantage is thermally labile compounds such as proteins can be processed with minimal damage as low temperatures can be employed by SCF technologies. On these accounts, the use of supercritical carbon dioxide can offer a substitute for an organic solvent in the many industrial applications such as the food industry and medical supplies. But scCO₂ but requires high-pressure equipments and expertise, leading to high capital investment for equipment. Moreover, compression of CO₂ requires elaborate recycling measures to reduce energy costs.⁶

Table 1.2 Critical properties of various solvents^{5,7}

Gas Name	Chemical Formula	Molecular Weight (g/mol)	Critical Pressure, Pc (bar)	Critical Temperature, Tc (°C)
Acetone	C ₃ H ₆ O	58.08	47.0	235.1
Carbon dioxide	CO ₂	44.01	73.8	31.1
Chloroform	CHCl ₃	119.38	53.7	263.4
Cyclohexane	C ₆ H ₁₀	82.15	43.4	287.5
Dichloromethane	CH ₂ Cl ₂	84.93	63.0	237.0
Ethanol	CH ₃ CH ₂ OH	46.07	61.4	243.2
Ethane	C ₂ H ₆	28.05	48.8	32.4
n-Hexane	C ₆ H ₁₄	86.18	30.1	234.4
Methanol	CH ₃ OH	32.04	80.9	240.1
Water	H ₂ O	18.02	221.2	374.4

Currently, the non-toxic and environmentally friendly nature of supercritical fluids carbon dioxide (scCO₂) has led to the exploration of their use in many processes of both laboratory and industrial scale in order to replace hazard solvents. Even though CO₂ does have some shortcomings, primarily associated with poor solvent strength and high pressure operation,

numerous successful applications of sc CO₂ have been found in the areas of supercritical fluid extraction⁸⁻¹¹, supercritical fluid chromatography,^{12,13} catalysis/reactant fluid,¹⁴⁻¹⁶ injection modeling and extrusion,¹⁷ particle formation,¹⁸⁻²⁰ electronic chip manufacturing,^{21,22} dry cleaning,²³ and polymerization media.^{24,25}

1.2 SUPERCRITICAL-CARBON DIOXIDE-BASED MATERIAL SCIENCE APPLICATIONS

1.2.1 Polymerization

Taking advantages of the unique physical properties, supercritical carbon dioxide using as a medium for polymer synthesis and for polymer processing has attracted great attention recently. There are a number of factors that make carbon dioxide a desirable solvent for carrying out polymerization reactions. CO₂ is inexpensive, non-toxic, non-flammable, and readily available in high purity. In addition, the separation of solvent from product is simplified because CO₂ can be completely released upon depressurization, eliminating energy intensive drying steps. DeSimone's group's pioneering efforts showed that amorphous fluoroacrylate polymers could be synthesized by homogenous solution polymerization in sc CO₂ which exhibits to be an excellent alternative to chlorofluorocarbons (CFCs), the conventional solvents for fluoropolymer synthesis and processing.²⁶

However, with the exception of polyfluoroacrylates and siloxanes, nearly all the high molecular weight polymers show negligible solubility in CO₂ under practical conditions of several tens of MPa. The synthesis of these materials in CO₂ has therefore involved

heterogeneous polymerization methods such as precipitation, dispersion emulsion polymerization. In precipitation polymerization, the monomer and initiator are soluble in the continuous phase and the polymer precipitates as it forms agglomerated powder. Romack and coworkers investigated the free-radical precipitation polymerization of acrylic acid in sc CO₂.²⁷ Even though the polymer precipitated from the solution, the very fast propagation rate of this reaction allowed the achievement of high molecular weight poly (acrylic acid) ($M_n=1.5 \times 10^5$ g/mol). They also showed that the molecular weight of the product could be controlled by the presence of chain transfer agents. Cooper et al. prepared highly cross-linked copolymers in sc CO₂ through free-radical precipitation polymerization.²⁸ It was shown that the cross-linked polymers could be synthesized in the form of relatively uniform micro-spheres, even in the absence of any surfactants.²⁹

Dispersion polymerization is also characterized by initially homogeneous conditions; however, the resulting insoluble polymer is stabilized by specifically designed surfactants in order to prevent flocculation and aggregation. The surfactants contain a CO₂-phobic region and a CO₂-philic region. The CO₂ phobic region acts as anchor to the growing polymer, either by physical adsorption or by chemical grafting. A long-range steric repulsion between particles were imparted to the polymer-solvent system, preventing flocculation and precipitation.³⁰ The first sample of dispersion polymerization was reported by DeSimone and colleagues. Methyl methacrylate had been polymerized in CO₂ using poly (1,1-dihydroperfluorooctylacrylate) (PFOA) as the stabilizer. Without added any stabilizers, the precipitation polymerization of MMA in scCO₂ resulted in poly(methyl methacrylate) (PMMA) with relatively low molecular weights ($(77-149) \times 10^3$ g/mol) and low conversions (10-40 %). The polymer was collected on the wall. In the presence of the stabilizers, PMMA molecular weight ($(190-325) \times 10^3$ g/mol) and

monomer conversions (>90%) improved dramatically, and the product could be recovered from the reactor as a dry, free-flowing powder. By increasing the concentration of the stabilizer, smaller and more uniform particles were created.²⁴ More detailed studies on the use of PFOA as a stabilizer for the dispersion polymerization of MMA were made by Hsiao and coworkers.³¹ Other than MMA and PFOA system, other systems, such as MMA and poly(dimethylsiloxane) (PDMS),³² vinyl acetate and PDMS,³³ and styrene and poly(styrene-*b*-FOA),³⁴ were also investigated for free-radical dispersion polymerization.

In emulsion polymerization the monomer has very low solubility in CO₂ but the initiator is CO₂ soluble. The monomer is dispersed as droplets in the CO₂ that are stabilized by surfactant molecules adsorbed to the surface. The initiator is soluble in the continuous CO₂ phase but in the monomer droplet. The polymerization starts when the initiator meets the monomer in the micelle. Adamsky and Beckman investigated the water-in-oil emulsion polymerization of acrylamide in scCO₂. The polymer product exhibited a higher degree of linearity when compared with poly(acrylamide) produced by conventional emulsion polymerization.³⁵

Well-defined and ordered porous materials are used in a wide variety of applications, including catalytic supports, adsorbents, chromatographic materials, filters, tissue engineering scaffold, and thermal, acoustic, and electrical insulators.^{36,37} Recently, there has been dramatically increasing interests in the synthesis of macroporous materials using scCO₂, which can obviate the need for any toxic solvents and lead to materials that contain no solvent residues comparing with conventional techniques. Furthermore, the pore size is allowed to be finely-tuned with pressure.³⁸ Cooper and coworkers have shown for the first time that scCO₂ is an excellent porogenic solvent for the formation of cross-linked macroporous polymer monoliths. The results showed that, under appropriate condition, pore sizes could be fine-tuned by varying the CO₂

pressure and by reverse micellar imprinting.^{39,40} Most recently, a new method for producing well-defined porous materials by templating high internal phase CO₂-in-water (C/W) emulsion was developed by Cooper's group.⁴¹⁻⁴³ Providing that the CO₂-in-water emulsions are sufficient stable, it is possible to produce low-density materials (~0.1 g/cm³) with large pore volumes (up to 6 cm³/g) from water-soluble monomers such as acrylamide and 2-hydroxyethyl acrylate.⁴¹

1.2.2 Formation of Polymer Blends

The use of scCO₂ as a solvent for the formation of polymer blends was pioneered by McCarthy and colleagues. The general procedure was to use sc CO₂ as a swelling agent in order to infuse a CO₂-insoluble polymeric host with a mixture of monomer and an initiator. Polymerization is then initiated thermally within the host polymer to form a blend, either in the presence of scCO₂ or after venting the CO₂. Watkins and McCarthy studied the polymerization of styrene in a range of host polymers, including poly(chlorotrifluoroethylene) (PCTFE), poly(4-methyl-1-pentene) (PMP), polyethylene (PE), bisphenol A polycarbonate, poly(oxymethylene), and nylon-6,6.^{44,45} Significant incorporation of pure polystyrene in all polymer substrates was confirmed using differential scanning calorimetry (DSC) and IR analysis.

Although the solubility of most polymers in CO₂ is extremely low, CO₂ interacts with polymer sites, such as carbonyls, acting as a molecular lubricant and depressing the glass transition temperature (T_g) of the polymer, which is referred to as plasticization. This process enhances polymer chain mobility and acts as the underlying principle in many polymer processing techniques including polymer blending.^{38,46}

1.2.3 Encapsulation of Pharmaceuticals

Carbon dioxide has many advantages as a solvent for polymer particles formation, especially for controlled release applications. Conventional techniques for the micronization, co-precipitation, impregnation and encapsulation of pharmaceuticals can be problematic because the heat and mechanical stresses involved can cause thermal and chemical degradation of the drugs. Large amounts of organic solvents and surfactants/emulsifiers are also required which can lead to unacceptable levels of residual impurities necessitating further purification steps.^{47,48} Micronization and precipitation of pharmaceutical compounds using scCO₂ as a promising alternative have many advantages including enabling the processing of thermo-labile and chemically sensitive compounds, and producing particles that are free from solvent residues.

There are several techniques for the preparation of polymer particles using scCO₂, but these can be divided into two categories: those that involve precipitation from a homogeneous supercritical solution by rapid expansion and those that use the scCO₂ as an antisolvent. The former method is known as Rapid Expansion of Supercritical Solution (RESS), in which the homogeneous solution of the solutes, drug and polymer, in scCO₂ is expanded rapidly into a region of much lower pressure and then fine particles were precipitated with the substantial drop of their solubility.⁴⁹⁻⁵¹ However, the key drawback is that the compound must have a reasonable solubility in scCO₂ and thus RESS has been limited so far to a relatively narrow range of CO₂-soluble materials. Antisolvent techniques include several different processes, such as Supercritical Antisolvent precipitation (SAS),⁵² Precipitation by Compressed Antisolvents (PCA),^{53,54} Solution Enhanced Dispersion by Supercritical Fluids (SEDS),^{55,56} Aerosol Solvent Extraction System (ASES).^{57,58} Although these processes differ in important ways, the

fundamental principle behind all of these methods is essentially same: CO₂ is poor solvent for the solute compound in organic solution but completely miscible with the solvent, and thus precipitation occurs upon mixing. In a typical antisolvent technique, e.g. ASES, an organic solution of drug and polymer is injected into scCO₂ through a nozzle. The drug and polymer blends are precipitated when organic solvent contacts with scCO₂.⁵⁹ The design of the apparatus, particularly the injection nozzle, can have a profound influence on the resulting product morphology. Using these methods, many pharmaceutical substances including proteins, antibiotics and steroids, have been processed successfully into nanoparticles or encapsulated inside biodegradable polymers to form particles that can be used for drug delivery and controlled release.⁶⁰⁻⁶³

1.2.4 Scaffolds for Tissue Engineering Applications

A shortage of donor tissue limits the number of people who receive life-saving organ and tissue transplantations. This limitation has driven the development of the tissue engineering field, in which new tissues are created from cultured cells and biomaterials.⁶⁴ Novel materials are needed to induce cell attachment, differentiation and proliferation for tissue growth in vitro and/or in vivo. As one of important biomaterials, three-dimensional polymer porous scaffold can be used as cell supports to provide mechanical stability and structural guidance and to allow cells to be seeded before and after transplantation into the body.^{65,66} Conventional techniques for preparation of polymer scaffolds involve organic solvents and high temperatures that may be harmful to adherent cells, nearby tissues or biologically active factors. ScCO₂ technology is considered as an attractive approach for preparing a variety of polymer scaffolds.⁶⁷

Mooney et al. prepared porous foams for poly(L-lactic acid) (PLA), poly (glycolic acid) (PGA), poly(lactic-co-glycolic acid) (PLGA) with high pressure CO₂.⁶⁷ Poly(ethyl methacrylate)/tetrahydrofurfuryl methacrylate (PEMA/THFMA) foams with controlled porosity and pore geometry and interconnectivity were obtained by Howdle and colleagues using scCO₂.⁶⁸ Generally, the biomaterials are placed in a high-pressure vessel and saturated with CO₂ at a given conditions for a period of time range, e.g. 100bar, 40 °C and 8 h used by Barry and coworkers. The porous scaffold is obtained when venting CO₂.⁶⁸ By varying the magnitude of pressure drop and the rates of depressurization, the pore size within the foams can be controlled.⁶⁹ The biomaterials are plasticized with scCO₂, substantially lowering the T_g and viscosity, and allowing efficient incorporation of thermal and solvent sensitive bioactive guest materials such as growth factors into polymeric scaffold. Hile et al. used scCO₂ to produce PLGA foams containing a basic fibroblast growth factor (bFGF) mixed with bovine serum albumin (BSA).⁷⁰ The total protein release rates (bFGF and BSA) were found to be greater from foams prepared in scCO₂ than scaffolds made by solvent casting-salt leaching. The incorporation of proteins such as ribonuclease A, β-D-galactosidase, and vascular endothelial growth factor (VEGF) into PLGA and PLA scaffolds has also been carried out using scCO₂ at near ambient temperatures (35 °C) and modest pressures (200 bar).^{69,71}

1.3 CO₂ THICKENING AGENTS

Another important application of polymers is used as CO₂-thickening agents, which play a significant role in petroleum engineering. After natural forces have been depleted and water flooding has been completed, which are called primary (5-10% recovery) and secondary

recovery (additional ~20-40% recovery), respectively, much of the oil (typically more than 50%) still remains behind in pores of sandstone and limestone formations. With the increasing demand for petroleum versus limited resources, tertiary recovery methods, referred to as enhanced oil recovery (EOR) employ fluids other than water to displace additional oil from reservoir. Carbon dioxide floods have been used at low cost in an attempt to recover this residual oil for many years. This technology has had an opportunity to mature because of the availability of large amount of high purity, high pressure CO₂ obtained from natural reservoirs, for instance, Bravo Dome and MeElmo Dome and the establishment of pipeline distribution systems that allow CO₂ to be transported to oilfields. It is believed that CO₂ flood will remain one of the most viable EOR technologies for decades. CO₂ is injected into the oil-bearing porous media at the reservoir temperature, which is usually between 25 °C and 120 °C and the working pressure is maintained slightly above the “minimum miscibility pressure” (MMP). Candidate reservoirs are typically at a depth greater than 2000 ft and are able to withstand the CO₂ MMP which ranges from approximately 7-28MPa over the typical reservoir temperature range for light oils⁷². The working pressure is adjusted to be slightly above the MMP to ensure that solvent strength of the CO₂ is great enough to obtain a high degree of solvency for the oil. Thus unlike water flooding in the secondary oil recovery, CO₂ can dynamically develop effective miscibility with oil and can therefore displace oil left behind by water flooding. Further, when the reservoir fluids are produced, CO₂ can be readily separated from the oil simply by pressure reduction.

However, one of the inherent disadvantages of CO₂ as an oil-displacement fluid is its low viscosity, 0.03-0.1 cp at reservoir conditions, as shown in Figure 1.2,⁷³ compared with the viscosity of oil targeted for CO₂ floods, which varies from 0.1 cp to 50 cp. The low viscosity of CO₂ results in high mobility (defined as permeability/viscosity of that fluid in porous media)

compared to that of reservoir oil, causing the mobility ratio, defined as the ratio of mobility of displacing fluid to the fluid which is being displaced, be greater than one. Thus CO₂ “fingers” its way towards the production well, by-passing much of the oil in the reservoir (see Figure 1. (a)). Moreover, in stratified reservoirs, the high mobility of CO₂ induces it to preferentially enter highly permeable zones, leaving oil residing in less permeable layer not contacted by CO₂ and therefore not efficiently displaced. Consequently, if the carbon dioxide viscosity could be elevated to a level comparable with the oil to be displaced, typically a 2-20 fold increase, substantial improvement in oil recovery efficiency could be achieved. The shape of CO₂-flooding with thickening agents in a reservoir is shown in Figure 1.(b).

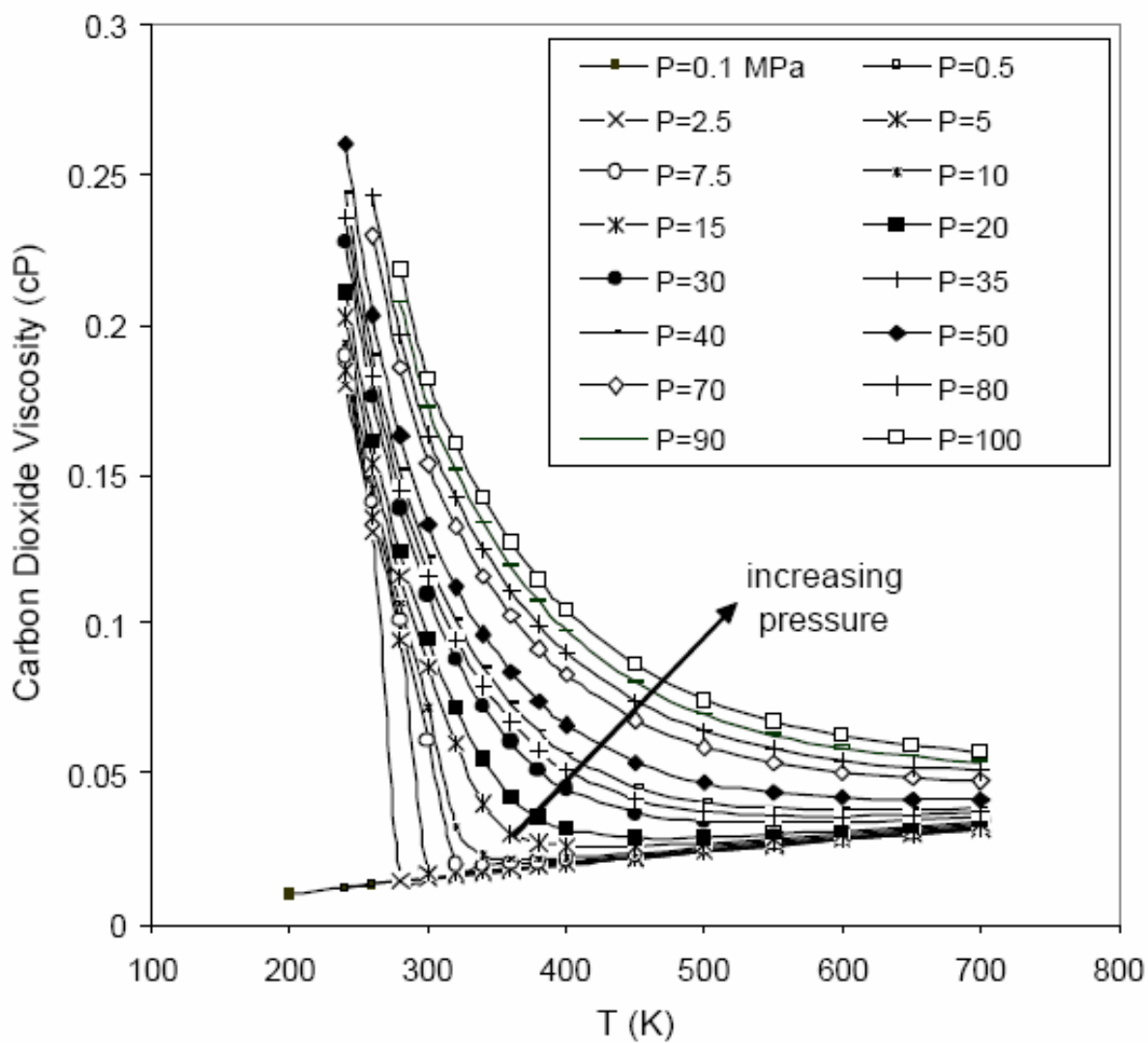


Figure 1.2 Viscosity of CO₂ as a function of temperature and pressure⁷³

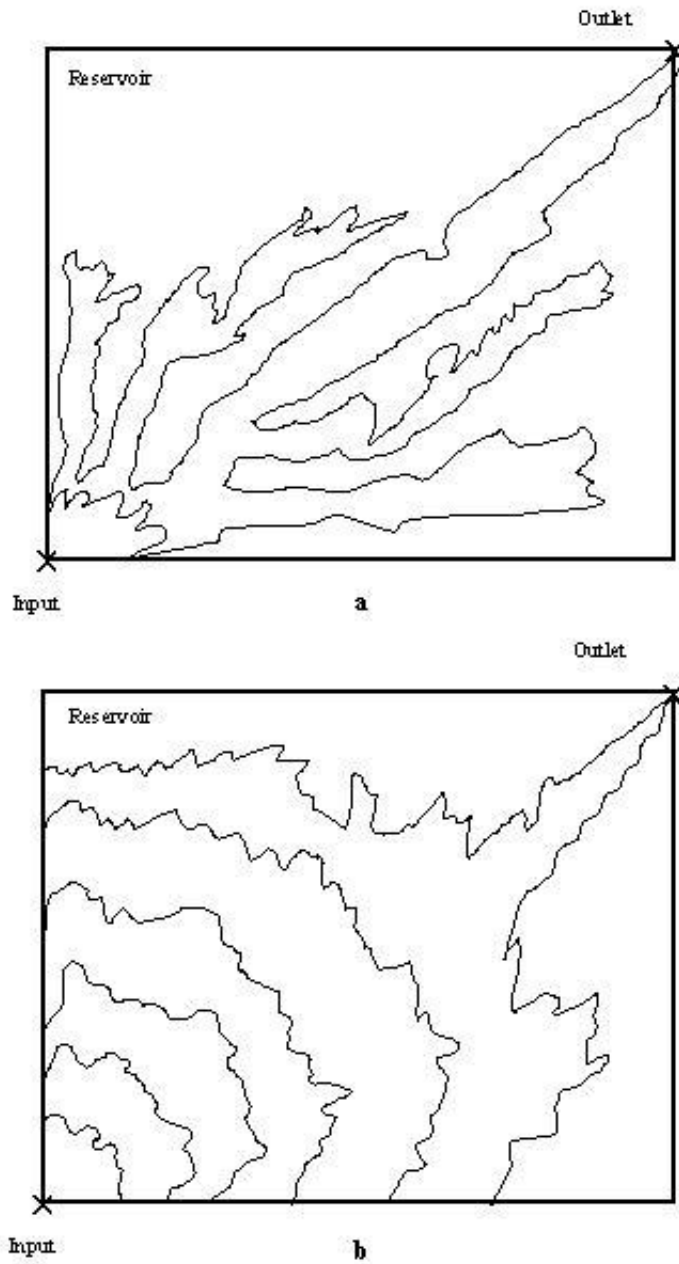


Figure 1.3 CO₂ flooding in a typical reservoir: (a) “fingering” phenomena without mobility control, (b) CO₂ flows with thickeners

1.3.1 Exploratory Research on Decreasing the Mobility of CO₂

Since 1980's, a number of attempts have been made to develop an effective CO₂ thickener. Many basic requirements must be satisfied, for example, a candidate material should be stable and soluble in CO₂ at reservoir conditions, and low cost which can be applied in a large quantity. It also must be remained in the CO₂-rich phase rather than partitioning into the brine or oil while the level of viscosity enhancement is easily controlled to the desired level by adjusting the concentration of the thickener.

Heller and his co-workers first studied conventional polymers for CO₂ viscosity enhancement. They evaluated a variety of commercially available polymers, amorphous polymers of various molecular weights. They also studied linear, weakly associative polymers composed of tri-alkyltin fluoride, and telechelic ionomers. However, none of the polymers were identified as a CO₂ thickener due to the very low solubility of these compounds in CO₂. Based on investigation, they generalized that amorphous stereoregularity favors dissolution of polymers in CO₂ which is able to maximize the entropy of mixing between CO₂ and polymers.⁷⁴⁻⁷⁶

To dissolve the compounds into CO₂, a large amount of cosolvent was introduced into the CO₂ solution. Heller's group presented the results of their attempts to gel organic fluids and CO₂ with 12-hydroxystearic acid (HSA). Even though HSA was essentially insoluble in dense carbon dioxide, the addition of a significant amount of cosolvent, such 10-15wt% ethanol, resulted in the dissolution of HAS and the formation of a translucent or opaque gel phase. For example, only a slight increase in solution viscosity was observed for a 3wt% HSA/15wt% ethanol/82wt% CO₂ mixture at 34°C and 1800 psi, although a 100-fold increase in viscosity was observed in a capillary viscometer at 28 °C.⁷⁷

Terry's research group at University of Wyoming attempted to increase the viscosity of CO₂ via in-situ polymerization of CO₂-soluble monomers, producing high molecular weight polymer that was CO₂-soluble and capable of increasing viscosity.⁷⁸ However, the hydrocarbon polymers precipitated when molecular weights increased, rather than staying in solution to render any viscosity enhancement.

The direct use of "entrainers" as CO₂-thickeners was presented by Llave and coworkers.⁷⁹ These compounds were relatively low molecular weight, CO₂-soluble compounds such as alcohols, ethoxylated alcohols, and hydrocarbons. Although the viscosity increased substantially with the presence of entrainers, the entrainer concentrations were very high. For example, 1565% increase of CO₂ viscosity was obtained as 44 mol% 2-ethylhexanol was added into CO₂. When presenting in a more dilute concentration, such as 2 mol%, the viscosity enhancement was only 24% for 2-ethylhexanol.

High molecular weight silicone oils were also considered to enhance CO₂ viscosity.⁸⁰⁻⁸² Although the viscosity of CO₂ at 55 °C and 17.2 MPa could be raised to 1.5 cp with 4 wt% siloxane (M_w=197,000), large amounts of toluene, 20 wt%, had to be introduced as a cosolvent, which was undesirable for the field use of EOR. Nonetheless, this research indicated that a substantial decrease in CO₂ mobility enhanced oil recovery from lab cores.

Our group's attempts to enhance the viscosity of carbon dioxide⁸³⁻⁸⁶ began with the evaluation of surfactants (amphiphilic compounds containing a hydrophilic head group and a hydrophobic tail). At concentrations above the critical micelle concentration (CMC), these compounds can aggregate as spheres or cylinders. Geometries such as rods or cylinders can lead to substantial increases in solution viscosity. Approximately 80 commercially available oil-soluble surfactants were evaluated in our labs. None of the commercially available surfactants

were soluble enough in CO₂ to induce a viscosity increase. Although hydroxyaluminum bis(2-ethylhexanoate), the surfactant used to thicken gasoline in the production of Napalm, was capable of increasing the viscosity of alkanes as light as propane, it was CO₂ insoluble. Other investigators have also reported the extremely low solubility of surfactants in CO₂.

Semifluorinated alkanes, diblock compounds (an alkane segment and a perfluorinated alkane segment) had previously been used to form gels in light alkanes. This occurred when the alkane was heated, dissolving the semifluorinated alkane, and then cooled. Upon cooling, microfibriles of the semifluorinated alkane formed, which interlocked with the alkane in the voids, forming a “gel”. These fibers formed due to the alignment of perfluorinated and hydrocarbon segments of neighboring semi-fluorinated alkanes. Similar results were obtained when liquid CO₂ was used as the fluid. Because this ‘gel’ was not a single, viscous, transparent fluid phase, but rather a dispersion of carbon dioxide in a network of solid fibers, it was unsuitable for flow in porous media or in fractures.

Light alkane cosolvents were used to enhance the solubility of tributyltin fluoride, a known alkane-gelling agent, in CO₂. The viscosity of the fluid phase increased several orders of magnitude using only 1wt% tributyltin fluoride, yet pentane cosolvent concentrations of 40-50 wt% were required.

We also investigated several polymers for their ability to raise the viscosity of dense carbon dioxide. It had been previously reported that CO₂ could be used to fractionate perfluorinated ether oils, such as the Krytox series of oils manufactured by DuPont. The highest molecular weight (Mw=13,000 g/mol) commercially available perfluorinated oil was determined to be completely miscible with CO₂ at ambient temperature and a pressure of only 18 MPa (2600 psi). However, the viscosity enhancement was only 8% when the concentration of the polymer in

CO₂ is 10wt%. Fluoroether oils with molecular weight as high as 30,000 g/mol were recently evaluated as carbon dioxide-thickeners, but no substantial improvements were achieved at concentrations of several weight percent. Using a fluoroether diol and a fluoroether diisocyanate, we generated a cross-linked fluoroether-based polyurethane in CO₂. Although the resultant polymer was soluble to 4 wt% in dense carbon dioxide, only marginal increases in CO₂ viscosity were observed.⁸⁷

1.3.2 Success of Fluorinated Copolymers as CO₂ Thickeners

In early 1990s, investigators began tailoring the properties of compounds to dissolve in CO₂ rather than hoping that a hydrocarbon soluble compound would fortuitously dissolve in CO₂.

DeSimone and coworkers^{24,26,88,89} have conducted numerous polymerizations in liquid and supercritical carbon dioxide. CO₂ has been shown to be a suitable reaction medium for homogeneous, precipitation, dispersion, and emulsion polymerizations. DeSimone has observed that fluoroacrylate polymers exhibit remarkably greater solubility in carbon dioxide than other types of polymers. Modest viscosity changes associated with low concentrations (several wt%) of a highly CO₂ soluble homopolymer in dense carbon dioxide were first documented by DeSimone's group.⁸⁸ Poly(1,1-dihydroperfluorooctyl acrylate), PFOA, Mw = 1.4×10⁶ g/mol, was formed by performing a homogeneous polymerization of the fluorinated monomer in carbon dioxide. The resultant homopolymer was also CO₂ soluble, and induced an increase in solution viscosity as measured in a falling sinker viscometer. For example, at 50 °C, the viscosity increased from 0.08 cp for neat CO₂ to 0.20- 0.25 cp at 280-360 bar using a 3.7 wt/vol% (3.7 gm polymer per 100 cm³ solution) mixture of PFOA in carbon dioxide. At 6.7 wt/vol%, the viscosity

increased from about 0.2-0.6 cp over the 230-350 bar pressure range. No co-solvent was required to dissolve this CO₂-philic polymer. Figure 1.4 is an illustration of the increase in carbon dioxide viscosity attained with PFOA at 50 °C. This is the only successful documentation of a polymer increasing the viscosity of carbon dioxide without the need for a co-solvent prior to 1999. The concentration (about 5-10 wt%) required to attain this viscosity increase (3-8 fold) illustrates that even for high molecular weight CO₂-soluble polymers, it is challenging to attain a 10-100 fold increase in viscosity using dilute concentration (1wt% or less).

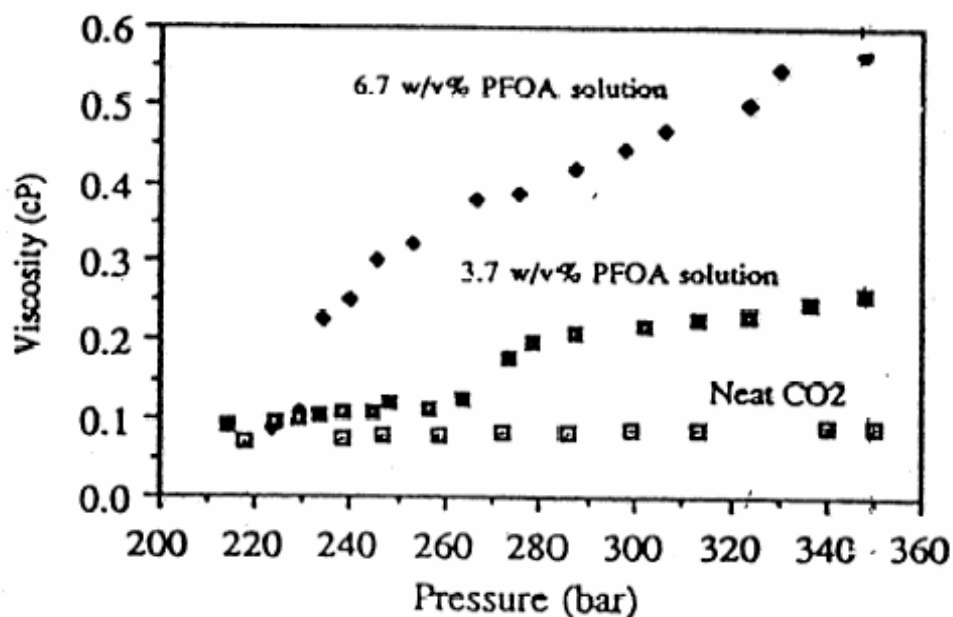
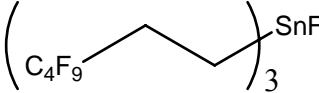

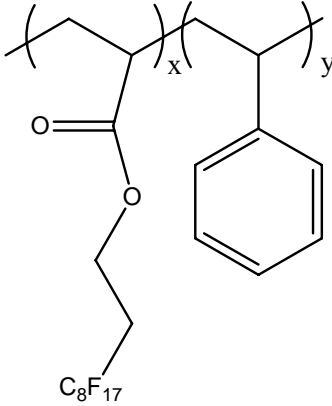


Figure 1.4 Viscosity of PFOA in CO₂ at 323K under different concentrations.^{88,89}

However, if some sort of associating groups could be incorporated into the CO₂-soluble polymers, the formation of viscosity-enhancing, formation of macromolecular associating networks in CO₂ is likely to promote CO₂ viscosity to a desired level. Our lab has possessed abundant experience in designing CO₂ thickening agents. Our group has designed and synthesized several CO₂ thickeners that incorporated CO₂-philic segments and CO₂-philic

segments, such as semifluorinated trialkyltin fluoride,⁹⁰ fluorinated telechelic ionomers,⁹⁰ fluoroacrylate-styrene copolymers (PHFDA-xPSt)^{91,92} (see Table 1.3). Each compound was evaluated for both CO₂ solubility and enhancement in solution viscosity.

Table 1.3 Formulas of fluorinated CO₂ thickeners

Name	Formulas	Reference
Semi-Fluorinated Trialkyltin Fluoride		90
Fluorinated telechelic disulfates	NaOO_3S  SO_3ONa	90
PHFDA-xPSt		91

The semifluorinated trialkyltin fluoride was soluble in liquid carbon dioxide at moderate pressures of 10-18 MPa over 1-4wt% concentration ranges at 297 K. The fluorinated telechelic ionomers were soluble in carbon dioxide within the molecular weight range of 13,800 and 29,900. The optimal molecular weight for solubility was 18,700. The degrees of viscosity enhancement of both compounds were quite low, however. At 297 K and 34 MPa, the relative viscosity of semifluorinated trialkyltin fluoride solution increased by a factor of 3.3 at 4 wt%,

while the viscosity of the fluorinated telechelic ionomers ($M_w=29,900$ g/mol) solution increased 2.7 times comparing to that of neat carbon dioxide.⁹⁰

Our most successful thickeners were a series of bulk polymerized random copolymers (PHFDA-xPSt) of 3,3,4,4,5,5,6,6,7,7,8,8,9,9-10,10-heptafluorodecyl acrylate (PHFDA) and styrene (PSt), where x represent the molar fraction of styrene in the copolymer.⁹¹ The optimum level of styrene proportion, approximately 30 mol%, was observed with respect to viscosity thickening behavior in carbon dioxide. Figure 1.5 shows the phase behavior of the PHFDA-xPSt copolymers at 298 K. The copolymer with styrene composition as high as 30 mol% were very soluble in CO₂, exhibiting solubilities of 1–5 wt% at pressure of 11-16 MPa. In general, the cloud point pressures increased with increasing molar fraction of styrene in the copolymers because styrene repeat units are known to be CO₂-phobic. Significant increase in the cloud point pressure was observed for copolymers when styrene compositions approach 35 and 40 mol% in the copolymer. Therefore, solubility considerations would restrict the styrene proportion of these copolymers <30 mol%.

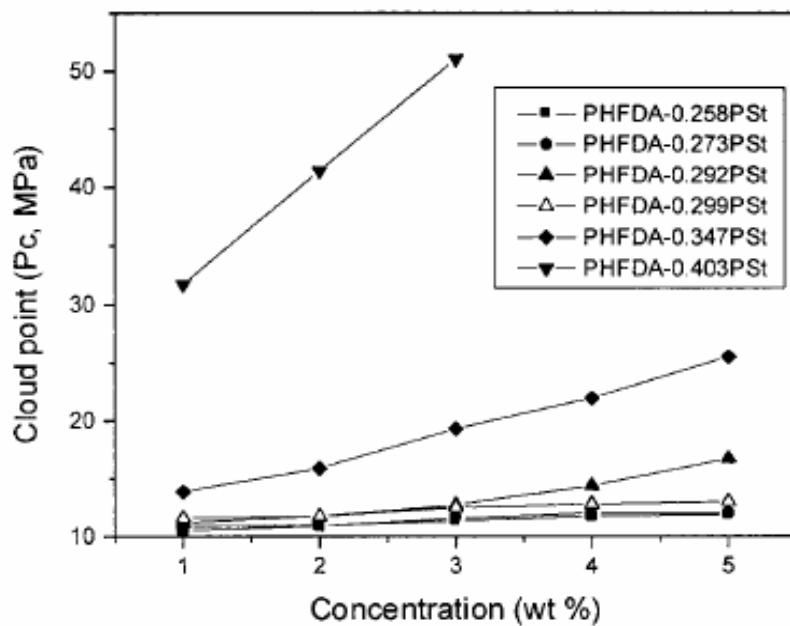


Figure 1.5 CO₂ solubility of PHFDA-xPSt copolymers at 298K⁹¹

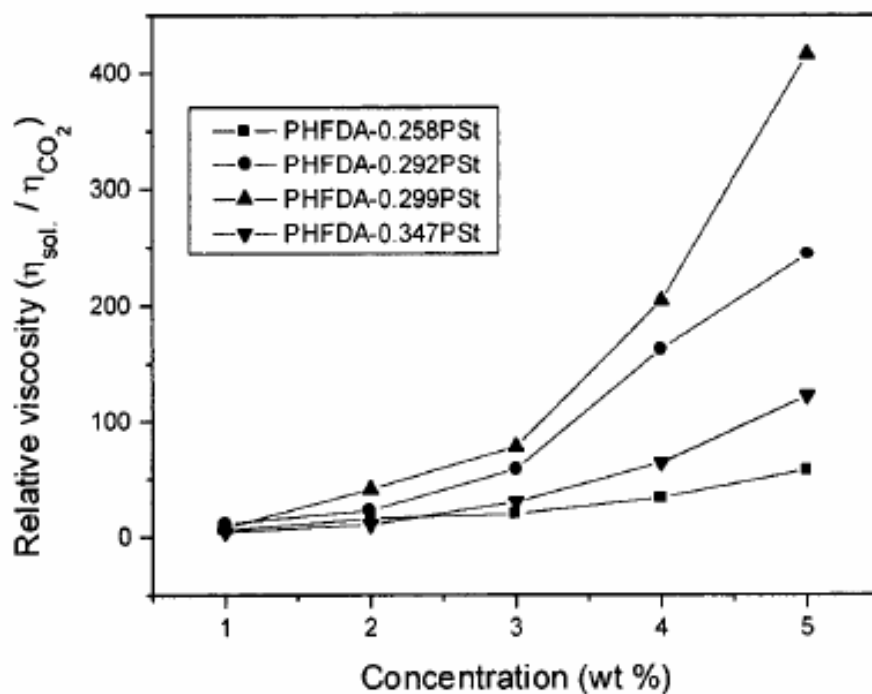


Figure 1.6 CO₂ viscosity enhancement achieved with the fluoroacrylate-styrene copolymers⁹¹

The viscosity increases evaluated for the solutions of these copolymers in CO₂ were dramatic at 297 K and 35 MPa, shown in Figure 1.6. The effectiveness of the thickener increased as the styrene concentration increased from 25 to 30 mol% but decreased at higher concentrations. At higher phenyl group content, the copolymers showed less solubility in carbon dioxide. As a result, the polymer coils could not extensively expand in solution and potentially lead to fewer inter-chain associations rather than a large number of intra-chain associations. This would have reduced the prevalence of macromolecules, thereby diminishing the effectiveness of the thickener.

It is believed that the strong viscosity enhancement of the copolymers is attributed to π - π stacking between aromatic rings. Because H atoms are positively charged and C atoms are negatively charged with respect to one another in aromatic molecules. The Coulomb force in favors close C \cdots H approaches. This effect gives rise to T-shaped, edge-to-face aromatic-aromatic interactions (Figure 1.7). H atoms at the edge of one molecule point toward negatively charged C atoms on the faces of the adjacent molecule. Hence, the dihedral angles between phenyl-ring planes are often close to the perpendicular.⁹³⁻⁹⁶ These non-bonded interactions between the aromatic rings impede the motion of the polymeric chains in CO₂ solution, finally resulting in a viscosity enhancement.

Figure 1.8 clearly illustrates that these solutions are shear thinning as expected and that the viscosity of CO₂ flowing through porous media can also be increased with this copolymer in dilute concentration. This result remains the only data demonstrating that polymeric compound can successfully reduce the mobility of CO₂ flowing through porous media without the need for co-solvent.⁹⁷

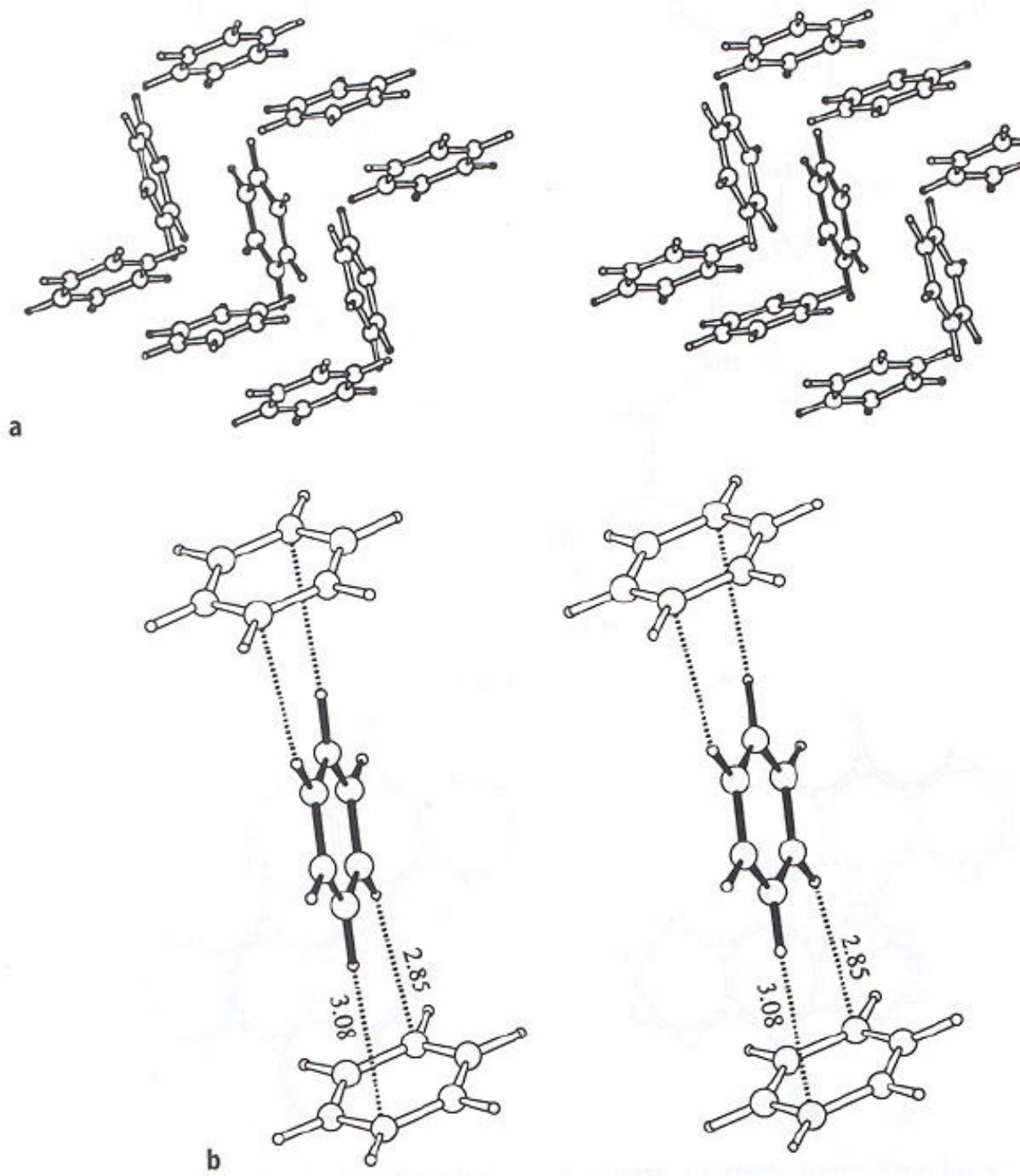


Figure 1.7 π - π stacking of the aromatic phenyl groups, (a) an overview structure; (b) a close view structure³⁷

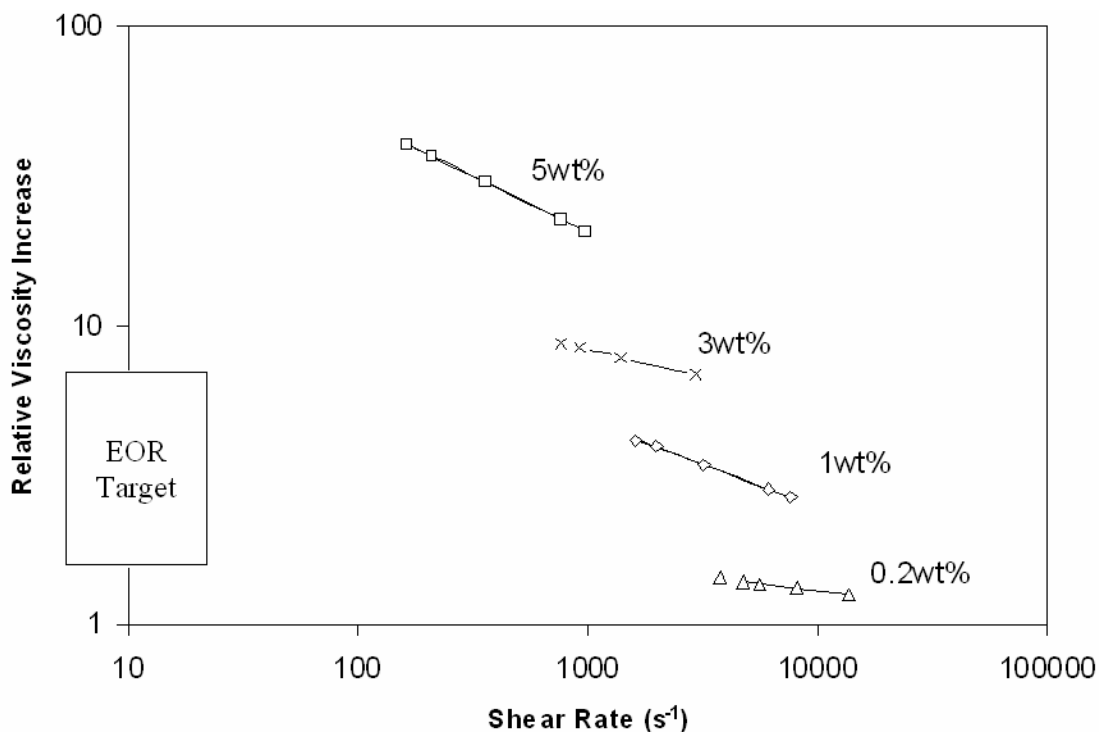


Figure 1.8 Effect of shear rate and concentration on the viscosity of fluoroacrylate-styrene copolymer solution in CO₂; Glass tube inside radius=1.588 cm; copolymer of 29mol% Styrene-71mol% fluoroacrylate; T=298K; P=34 MPa.^{92,98}

Drawing from previous studies of polymeric CO₂ thickeners, a successful thickener should have two functional parts identified in two successive steps: a CO₂-philic group which impart certain solubility of the thickener in CO₂, and associative groups (usually being CO₂-phobic, e.g. styrene) which can improve CO₂ solution viscosity. Of these two segments, design and synthesis of CO₂-philic polymers must be done first. This dissertation details research into the first step: the identification of novel, (preferably) non-fluorous, highly CO₂ soluble compounds, oligomers, and polymers. (Unfortunately, none of these were so CO₂ soluble as to merit their modification into thickeners to date, therefore, no results on the second step are presented.)

1.4 RESEARCH OBJECTIVES

Although fluoropolymers have received substantial prestige in scCO₂ technology, high cost may prohibit industrial scale use for many applications. In addition, fluorinated materials often have poor environmental degradability and upon degradation may yield dangerous compounds, potentially negating the environmental advantages associated with the use of scCO₂. For example, the approximate price of high-pressure and dry CO₂ from natural reservoirs to oilfields is roughly \$10/ton. In the case of EOR, if the cost of the thickener were \$1/lb, the addition chemical cost of the thickener present at 0.05wt% would add \$1 for every \$10 of CO₂. If the thickener costs \$2/lb and 0.2wt% is required, then the addition cost for the thickening agent would be \$9 for every \$10 of CO₂. Such costs could be acceptable because roughly 3 barrels of liquid CO₂ are required for each barrel of oil recovered, and the volume of thickened CO₂ could reduce this requirement by 50% or more while reducing or eliminating the need to co-inject water. Although the substantial increases in viscosity were attained with high molecular weight PHFDA-xPSt at a concentration as low as 0.25wt%, the fluorous monomer alone cost roughly \$2500/lb. Therefore, fluorinated thickeners would substantially increase the cost of CO₂ flood in EOR, consequently, the price of oil.

The primary objective of this project is to develop novel polymers with high CO₂ solubility are solely composed of C, H, and O, avoiding the use of fluorine and silicone which are expensive and environmentally unacceptable. To date, poly(vinyl acetate)s (PVAc)s were found to be the most CO₂ soluble polymers in all the non-fluorous and non-silicon polymers. However, its CO₂-philicity is still not strong enough for practical applications which usually require the pressure under moderate conditions (<100 °C, <40 MPa).⁹⁹ For example, the cloud

point pressure for oligo(vinyl acetate) sodium sulfate surfactant with 17 repeat units is higher than 35 MPa at 1 wt% and 298K.¹⁰⁰ The novel polymers will have a highly CO₂ soluble strength which will be comparable with amorphous fluoropolymers and polysiloxanes.

The ultimate research objective is to design novel surfactant, copolymers, and thickeners by functionalizing the highly CO₂-soluble polymers. For example, new CO₂ thickening polymers, considering both environmental and economical aspects, could be prepared by incorporating associative groups (e.g. styrene or vinyl amino ether). As well, high CO₂ soluble copolymer and surfactants could be developed for many potential applications including protein extractions, polymerizations, and dry cleaning based on scCO₂. (This project, however, relates only to the identification of new highly CO₂-philic polymers, oligomers and compounds.)

2.0 BACKGROUND

2.1 SOLVENT PROPERTIES OF CO₂

CO₂ has been considered as a nonpolar solvent for a long time because the absence of a dipole moment and its low dielectric constant. Liquid and supercritical CO₂ was commonly assumed to have comparable solvent properties with hexane. However, hexane failed to screen CO₂-philic compounds because many materials that are miscible with hexane were reported to be insoluble in supercritical CO₂ and vice versa. Recently, it is noted that quadrupolar effects are responsible for the solvation properties of supercritical CO₂.¹⁰¹

Although CO₂ has a zero dipole moment, it is a charge-separated molecule with significant nonzero bond dipole moment.¹⁰²⁻¹⁰⁴ This charge separation results in a significant quadrupole moment, and CO₂ is described as a quadrupolar solvent. The solvation behavior of CO₂ is attributed to its large quadrupole moment. The quadrupolar charge separation present in CO₂ results in a partial positive charge on the carbon and partial negative charges on the electronegative oxygens, as shown in Figure 2.1. This electronic structure suggests that CO₂ can act as either a Lewis acid or Lewis base. As a Lewis acid, the electron deficient carbon atom can interact with a Lewis base group such as a carbonyl oxygen atom (C=O···C). CO₂ can also act as a Lewis base by showing that in the interaction between CO₂ and a carbonyl functional group, such as an acetate group, one of electronegative oxygen atom of CO₂ can interact as a Lewis base

with one of the electron deficient hydrogen atoms attached to the carbonyl carbon atoms through a relatively weak cooperative C–H···O hydrogen bond (Figure 2.2).¹⁰⁵⁻¹⁰⁷ This interaction provided approximately 0.5 kcal/mol additional stabilization energy.¹⁰⁸

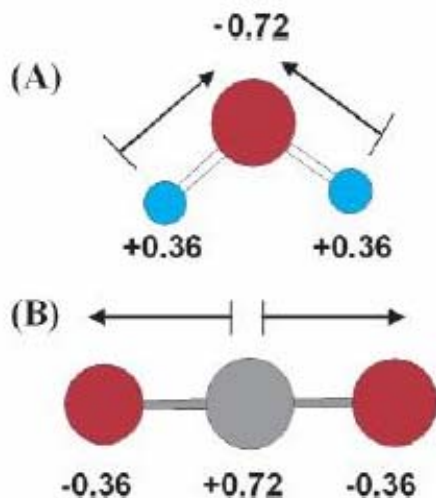


Figure 2.1 Comparison of the partial charges on the individual atoms of H₂O (A) and CO₂ (B) with the charges derived by fitting the electrostatic potentials (CHELPG charges) in electrons calculated at the MP2/aug-cc-pVDZ level.¹⁰⁹

Figure 2.1 also shows that the charge separation is similar for CO₂ and H₂O except for the reversal of the sign in the charges of the end versus central atoms. It is well known that the cooperative hydrogen bond net works make H₂O a unique solvent for polymer materials unlike CO₂. Although much less efficient, CO₂ also should be taken account as a polar molecule with two active and considerably strong bond dipole.¹¹⁰ Those distinguishing characteristics of CO₂ have been firmly confirmed by spectroscopic methods^{106,107,111} and phase behavior descriptions.^{112,113}

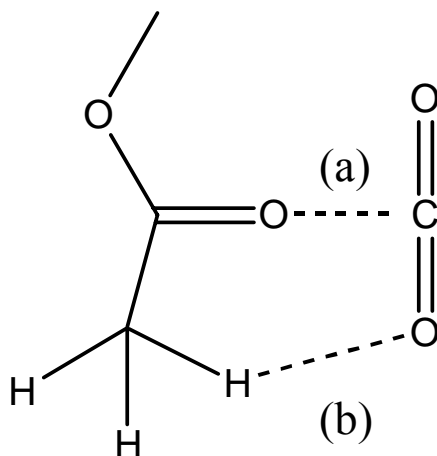


Figure 2.2 Schematic diagram of interactions between CO₂ and CO₂-philic group, (a) CO₂ as a Lewis acid (C=O···C); (b) CO₂ acts as a Lewis base (C-H···O)

2.2 THERMODYNAMIC FUNDAMENTALS OF SUB/SUPERCRITICAL CO₂ SOLUTION

To dissolve polymers in liquid/supercritical CO₂ at a given temperature and pressure, the Gibbs free energy must be negative and at a minimum. The Gibbs free energy of mixing is defined as

$$\Delta G_{mix} = \Delta H_{mix} - T\Delta S_{mix}$$

Equation 2-1

Where ΔH_{mix} represents the change of enthalpy and ΔS_{mix} represents the change of entropy in mixing processes. To form a stable polymer-CO₂ solution at a given temperature and pressure, the Gibbs free energy must be negative and at a minimum.¹¹⁴ Enthalpic interaction of a given compound in liquid/supercritical CO₂ depends predominantly on the intermolecular forces between solvent-solvent, solvent-compound, and compound-compound pairs in solution. From

the enthalpic consideration, whether a compound is soluble or not in a given solvent depends on the interchange energy, ω , defined as

$$\omega = z \left[\Gamma_{ij}(r, T) - \frac{1}{2} (\Gamma_{ii}(r, T) + \Gamma_{jj}(r, T)) \right]$$

Equation 2-2

Where z is the coordination number, Γ is the intermolecular pair potential energy. i, j represent solute and solvent molecules, respectively. An approximate form of Γ_{ij} for small molecules is

$$\Gamma_{ij}(r, T) \approx - \left[C_1 \frac{\alpha_i \alpha_j}{r^6} + C_2 \frac{\mu_i^2 \mu_j^2}{r^6 kT} + C_3 \frac{\mu_i^2 Q_j^2}{r^8 kT} + C_4 \frac{\mu_j^2 Q_i^2}{r^8 kT} + C_5 \frac{Q_i^2 Q_j^2}{r^{10} kT} + \text{complexformation} \right]$$

Equation 2-3

Where α is the polarizability, μ is the dipole moment, Q represents the quadrupole moment, C_{1-5} are constants, r is the distance between the molecules, k is Boltzmann's constant, and T is absolute temperature. Induction interactions are neglected in Equation 2-3 since their contribution to the potential energy tends to be much smaller compared with dispersion and polar interactions. Furthermore, Equation 2-3 is not expected to describe rigorously the interaction of a polymer segment with another segment or with the solvent since segmental motion is constrained by chain connectivity and this architectural feature is not taken into account. Nevertheless, Equation 2-3 can serve as a guide to qualitatively interpret the effects of intermolecular interactions on polymer-solvent phase behavior.

The first term represents nonpolar dispersion interactions that are only dependent on the polarizability of compounds and distance between the compound molecules, but not on

temperature. It is predicted that CO₂ is not a good solvent unless the density of CO₂ is increased to high values (but this may lead to unacceptable large pressures for CO₂ floods). In order to discuss dipole interactions (the 2nd term on the right side in Equation 2-3), dipole–quadrupole interactions (the 3rd term on the right side in Equation 2-3), and interactions of quadrupole–quadrupole (the 4th term on the right side in Equation 2-3), the polarity of CO₂ must be considered. Although CO₂ does not have a dipole moment, it does have a substantial quadrupole moment ($-4.3 \times 10^{-26} \text{ erg}^{1/2} \text{ cm}^{5/2}$) that operates over a much shorter distance than dipolar interactions. It is noted that the dipolar and quadrupolar interaction terms in Equation 2-3 are inversely proportional to temperature. Hence, it may be possible to dissolve a nonpolar polymer in CO₂ if the temperature is high enough to diminish CO₂-CO₂ quadrupolar interactions relative to CO₂-polymer segment nonpolar dispersion interactions. On the other hand, CO₂ is a weak solvent for polar polymers since the effect of dipole interactions outweighs that of quadrupole interactions, especially at low temperatures where polar interactions are more significant. Therefore, the dissolution capability of CO₂ mediates between polar and nonpolar solvent. The challenge that remains is to predict the level of polarity needed in the polymer to make it soluble in CO₂ at modest pressures and temperatures. In addition, specific interactions such as electron acceptor-donor complex formation or hydrogen bonding cannot be ignored, especially at low and moderate temperatures because of their inverse temperature dependence. For example, certain polymers that possess electron-donating groups, such as carbonyls, have been shown to exhibit specific interactions with CO₂ where the carbon atom of CO₂ acting as an electron acceptor can form a Lewis acid and base complex with carbonyl oxygen that acts as an electron donor. Although the strength of this kind of Lewis acid: base complex was shown less than 1kcal/mol,

which is slightly stronger than dispersion interactions, the CO₂-polymer complex is expected to be significant in a dense CO₂-polymer solution at low or moderate temperatures.¹¹⁵

Besides energetic interactions, entropy of mixing plays a very important role in assessing the possibility of compounds in CO₂, especially when compound's molecular weight is high. The entropy of mixing is related to the free volume difference between the compound and CO₂. Generally, to dissolve a compound in CO₂, it is necessary for CO₂ molecules to aggregate around the compound molecules (solute). This process reduces the number of conformations available to the pure CO₂ leading to negative entropy of mixing which can dominate favorable enthalpic interactions and prevent the formation of a single phase. If the free volume of a compound is increased, it becomes easier to dissolve it in CO₂. Compared with linear molecules, branching molecules have much more free volume. To molecules with relative large molecular weight, as the rotational flexibility of the chain segments decreases, the number of possible conformations available to the polymer is expected to decrease, which makes the entropy of mixing of the polymer with an SCF solvent more negative.¹¹⁶

Although it is impossible to rigorously decouple the impact of energetic and entropic contribution to Gibbs free energy since both of these considerations depend on temperature in complex ways, it is possible to interpret compound – CO₂ phase behavior as being dominated by either enthalpy or entropy, and to design structures that magnify or attenuate the impact of energetic relative to entropic contributions.^{115,117}

2.3 PROGRESS IN IDENTIFICATION OF NON-FLUOROUS/SILICONE CO₂ SOLUBLE FUNCTIONAL GROUPS

2.3.1 Experimental Study

Recently, a number of compounds have been designed, synthesized and evaluated to be candidates for inexpensive and environmentally benign CO₂-philic segment of a thickener (i.e. the replacement for the fluoroacrylate). Table 2.1 provides a compilation of compound (e.g. oligomers, polymers)-SCF phase behavior studies found in the literature and performed in our laboratory. Figure 2.3 collects nearly all the oxygenated hydrocarbon-based CO₂ soluble polymers to date.

Table 2.1 Summary of prospective CO₂-philic functionalities

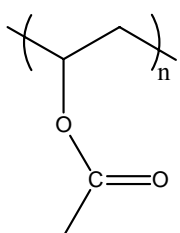
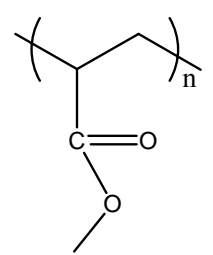
#	Polymer Name	Functional groups	Structures	CO ₂ solubility result at 298K, 68.9 MPa and 1-5wt%*	References and/or Resources
1	Poly(vinyl acetate)	Acetate group		The most CO ₂ -soluble high MW oxygenated hydrocarbon polymer	118,119
2	Poly(methyl acrylate)	Carbonyl and ether		Soluble	118,119

Table 2.1 (Continued)

3	Poly(lactide)	Carbonyl and ether oxygen		The Second most CO ₂ soluble oxygenated hydrocarbon polymer	120
4	Poly(propylene oxide)	Ether oxygen		Soluble at low MW (<2500)	119,121,122
5 [†]	β-cyclodextrin heneicosaacete (Also 6- and 8-membered acetylated cyclodextrins)	Acetate group		Soluble	123
6 [†]	β-D-galactose pentaacetate	Acetate group		Extremely Soluble	112,124
7	Grafted silicone polymers (this structure does not imply the use of silicon copolymers as thickeners; they served to provide a way to compare side groups composed of C, H and O)	Carbonyl and ether oxygen		Soluble	125,126
			R=propyl acetate, methyl butyrate, butyl methyl ketone, propyl methyl carbonate, propyl ethyl ether		
8	Poly(ethylene glycol)	Ether oxygen		Soluble	121
9	Poly(propylene glycol)	Ether oxygen and branching		Soluble	121
10	Poly(tetrahydrofuran)	Ether oxygen		Insoluble	121

Table 2.1 (Continued)

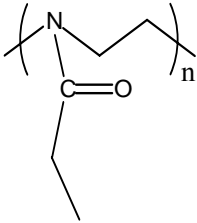
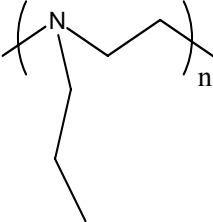
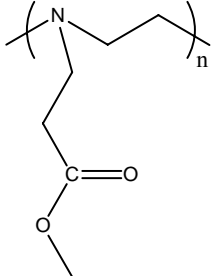
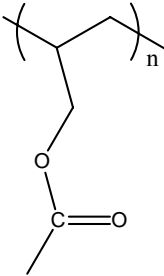
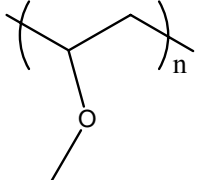
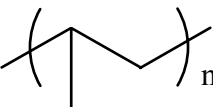
11	Poly(2-ethyl-2-oxazoline)	Carbonyl and amine		Insoluble	Investigated by previous group members (unpublished results)
12	Poly(propyl ethyleneimine)	Amine		Insoluble	Investigated by previous group members (unpublished results)
13	Poly(propyl methylacrylate-ethyleneimine)	Carbonyl, ether, and amine		Insoluble	Investigated by previous group members (unpublished results)
14	Poly(allyl acetate)	Acetate group		Insoluble	Investigated by previous group members (unpublished results)
15	Poly(vinyl methyl ether)	Ether oxygen		Less soluble than PVAc	Investigated by previous group members (unpublished results)
16	Poly(propylene)	Branched hydrocarbon		Less soluble than PVAc Insoluble at high MW	Investigated by previous group members (unpublished results)

Table 2.1 (Continued)

17	Partially sulfonate-functionalized poly(propylene glycol), $x=0.44$	Sulfonyl and ether		Insoluble	Investigated by previous group members (unpublished results)
18	Partially methyl ether functionalized Poly(propylene glycol), $x=0.12, 0.22, \text{ and } 0.44$	Ether oxygen		Insoluble	Investigated by previous group members (unpublished results)
19	Partially acetate ether functionalized poly(propylene glycol), $x=0.12, 0.22, 0.44$	Acetate group		Less soluble than PVAc	Investigated by previous group members (unpublished results)
20	Poly(methylene acetate)	Acetate group		Insoluble	Investigated by previous group members (unpublished results)
21	Poly(vinyl ethyl ether)	Ether oxygen		Less soluble than PVAc at low MW (Mw=3700)	Investigated by previous group members (unpublished results)
				Insoluble at high MW (Mw=100,000)	Investigated by Lei Hong (unpublished results)
22	Poly(propylene glycol) monobutyl ether (Mw=340, 1000, 1200)	Ether oxygen		Soluble	Investigated by Lei Hong (unpublished results)

Table 2.1 (Continued)

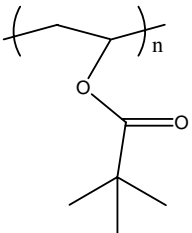
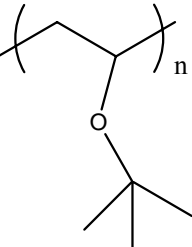
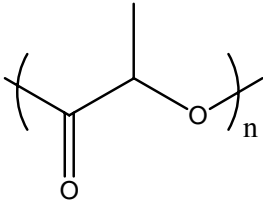
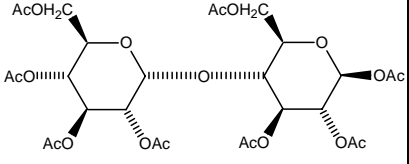
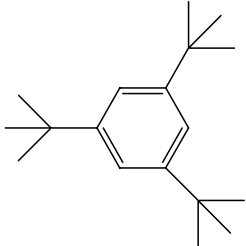
23	Poly(vinyl pivalate) (Mw=100,000 g/mol)	Acetate group and branched structure		Insoluble	Investigated by Lei Hong (unpublished results)
24	Poly(vinyl tertbutyl ether)	Ether and branched structure		Insoluble	Investigated by Lei Hong (unpublished results)
25	Poly(D-lactide) (Mw=44,000 g/mol; Mn=34,000 g/mol)	Carbonyl and ether oxygen		Insoluble (The solubility was measured up to 138 MPa.)	Investigated by Lei Hong (unpublished results)
26	Maltose octaacetate	Acetate group		Soluble	Investigated by Lei Hong (published) 113
27 [†]	Lactose octaacetate			Soluble	Investigated by Lei Hong (unpublished results)
28	Sucrose octaacetate			Insoluble	Investigated by Lei Hong (unpublished results)
29	1,3,5-tri- <i>tert</i> -butylbenzene (TTBB)	Branched structure		Highly soluble	Investigated by Lei Hong (unpublished results)

Table 2.1 (Continued)

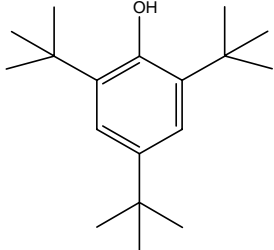
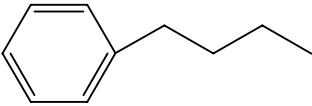
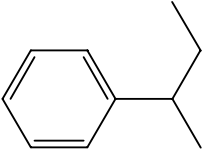
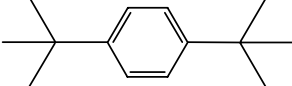
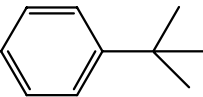
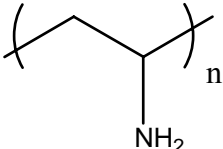
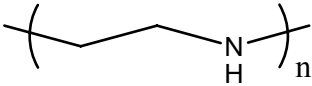
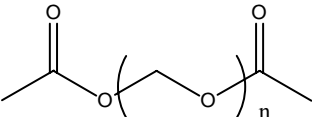
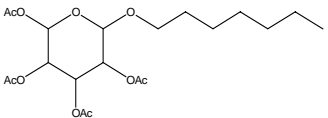
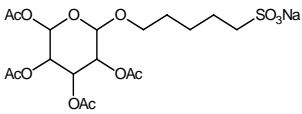
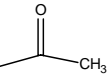
30	2,4,6-tri- <i>tert</i> -butylphenol (TTBP)	Branched structure		Highly soluble	Investigated by Lei Hong (unpublished results)
31	butylbenzene	Branched structure		Highly soluble	Investigated by Lei Hong (unpublished results)
32	Sec-butylbenzene	Branched structure		Highly soluble	Investigated by Lei Hong (unpublished results)
33	1,4-di- <i>tert</i> -butylbenzene	Branched structure		Highly soluble	Investigated by Lei Hong (unpublished results)
34	Tert-butylbenzene	Branched structure		Highly soluble	Investigated by Lei Hong (unpublished results)
35	Polyethyleneamine	Nitrogen		Insoluble	Investigated by Lei Hong (unpublished results)
36	Polyethyleneimine	Amine		Insoluble	Investigated by Lei Hong (unpublished results)
37	Ethylenediamine-ethyleneimine copolymer	Amine	N/A	Insoluble	Investigated by Lei Hong (unpublished results)
38	Poly(oxymethylene) acetate end-capped	Carbonyl and ether oxygen		Insoluble	Investigated by Lei Hong (unpublished results)
39 [†]	Sugar acetate	Carbonyl oxygen		Soluble (<4wt%)	Investigated by Lei Hong (unpublished results)

Table 2.1 (Continued)

40 [†]	Sugar surfactant acetate	Acetate group		Insoluble	Investigated by Lei Hong (unpublished results)
41	PIM-1 (polymer of intrinsic microporosity)	High free volume	The structure was given in reference ^{127,128}	Insoluble	Investigated by Lei Hong (unpublished results)

- * The pressure is the limit of our equipment.

- [†] R=Ac=acetate group: 

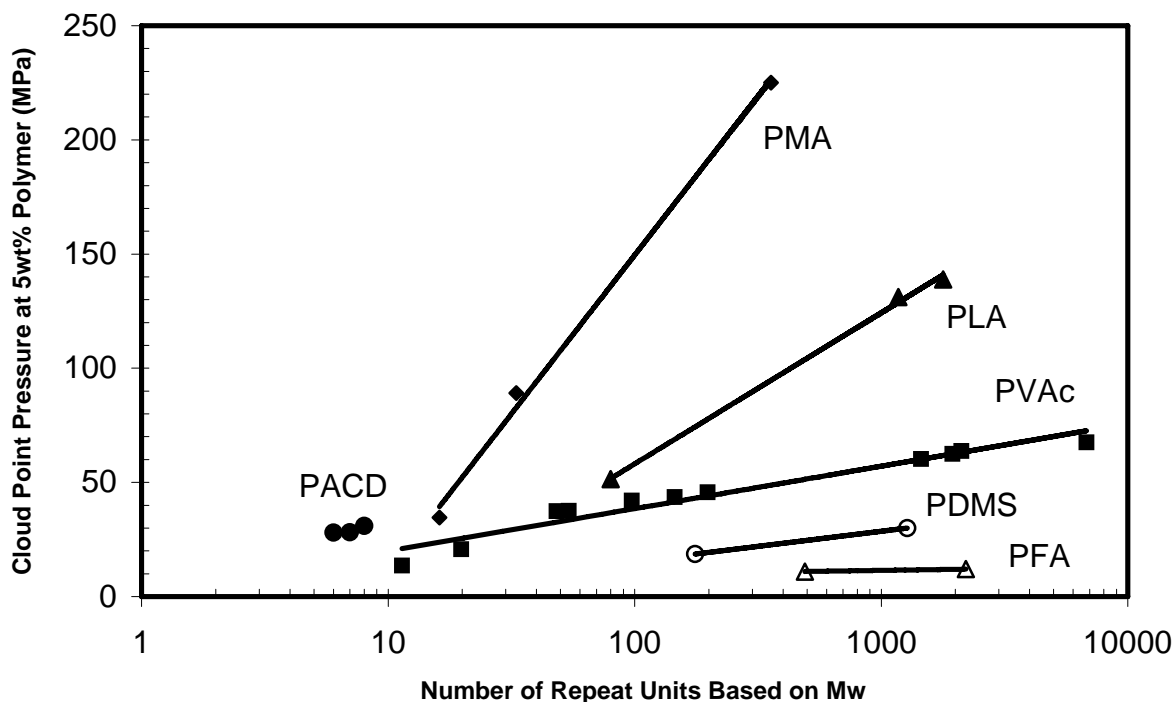


Figure 2.3 Cloud point pressures at ~5% polymer concentration and 298 K for binary mixtures of CO₂ with polymers as a function of number of repeat units based on Mw, where PFA, PDMS, PVAc, PLA, PMA and PACD represent poly(fluoroalkyl acrylate), poly(dimethyl siloxane), poly(vinyl acetate), poly(lactic acid), poly(methyl acrylate) and per-acetylated cyclodextrin, respectively. ^{119,123}

2.3.2 Empirical Heuristics of Designing Oxygenated Hydrocarbon-Based CO₂-Soluble Functional Groups

2.3.2.1 Characteristics for a “CO₂-phile”

Flexible chains and high free volume. Both flexible chains and high free volume enhance the entropy of mixing and, consequently, the solubility of compounds in CO₂. Elevating free volume and flexibility can, for example, be achieved through (e.g. tert-butylation) branching and use of ether linkages in the main chain. A flexible polyether backbone which has a low T_g is highly recommended for candidates of CO₂ soluble polymers. Branched AOT analogs terminated with a t-butyl group also exhibit 1-2 wt% solubility in CO₂ while AOT is essentially CO₂-insoluble.^{129,130} Tert-butyl compounds (e.g. TTBB and TTBP in Table 2.1) were observed highly CO₂-soluble. These results suggest that branching may increase the free volume of solute, weaken intermolecular interaction between polymer segments, and then favor the mixing of polymer and CO₂.

Multidentate interactions between CO₂ and solute functional groups. Both carbon and oxygen atom in carbon dioxide can interact with oxygen-containing functional groups with multidentate binding.

Weaker self-interactions O'Neill and colleagues found that more of CO₂-philes share a same characteristic, weak self-interaction.¹³¹ Our research confirmed that all aminated polymers were CO₂ insoluble despite expectations that the favorable interactions expected between CO₂ and amine groups would enhance solubility. Apparently, self-interactions between these amine groups predominated over CO₂-amine interactions. The molecular modeling calculation achieved by Dr. Johnson's group confirms this conclusion. Calculation on the base of MP2/6-

31+g(d), the interaction of amine+CO₂ and self-interactions between amines is -4.3 and -6.9 kcal/mol, respectively.

The presence of acetate groups. Per-acetylated monosaccharides and di-saccharides exhibited remarkable CO₂ solubility.^{118,119} Per-acetylated cyclodextrins composed of six, seven or eight saccharides were also very soluble in CO₂. Poly(vinyl acetate) remains the most CO₂ soluble oxygenated hydrocarbon polymer yet identified, as illustrated by the solubility of PVAc with a molecular weight of 585000 exhibiting >5wt% solubility in CO₂ at pressures of roughly 10,000 psi. (Silicone polymers functionalized with acetate groups also exhibited high CO₂ solubility relative to other side groups^{125,126}). Earlier *ab initio* calculations^{102,105} and Fourier transform IR spectroscopy¹⁰³ results indicated that the carbonyl was CO₂-philic, but the acetate seems to have a greater degree of CO₂-philicity than the carbonyl. However, the acetate group must be placed onto the polymer judiciously. For example poly(vinyl acetate) exhibits much higher CO₂-solubility than poly(methyl acrylate) although they are isomers.

Attention on ether group. Although ether-CO₂ interactions did not receive significant attention as much as carbonyl groups and CO₂ did, *ab initio* calculations suggest that ethers can interact at least as favorably with CO₂ as carbonyls through calculations based on Møller-Plesset second-order perturbation theory (MP2) because the interaction energy between CO₂ and ether oxygen is comparable with the interaction energy between CO₂ and carbonyl oxygen.¹²⁵ Furthermore, ether segment is “soft”, so that the flexibility is enhanced which favors the entropic dissolution. Therefore, a judicious application of both carbonyl and ether groups will be one of the keys for develop nonfluorous-CO₂ thickeners.

2.3.2.2 Factors Showing Negative Contributions to CO₂-Philicity

Allyl polymers are CO₂ insoluble. The inclusion of a -CH₂- spacer between the polymer backbone and the pendant group dramatically lowers CO₂ solubility. Although best illustrated by the dramatic loss of solubility induced by adding a methylene spacer to PVAc, yielding the CO₂-insoluble product poly(allyl acetate), the same phenomena has been noted for other polymers synthesized by our group. However, it is still a mystery for us why the methylene spacer significantly reduces the CO₂ solubility.

Acetylation alone does not ensure CO₂ solubility. High molecular weight cellulose triacetate (103,000 g/mol) neither dissolved, softened nor swelled in dense CO₂, even at 200 °C and 70 MPa, probably due to the crystalline nature of this polymer. Poly(methylene acetate), which contains an acetate on every carbon in the polymer backbone, had a very high melting point and was insoluble in CO₂, although it appeared to swell in CO₂. Surprisingly, sucrose octaacetate neither melts nor dissolves readily in CO₂ at 298 K and 1wt%, although similar acetylated disaccharides such as maltose octaacetate are extremely CO₂ soluble. These results suggest that a high degree of acetylation alone does not ensure CO₂ solubility. Steric hindrance and polymer crystallinity may inhibit the CO₂-acetate interactions; therefore the acetates must be accessible.

2.4 MODELING AIDED DESIGN ¹³²

Although the trial-and-error approach coupled with the set of empirical heuristics presented above has yielded some success, the fact is that the heuristics do not always work. Many

polymers have been predicted that “should” be highly CO₂ philic, according to the heuristics, but turn out to be relatively insoluble. So far polyvinyl acetate is the most CO-soluble oxygenated polymer. We also know that introduction of tert-butyl groups might enhance CO₂ solubility. However polyvinyl pivalate, a combination of polyvinyl acetate with a tert-butyl group (shown in Table 2.1), did not dissolve in CO₂ at 1 wt% under 298K and 68.9 MPa regardless of what molecular weight was. Molecular modeling offers an ability to look carefully into the energetics, structure and dynamics of CO₂-polymer phase behavior and to be able to ascertain precisely what makes a polymer CO₂-philic. From this information we will be able to suggest specific new polymer structures that should have higher solubility. This represents the first computation effort to design CO₂ philic functional groups. Synthesis and testing of the polymers will provide feedback to the modeling allowing an adjustment of the modeling techniques if necessary.

In principle, molecular modeling can be used to compute essentially all the thermodynamic properties of the polymer/CO₂ mixtures through statistical mechanical simulations. In practice, however, accurate thermodynamic properties depend critically on the accuracy of the molecular interaction models that must be used in the statistical mechanical simulations. An alternative is to use *ab initio* quantum mechanical methods to compute the zero-temperature interaction energies between CO₂ and functional moieties of the polymers of interest. This approach has the advantage of giving (in principle) highly accurate interaction energies for CO₂ and the functional groups of the polymers. Two obvious disadvantages are that the entire polymer cannot be modeled and that no finite temperature properties are calculable. It is difficult to compute accurate interaction energies for polymer/CO₂ systems because the interaction energies are very weak (compared with molecular bonds) and are dominated by electron correlation effects (van der Waals interactions). The Møller-Plesset (MP) perturbation

method for including electron correlation has been used for weakly interacting systems. MP2 (second-order Møller-Plesset perturbation theory) is the lowest order MP theory and is not generally adequate for computing intermolecular interaction energies, except when a substantial electrostatic interaction is involved. Methods that include triple excitations, e.g., fourth-order Møller-Plesset with single, double, triple, and quadruple excitations MP4 (SDTQ), or coupled cluster with perturbational triples, CCSD-(T), are required for many applications.

Although the interplay of solute-solute, solute-solvent, and solvent-solvent interactions should be completely considered when the dissolution behavior of polymers in CO₂ is being explored, we realize that the polymer-polymer interactions are also of great importance in determining the solubility of the polymer. However, the interaction energies between polymer segments cannot be computed at the same level of theory as the segment-CO₂ interactions because two polymer segments have too many atoms. If we use a lower level theory, such as Density Functional Theory (DFT), then the answers would be largely meaningless (DFT is basically more accurate for representing the system with strong interaction potentials such as molecular bonds. However, polymer and CO₂ systems we are interested in are dominated by van der Waals interactions which are weak interactions. Hence, high-level theories are required). To perform the calculation based on high-level theories, better computational algorithms and faster computers need to be developed. Therefore, we only calculated and estimated the binding energies between polymer segment and CO₂. Another inherent deficiency of *ab initio*-modeling-designing is that the model is not able to simulate the entropic changes of the mixture and to reflect a proper change of Gibbs free energy of mixing (shown as Equation 2-1). Consequently, the CO₂-philicities of designed polymers might not be as good as what they are predicted.

In this project, we perform MP2 modeling simulations to compute the interaction energies of CO₂ with various polymer moieties including the simplified repeat unit of polyvinyl acetate fragment, isopropyl acetate (IPA). Polyvinyl acetate will serve as a control against which all other candidate polymers will be compared because it is currently the most CO₂ soluble high molecular weight oxygenated hydrocarbon polymer. All this molecular modeling work was finished by Dr. Johnson's group.

2.5 PHASE BEHAVIOR MEASUREMENTS

Phase behavior study of CO₂ solutions plays a significant role in this project. First of all, as discussed above, phase behavior study provides the feed-back to the modeling design, finishing the design loop which is composed of proposing polymer structure with modeling computation, preparing the polymers from functional group modification or direct polymerization, and testing the solubility of the polymers in dense CO₂. Secondly, phase behavior study is used to identify the CO₂-philic functional groups and structures, and provides the fundamental data for applications such as extraction, particle formation, supercritical micelles, and reaction. Bubble-point, dew-point, and liquid-liquid loci were determined using a non-sampling technique involving isothermal compression and expansion of binary mixtures of known overall composition. This method is also known as the synthetic method and is described in detail elsewhere.^{113,123,133} A schematic experimental layout is presented in Figure 2.4 and a short summary of the procedure is described below.

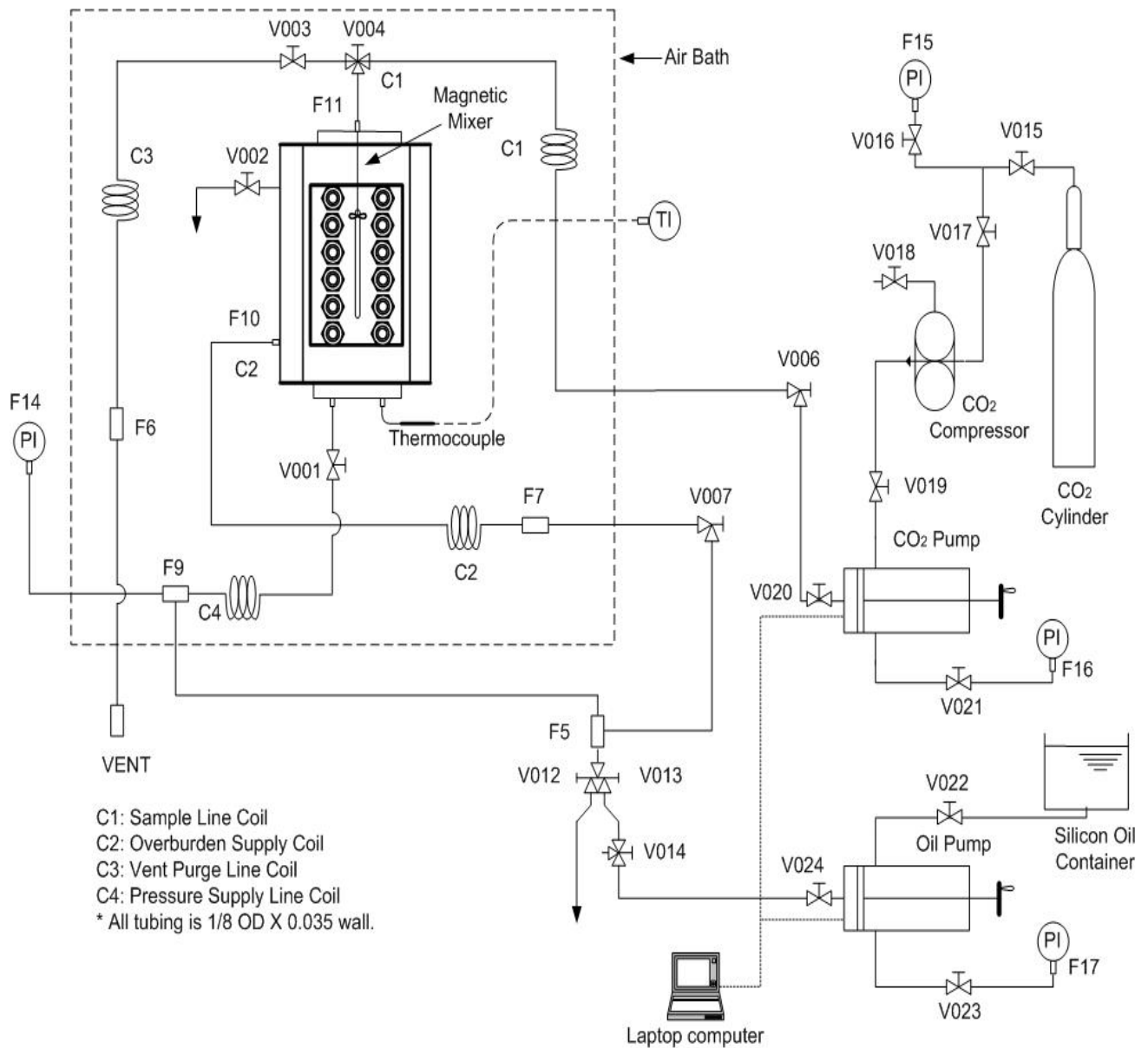


Figure 2.4 Schematic of experimental apparatus for phase behavior study with a high pressure, variable volume, windowed cell (D.B. Robinson Cell)

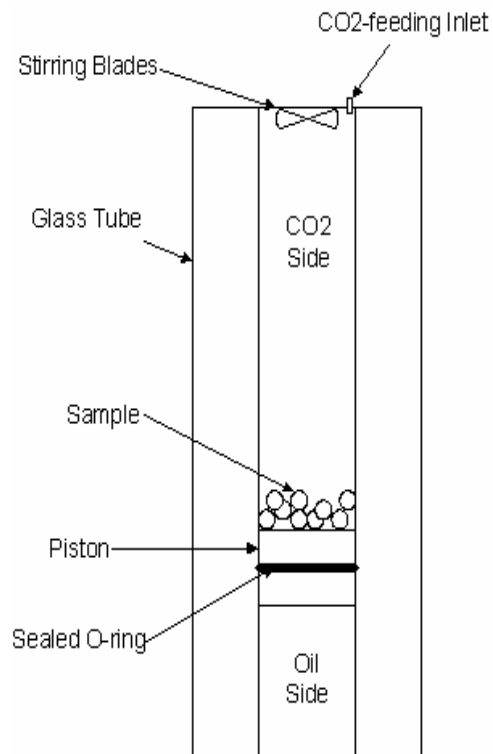


Figure 2.5 Detailed drawing of a high pressure, windowed, stirred, variable-volume view cell

In a typical experiment, a specified amount of the sample (e.g., 2.0000 ± 0.0001 g) was introduced to the sample volume of a high pressure, windowed, stirred, variable-volume view cell (DB Robinson & Assoc., 3.18 cm i.d., ~ 120 cm³ working volume, shown in Figure 2.5). In this cell, the sample volume is separated from the overburden fluid by a steel cylinder (floating piston) that retains an O-ring around its perimeter. The O-ring permits the cylinder to move while retaining a seal between the sample volume and the overburden fluid. After purging with carbon dioxide at 0.2MPa, the sample volume was minimized by displacing the floating piston to the highest possible position within the cell that did not result in the compaction of the sugar

acetate particles. High pressure liquid carbon dioxide (295 K, 13.78MPa) was then introduced to the sample volume as the silicone oil overburden fluid was withdrawn at the equivalent flow rate using a dual-proportioning positive displacement pump (DB Robinson). This technique facilitated the isothermal, isobaric addition of a known volume of CO₂ (e.g., 20.44±0.01 cm³) into the sample volume. The mass of CO₂ introduced was determined from the displaced volume, temperature, and pressure using an accurate equation of state for carbon dioxide.¹³⁴ Based on the uncertainties associated with the measurement of temperature, pressure, and volume, and the precision of the equation of state, compositions were estimated to be accurate to within 1% of the specified value (e.g. 0.10±0.001 wt fraction).

The sample and CO₂ mixture was then compressed to 62MPa. At these elevated-pressure conditions, either a single, transparent liquid phase or solid–liquid equilibrium was observed. The sample volume was then slowly expanded, and observations of two-phase or three-phase equilibrium were recorded. Bubble points were characterized by the coexistence of a minute amount of vapor phase in equilibrium with the liquid phase. Dew and liquid–liquid cloud points were designated as the pressure at which it was no longer possible to see through the solution; after maintaining the sample volume under quiescent conditions for 30 min, several drops of liquid would slowly accumulate at the bottom of the sample volume. Three-phase pressures were characterized either by vapor–liquid–liquid or vapor–liquid–solid equilibrium. Pressure was measured with a Heise pressure gauge accurate to within ±0.07 MPa for measurements up to 70 MPa. Temperatures were measured with a type K thermocouple to an accuracy of ±0.2K that was calibrated against ice water and boiling water. The pressures for two-phase boundaries were measured three times, with a reproducibility of ±0.2 MPa. Three-phase pressures were also recorded three times, with a reproducibility of ±0.1 MPa.

2.6 VISCOSITY MEASUREMENT

The viscosities of single-phase thickener- CO₂ solutions were determined with a falling cylinder viscometer.^{87,92,97,135,136} The technique was selected because of its simplicity in monitoring large viscosity increases in high-pressure fluids as evidenced by reductions in the terminal velocity of a falling object. The viscosity measurements were conducted in the same apparatus used for the phase behavior determinations, illustrated in Figure 2.4 and Figure 2.5.

In a typical viscosity measurement, an aluminum cylinder was introduced to the quartz tube prior to the addition of the sample and carbon dioxide. The outer diameter of the cylinder is slightly less than the inside diameter of the quartz tube. After a single and transparent phase was yield at the given pressure, the entire cell was then rapidly inverted (Figure 2.6), causing the aluminum cylinder to fall through the neat or thickened carbon dioxide. The time required for the cylinder to fall a specified distance with a steady velocity was then recorded and the terminal velocity of the cylinder in the fluid was calculated. Each measurement was repeated at least six times.

The governing equation for the viscometer, shown as Equation 2-4, relates the fluid viscosity μ , to the product of the calibration constant, K , and the density difference between the aluminum cylinder and the fluid ($\rho_c - \rho_f$), divided by the terminal velocity of the cylinder, u_c .

$$\mu = \frac{K(\rho_s - \rho_f)}{u_c}$$

Equation 2-4

Although Equation 2-4 is only valid for Newtonian fluids, it can also be used for estimating the viscosity of non-Newtonian fluids provided that the shear rate is low and shear dependence of the viscosity is not considered. The other assumptions include: (a) changes in the solution density relative to that of neat CO₂ is small relative to the density difference between aluminum falling cylinder and carbon dioxide; (b) the cylinder has a uniform diameter and falls coaxially through the quartz tube; (c) no turbulence is present. By solving the combination of Navier-Stokes equation and a mass balance, the calibration constant K can be theoretically determined from the viscometer geometry using Equation 2-5.

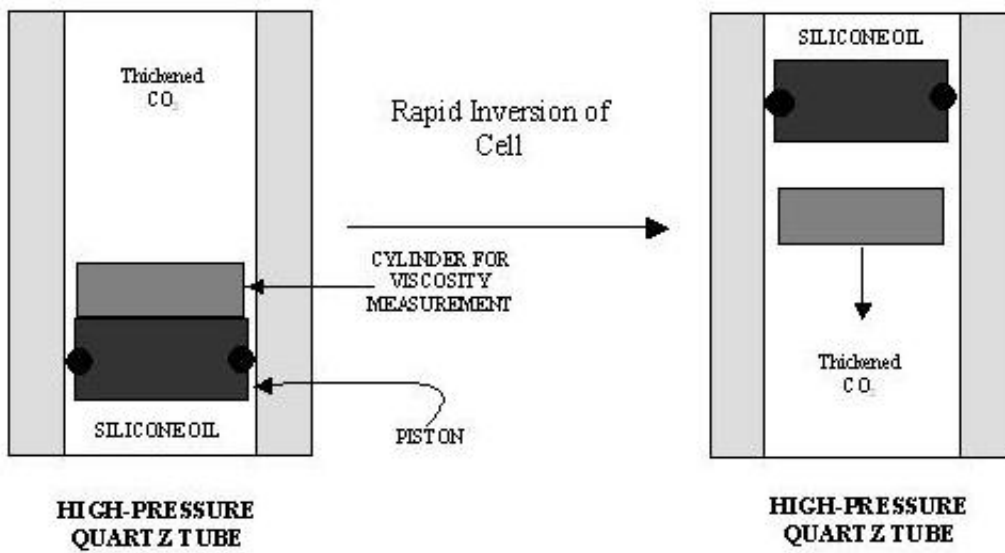


Figure 2.6 Schematic diagram for a falling cylinder viscometer

$$K = \frac{r_c g}{\frac{-4r_c}{\ln\left(\frac{r_c}{r_t}\right)(r_t^2 + r_c^2) + (r_t^2 - r_c^2)} - 2 \left[\frac{-2r_c - (r_t^2 - r_c^2) \frac{1}{r_c \ln\left(\frac{r_c}{r_t}\right)}}{\ln\left(\frac{r_c}{r_t}\right)(r_t^2 + r_c^2) + (r_t^2 - r_c^2)} + \frac{1}{r_c \ln\left(\frac{r_c}{r_t}\right)} \right]}$$

Equation 2-5

Where r_c and r_t represents the radius of aluminum cylinder and inside radius of the tube, respectively, and g is the acceleration of gravity.¹³⁵ The inner diameter of the quartz tube is 1.250 inch. The calibration constants for the two falling cylinders with outer diameter 1.228 inch and 1.244 inch were $2.54 \times 10^{-9} \text{ m}^3/\text{s}^2$ and $7.20 \times 10^{-11} \text{ m}^3/\text{s}^2$, respectively.

The solution relative viscosity is defined as the ratio of solution viscosity to neat carbon dioxide viscosity. With the assumption that the change in density of the fluid could be ignored upon the addition of thickener, it is clear that the relative viscosity is inversely equal to the ratio of terminal velocities from Equation 2-4. The relationship is indicated in Equation 2-6:

$$\frac{\mu_{\text{solution}}}{\mu_{\text{CO}_2}} = \frac{u_{c,\text{CO}_2}}{u_{c,\text{solution}}} = \frac{t_{\text{solution}}}{t_{\text{CO}_2}}$$

Equation 2-6

Where t_{solution} and t_{CO_2} are falling times of the cylinder across a fixed distance in the solution and neat CO_2 , respectively.

2.7 SYNTHESIS CHARACTERIZATIONS

Chemical characterization of the synthesis products was accomplished via a Bruker 300 MHz NMR spectrometer. The molar mass of compounds were obtained by either a matrix assisted laser desorption ionization (MALDI) time of flight (TOF) mass spectrometer or a quadrupole field ion trap mass spectrometer with electrospray ionization (ESI). Fourier transform infrared (FTIR) spectra were obtained at room temperature using a Nicolet FTIR spectrometer. Differential scanning calorimetry (DSC) was performed in a Thermal Analyst 2000 (TA Instruments) DSC 2910 differential scanning calorimeter. Scanning rates of 20°C/min were used over a temperature range of -130 to 250 °C. The glass transition temperature (T_g) on the basis of the total polymer weight was analyzed with software supplied with the DSC 2910 differential scanning calorimeter.

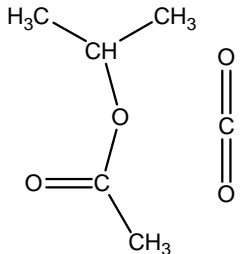
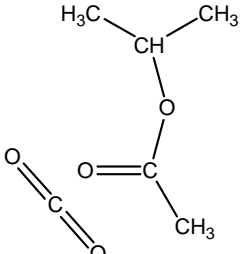
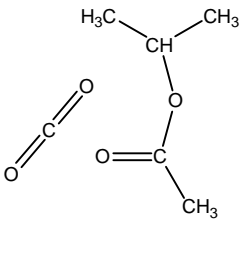
3.0 POLYMERS DESIGNED BY MODELING COMPUTATION

3.1 POLY(VINYL ACETATE)

Poly(vinyl acetate)s (PVAc) have been identified as the most CO₂-philic, high molecular weight, polymer composed solely of C, H, and O. Three possible binding configurations for poly(vinyl acetate) fragments, isopropyl acetate (IPA), were determined by the molecular modeling. The specific binding energies and configurations are illustrated in Table 3.1. The average binding energy is -14.9 KJ/mol. In every case, the CO₂ molecule always migrates around the molecule to bind with the carbonyl or ester oxygen of the IPA molecule. Specific interactions between carbonyl groups and CO₂ have received significant attention in the literature, from both experimental and theoretical perspectives. Ether oxygen and CO₂ interactions, by contrast, have received less attention, perhaps because of the perception that such interaction is too weak to make much of an impact on the thermodynamics of mixing. The modeling computations, however, strongly suggest that ethers will interact at least as favorably with CO₂ as carbonyls. Moreover, ether groups usually add less to the cohesive energy density of a material, probably proving to be far more important than carbonyls in the design of CO₂-philic functional groups if judiciously employed.¹³⁷

Many attempts have been achieved to understand the high CO₂ solubility of PVAc by comparing the difference between PVAc and its analogues. Within all the studies, it is well

Table 3.1 Binding configurations and energies for IPA/ CO₂¹³⁷

Binding Configurations of IPA + CO ₂	Interaction Energies ΔE (KJ/mol)
	-14.7
CO ₂ interacting with ether oxygen	
	-14.2
CO ₂ binding with carbonyl oxygen, tilting toward to the methyl group	
	-15.9
CO ₂ binds with the carbonyl oxygen, tilting toward the ester group side	

noted that PVAc and poly(methyl acrylate) (PMA) exhibit very different CO₂ solubility although they are isomers (See Figure 2.3). Kazarian et al. suggested that high flexibility of the ether group between the carbonyl group and the backbone makes CO₂ easier accessing to the carbonyl group in PVAc, resulting easier in formation of interaction between CO₂ and PVAs¹⁰³. Poly(vinyl methyl ether) (PVME) and poly(vinyl ethyl ether) (PVEE) showed CO₂ solubility under our equipment limit, which are yet lower than that of PVAc.¹³⁸ Suggested by the molecular modeling, the higher solubility of PVAc may be attributed to the fact that the acetate group has more binding modes available for CO₂ than the isolated ether group. PVAc has three binding modes per repeat unit while PVME and PVEE only have one binding mode with CO₂. Therefore, the total interaction energy of PVAc/CO₂ surpasses those of PVME/CO₂ and PVEE/CO₂.¹³⁹ Interestingly, poly(allyl acetate) did not exhibit solubility in CO₂ at the condition of 68.9 MPa, 298 K and 1 wt%. Wang calculated the average interaction energy between the repeat unit of poly(allyl acetate), isobutyl acetate (IBA), and CO₂ is -14.5 kJ/mol while the average interaction energy between the repeat unit of poly(vinyl acetate), isopropyl acetate (IPA), and CO₂ is -14.9 kJ/mol. The difference in the average interaction energies is smaller than the expected accuracy of the calculations and is not substantially enough to fully explain the distinct differences in solubilities.¹³⁷ Further study, probably not by the *ab initio* modeling, must be done to uncover the mystery of the methylene spacer.

3.2 POLY(3-ACETOXY OXETANE)

3.2.1 Modeling Design

If the designed polymers would have multiple binding sites with neighboring CO₂ molecules, we could obtain higher binding energies. Oxygen atoms will be placed judiciously on the polymer backbones and side chains in order to produce as many as multiple binding sites for CO₂ with the novel oxygenated hydrocarbon polymer. We have performed a series of calculations on different candidate repeat unit in an attempt to use molecular modeling to guide the design of the polymers. We have identified methoxy-isopropyl acetate as a promising candidate for a highly CO₂ soluble polymer precursor. Methoxy-isopropyl is a representative fragment of a novel polymer, poly(3-acetoxy oxetane), PAO, that has never been reported in the literature, shown in Figure 3.1.

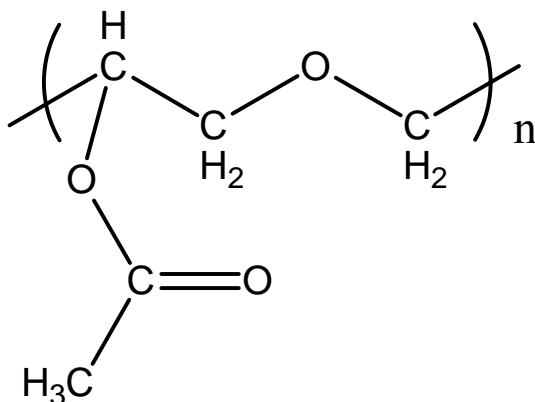


Figure 3.1 Structure of poly(3-acetoxy oxetane), PAO

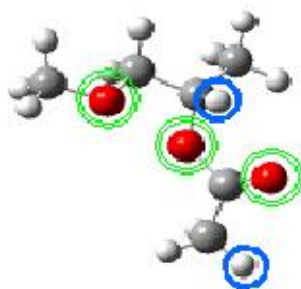


Figure 3.2 Three dimensional view of methoxy-isopropyl acetate, MIA

Shown in Figure 3.2, the oxygen atoms (larger double circles) are all potential Lewis base sites available for interactions with CO_2 . The two hydrogen atoms (smaller solid circles) are potential Lewis acids for interacting with oxygens of CO_2 because the modeling calculations demonstrate that the hydrogens are especially acidic. The binding geometries and energies for CO_2 interacting with methoxy isopropyl acetate have been computed and five optimized binding configurations were identified. Three of these binding geometries have quadridentate binding with CO_2 as shown in Figure 3.3. The binding energies for the three configurations A, B, and C are -22.5 , -23.6 , and -21.9 KJ/mol, respectively, and the average binding energy for all five configurations is -19.7 KJ/mol. Comparing with the binding energies between IPA and CO_2 , the polymer analogue of methoxy isopropyl acetate, which is poly(3-acetoxy oxetane), should have a higher solubility and a lower cloud point pressure than poly(vinyl acetate).

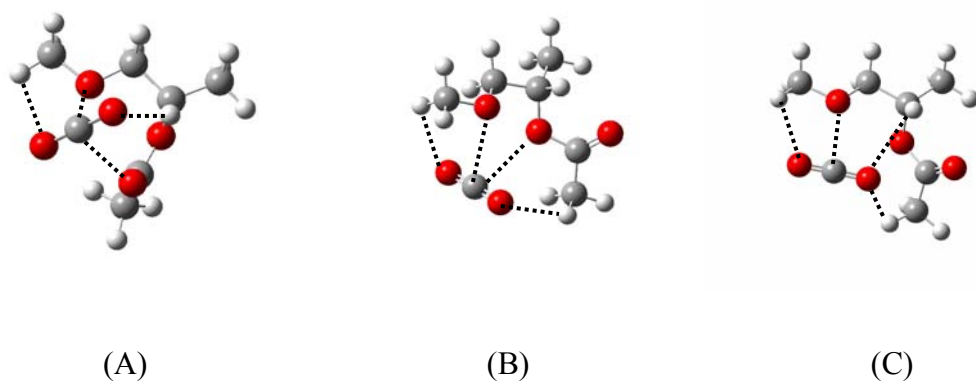


Figure 3.3 Three multiple binding geometry of CO₂ with methoxy isopropyl acetate

3.2.2 Preparation

3.2.2.1 Materials

Boron trifluoride diethyl etherate, imidazole, chlorotrimethylsilane, triisobutylaluminum solution (1M), acetic anhydride, and ferric(III) chloride was purchased from Aldrich. Dichloromethane, ethyl acetate, and toluene were obtained from EMD Chemicals Inc. Sodium bicarbonate and magnesium sulfate powders were obtained from J.T. Baker. Dichloromethane, ethyl acetate, and toluene were distilled and the other chemicals were used as received.

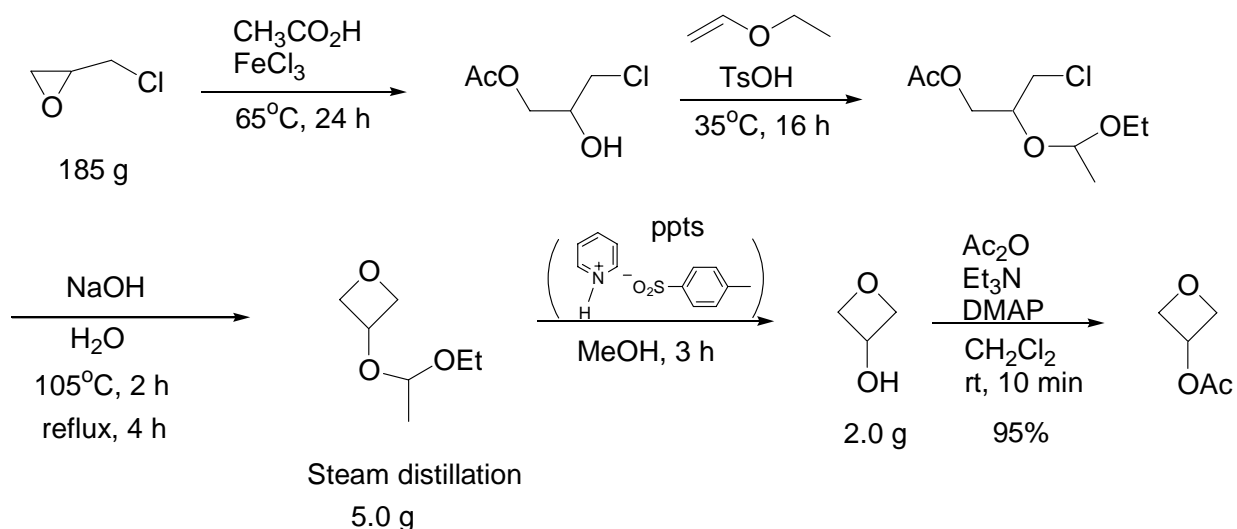


Figure 3.4 Synthesis scheme for monomer 3-acetoxyoxetane^{140,141}

The monomer was synthesized by Dr. Hamilton's group after five-step synthesis (Figure 3.4). ¹H-NMR spectrum of the 3-acetoxyoxetane is given in Figure A. 1 in Appendix. ¹H-NMR (300MHz, CDCl₃), δ_H: 2.11 (s, 3H), 4.65 (t, J=7.0, 2H), 4.89 (t, J=7.0, 2H), 5.47 (m, 1H).

3.2.2.2 Synthesis Procedure

Polymerization I^{140,142} In a typical experiment, prepare a solution of 3-acetoxyoxetane in dichloromethane, 1M, at -30 °C in a 100mL three way round bottomed flask. Stir the solution and keep the solution under non-flowing nitrogen. Add Boron trifluoride diethyl etherate at 0.5 equiv dropwise by syringe while stirring. In a few minutes, the mixture turned to be a thick gel. Slowly add 4mL of saturated aqueous solution of NaHCO₃ into the reaction solution. After shaking the liquid-liquid extraction glassware, let the phases segregate. Two phases formed, an aqueous phase on the top and the dichloromethane phase on the bottom. The synthesis scheme is shown in Figure 3.5.

Separate the organic phase from the aqueous phase. Most of the polymer product should stay in the organic solvent phase. After drying over 4 grams of MgSO₄ with gentle swirling for about 10 minutes, then remove dichloromethane via evaporation and let it dry for half an hour under high vacuum. Recover and characterize the polymer which was given thick oil. The ¹H-NMR and MALDI spectra are showed in Figure A. 2 and Figure A. 3. ¹H-NMR (300MHz, CDCl₃), δ_H: 2.11 (s, -CH₃), 3.56-4.34 (m, -CH₂CHCH₂O-). The molecular weight was given by MALDI is 800 g/mol.

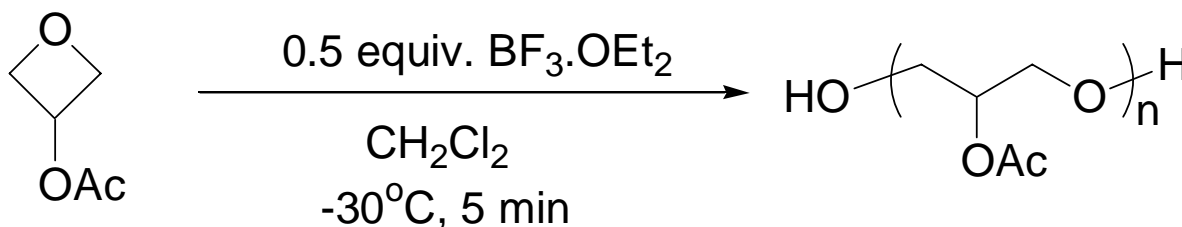


Figure 3.5 Synthesis scheme for poly(3-acetoxy oxetane) (PAO, Polymerization II)

*Polymerization II*¹⁴³ In a 25 mL round bottomed flask equipped with a magnetic stirring bar, 5.0 mL of 1.0 M solution of triisobutylaluminum (*i*-Bu₃Al) solution in hexanes was cooled to 0 °C in an ice bath, and water (0.063 mL, 0.7 equiv) was added dropwise over 15 min under stirring. After stirring 1 hr at 0 °C, the temperature was allowed to rise to room temperature, and stirring was continued overnight. *i*-Bu₃Al·0.7·H₂O was obtained and used as catalyst for the following polymerization. The catalyst was a clear, colorless solution and was stored at room temperature under vacuum.¹⁴⁴

To a solution of 1.0 g of 3-hydroxyoxetane in 17 mL of dichloromethane were added imidazole (1.44 g, 1.5 equiv.) and chlorotrimethylsilane (2.13 mL, 1.2 equiv.) at 0 °C. The

mixture was stirred at 0 °C for 3 h. White precipitate was separated by filtration and the volume of filtrate was reduced to a quarter by evaporation. 3- trimethylsilyloxy-oxetane was obtained by careful distillation using aspirator (Figure 3.6).

In a 100 mL flask equipped with a stirring bar, a solution of 3- trimethylsilyloxy-oxetane (6.3 g, 43.2 mmol) in 40 mL of anhydrous toluene was prepared at -78 °C in a dry ice bath. Air was removal by oil vacuum pump and the reaction conduct under nitrogen environment. *i*-Bu₃Al-0.7 H₂O (3.0 mL, 7 mol%) was added dropwise to the solution. The reaction mixture was kept in a -78 °C freezer for 32 hours. Additional 7 mol% of catalyst was added at -78 °C and stirring was continued for 2 h at the same temperature. The reaction mixture was kept in the freezer for additional 48 hours with stirring. The reaction solution was then allowed to increase temperature to 0 °C in an ice bath. To the solution was added 15 mL of acetic anhydride and ferric (III) chloride (420 mg, 15 mol%). After stirring for 1 h at 0 °C, 30 mL of saturated NaHCO₃ solution was slowly added to the solution. The mixture was stirred for 20 min at room temperature and was extracted with ethyl acetate three times (50 mL×3). The combined organic layer was dried over MgSO₄ and concentrated under reduced pressure. 1.0 g poly(3-acetoxyoxetane), showing as sticky oil, was obtained (Figure 3.6). The ¹H-NMR and MALDI spectra are showed in Figure A. 4 and Figure A. 5. ¹H-NMR (300MHz, CDCl₃), δ_H: 2.13 (s, -CH₃), 3.59-4.17 (br m, -CH₂CHCH₂O-). The molecular weight was given by MALDI is 940 g/mol.

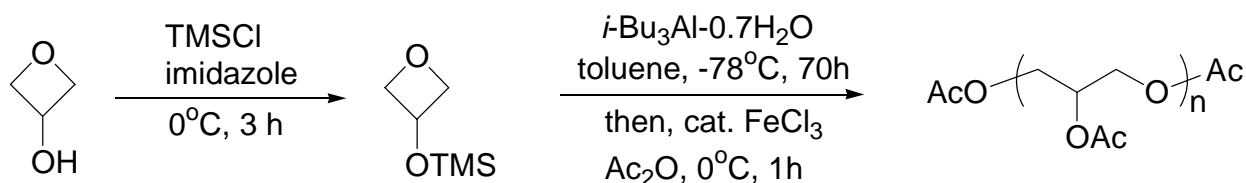


Figure 3.6 Synthesis scheme for poly(3-acetoxy oxetane) (PAO, Polymerization II)

3.2.3 Phase Behavior Study

The two polymers showed comparable cloud pressures (shown in Figure 3.7). The pressure difference probably is attributed to the PDI and impurity. Comparing the solubility with the poly(vinyl acetate) with same chain length, PAO showed higher cloud point pressure than poly(vinyl acetate), which is not agreement with the modeling prediction. Although it is possible that some important variables were not being counted in the modeling prediction, it is believed that the elevation of cloud point pressure is a result of high concentration of CO₂-phobic hydroxyl end groups of PAO with low molecular weights.¹³¹ We need to develop new polymerization technique to make high molecular weight PAO which could diminish the negative effect of hydroxyl group; but multiple attempts to attain high MW PAO have failed.

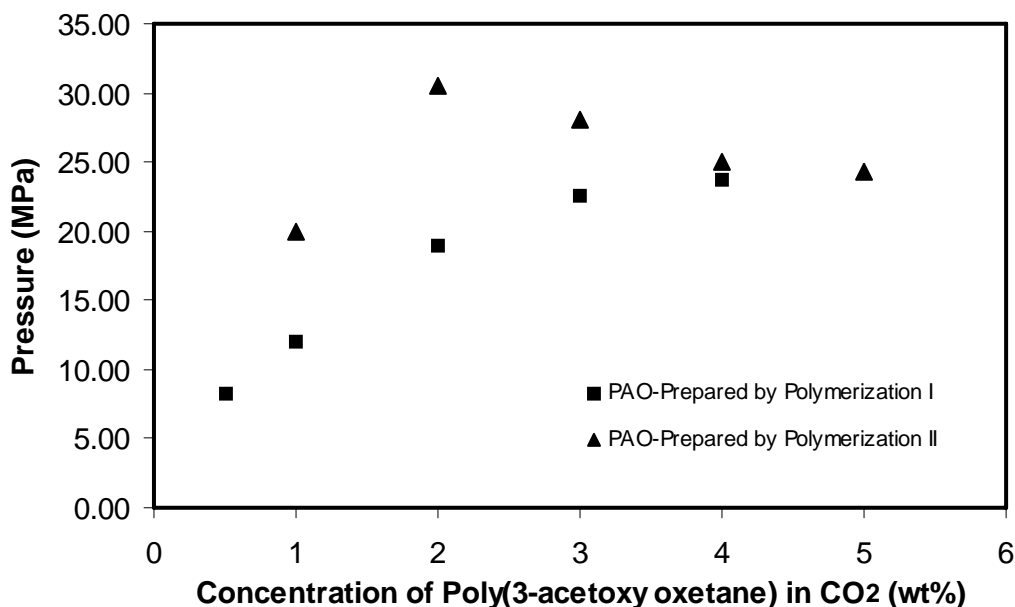


Figure 3.7 Pressure-composition diagram for CO₂ + poly(3-acetoxy oxetane) system at 298 K

3.3 POLY(VINYL ETHER)S WITH ACETAL GROUPS

3.3.1 Modeling Design

The other CO₂-philic polymer proposed by molecular modeling is poly(vinyl methoxymethyl ether) (PVMME), shown in Figure 3.8. Two optimized binding geometries of CO₂ with PVMME fragment representative, acetal, are identified by the modeling computation, illustrated in Figure 3.9, in which the binding energies are -20.2 and -22.6 KJ/mol for geometry A and B, respectively. The binding energies are approximately 5 KJ/more larger than IPA and CO₂ pairs.

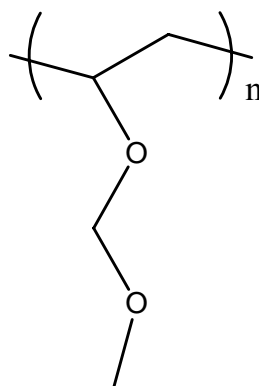


Figure 3.8 Structure of poly(vinyl methoxymethyl ether) (PVMME)

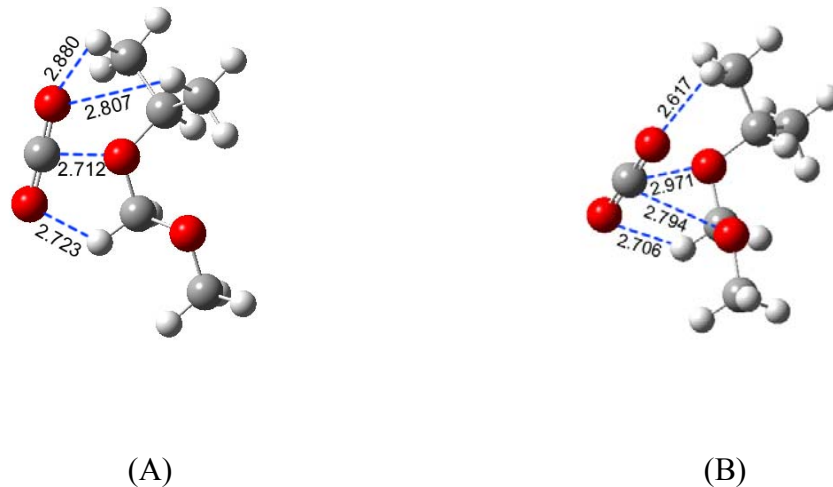


Figure 3.9 Optimized binding geometry of CO₂ with acetal group

3.3.2 Preparation

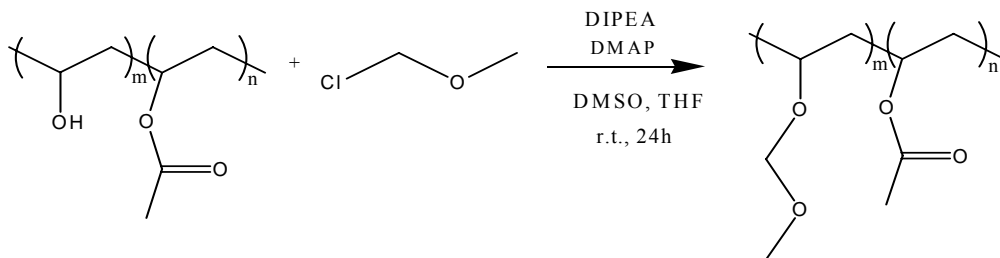
3.3.2.1 Materials

N,N-diisopropylethylamine, 4-(dimethylamino)pyridine, chloromethyl methyl ether, acetaldehyde, anhydrous methanol, anhydrous dimethyl sulphoxide (DMSO), and anhydrous tetrahydrofuran (THF) were purchased from Aldrich. Poly(vinyl alcohol) (Mw=2000, 78% hydrolyzed) was obtained from Scientific Polymer Products, Inc. Dialysis membrane tubing (Spectra/Por® BiotechRegenerated Cellulose, Molecular Weight Cutoff (MWCO): 1000 Daltons) was purchased from Spectrum Laboratories Inc. Acetaldehyde was distilled before use. Hydrogen chloride (99.995%) was obtained from Penn Oxygen.

3.3.2.2 Synthesis Procedure

*Poly(vinyl methoxymethyl ether)*¹⁴⁵ A 100 mL, three necked, round-bottomed flask was equipped with a magnetic stirring bar. The flask was charged with 25 mL DMSO and PVA (0.7 g, 10mmol in –OH). The mixture was heated to 90 °C. A clear solution was obtained. After the solution spontaneously cool down to room temperature, 4-(dimethylamino)pyridine (12.5mg, 0.1mmol), N,N-diisopropylethylamine (5.23mL, 30 mmol), and THF (10 mL) were added into the solution. Capped the flask with rubber stopper and vacuum the flask three times. The flask was equipped with a thermometer and then was conditioned with nitrogen. The flask was transferred to an ice-water bath. After the solution was cooled down to 0 °C, Methyl methoxymethyl chloride (3.8 mL, 50 mmol) was then added dropwise via syringe. The reaction mixture was then warmed to room temperature and stirred for 24 h (Figure 3.10).

I. Preparation of poly(vinyl methoxymethyl ether) (PVMME)



II. Preparation of poly(vinyl 1-methoxyethyl ether) (PVMEE)

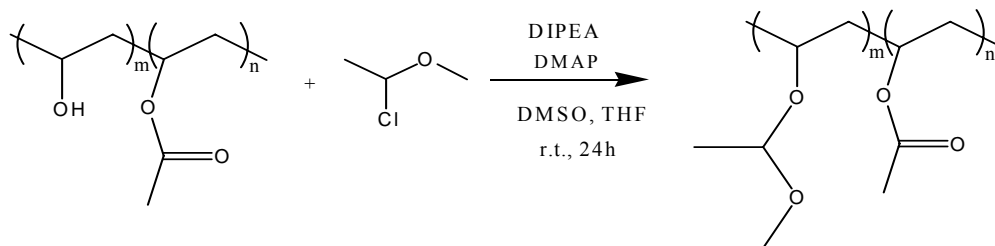


Figure 3.10 Synthesis scheme for poly(vinyl methoxymethyl ether) and poly(vinyl 1-methoxyethyl ether)

The reaction mixture turned to be brown solution after reaction. Transfer the solution to the dialysis membrane tubing and dialyzed against deionized water (1000 mL) for 24 h. Water was changed every eight hours. A light yellow sticky material was obtained in the tubing. After separate the polymer from water with a centrifuge (3000 rpm) for 20 min, pour out the water on the top. Wash the centrifuge tube with ethyl acetate. Collect all the liquid and separate the organic phase from aqueous phase with a separatory funnel (50 mL). The organic solvent was removed by a rotary evaporator under reduced pressure, yielding a yellow and very viscous material.

*1-chloroethyl methyl ether*¹⁴⁶ A 25 mL, three necked, round-bottomed flask equipped with a magnetic stirring bar was placed in an ice-water bath. The flask was charged methanol (3.2 g, 0.1 mol) and acetaldehyde (4.4 g, 0.1 mol) and capped by rubber stoppers. The solution was bubbled by gaseous HCl for 2 h. Two phases were obtained and the top phase was obtained by a separatory funnel. 1-chloroethyl methyl ether was used directly in the next step without further purification. ¹H-NMR (300MHz, CDCl₃), δ_H: 1.79 (d, J=5.4, 3H), 3.52 (s, 3H), 5.63 (q, J=5.4, 1H) (Figure A. 6).

Poly(vinyl 1-methoxyethyl ether) The synthesis procedure was same as poly(methoxy methyl vinyl ether) described above. Methyl methoxymethyl chloride was replaced by 1-chloroethyl methyl ether. The synthesis schemes were showed in Figure 3.10.

3.3.2.3 Characterization of Products

According to the molecular weight and proportion of hydrolysis, PVA (Mw=2000 g/mol) has 30 alcohol repeat units and 9 vinyl acetate units (m=30 and n=9 in Figure 3.10). ¹H-NMR spectra of PVA, PVMME and PVMEE are given in Figure A. 7, Figure A. 8, and Figure A. 9. PVA (Figure

A. 7): $^1\text{H-NMR}$ (300MHz, CDCl_3), δ_{H} : 1.34-1.59 (br m, $39 \times 2\text{H}$, $-\text{CH}_2-$), 1.93 (br s, $9 \times 3\text{H}$, $\text{CH}_3\text{COO}-$), 3.81 (br, $30 \times 1\text{H}$, $-\text{CH}(\text{OH})-$), 4.66 (br, $9 \times 1\text{H}$, $-\text{CH}(\text{COOCH}_3)-$); PVMME (Figure A. 8): $^1\text{H-NMR}$ (300MHz, CDCl_3), δ_{H} : 1.61-1.74 (br, $39 \times 2\text{H}$, $-\text{CH}_2-$), 1.93 (br, $9 \times 3\text{H}$, $\text{CH}_3\text{COO}-$), 3.26 (s, $30 \times 3\text{H}$, $\text{CH}_3\text{O}-$), 3.67 (br, $30 \times 1\text{H}$, $-\text{CHO}-$), 4.56 (br, $9 \times 1\text{H} + 30 \times 2\text{H}$, $-\text{CH}(\text{COOCH}_3)-$ and $-\text{OCH}_2\text{O}-$); PVMEE (Figure A. 9): $^1\text{H-NMR}$ (300MHz, CDCl_3), δ_{H} : 1.15 (s, $30 \times 3\text{H}$, $\text{CH}_3\text{CHOO}-$), 1.54-1.58 (br, $39 \times 2\text{H}$, $-\text{CH}_2-$), 1.94 (br, $9 \times 3\text{H}$, $\text{CH}_3\text{COO}-$), 3.19 (s, $30 \times 3\text{H}$, $\text{CH}_3\text{O}-$), 3.65 (br, $30 \times 1\text{H}$, $-\text{CHO}-$), 4.61 (br, $9 \times 1\text{H} + 30 \times 1\text{H}$, $-\text{CH}(\text{COOCH}_3)-$ and $-\text{OCH}(\text{CH}_3)\text{O}-$). Comparing the integral area between the methyl groups at the ether ends and the ester ends, the hydroxyl groups are completely protected for both PVMME and PVMEE. IR spectrum (Figure A. 10) confirms the conclusion. The peak at 1735 is the unreacted carbonyl group in ester in the unhydrolyzed poly(vinyl acetate). The responses of hydroxyl groups for PVMME and PVMEE are remarkably weaker than that of PVA. Therefore, the molecular weights of PVMME and PVMEE were obtained by calculation, 3400 and 3800 g/mol, respectively. DSC results (Figure A. 11, Figure A. 12, and Figure A. 13) are collected in Table 3.2.

Table 3.2 T_g of PVA, PVMME, and PVMEE

	PVA	PVMME	PVMEE
T_g ($^{\circ}\text{C}$)	61.97	-16.74	-1.20

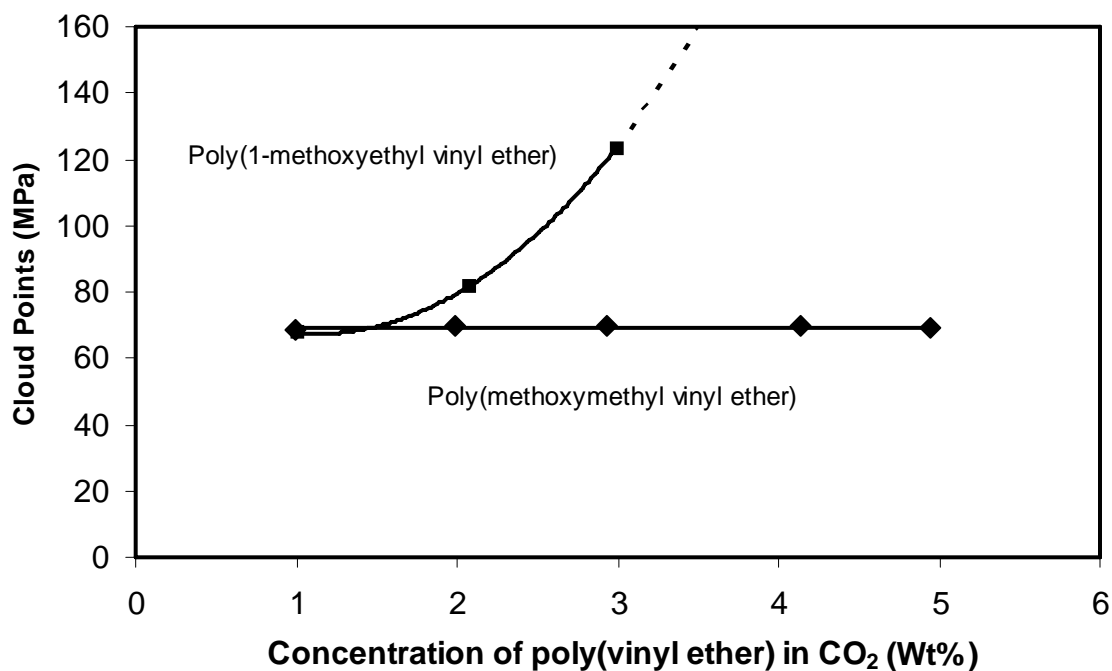


Figure 3.11 Pressure-composition diagram for CO₂ + poly(vinyl ether) systems at 298 K

3.3.3 Phase Behavior Study

It is hypothesized that increasing polymer free volume contributes a positive effects in determining the location of phase boundary via enhanced entropy of mixing.¹⁴⁷ PVMEE was anticipated to be more CO₂ soluble than PVMME did because PVMEE differs from PVMME by one extra methyl group in the side chain, resulting in a higher free volume. Surprisingly, the experimental results showed a reverse trend to the expectation that PVMME showed remarkably higher CO₂-philicity than PVMEE (Figure 3.11). The dissolution process is entropically favorable at low concentration. The two poly(vinyl ether)s have same number of repeat unit because both were synthesized from same poly(vinyl alcohol). Therefore, the two polymers exhibited comparable cloud point pressures at 1 wt%. With the increase of concentration, the

dissolution turns into being enthalpically favorable. The methyl group on the side chain might block the approaching of CO₂ to the carbonyl oxygen in PVMEE side chain. As a result, the cloud point pressures of PVMEE dramatically increase with the increase of concentration.

Concerning the contributions from entropy of mixing, a CO₂-philic polymer should have high free volume and high chain flexibility, which are evidenced by a low T_g. Theoretically, the glass transition temperature is lowered with increasing the ease of rotational motions of the side chains.¹⁴⁸ Although it is hypothesized that PVMEE would have a higher free volume than PVMME has, the extra methyl group on the side chain in PVMEE reduces the side chain mobility. As evidence, T_g of PVMEE is approximately 15 °C higher than that of PVMME, resulting in a higher T_g. Therefore, PVMME demonstrate higher CO₂-philicity than PVMEE.

3.4 CONCLUSIONS

PAO and PVMME were proposed as CO₂-soluble polymers based on the molecular modeling calculations. At the condition of 298 K and ~5 wt%, the cloud point pressures of PVMME (69 MPa) and PAO (24 MPa) are approximately 30 MPa and 11 MPa, respectively, higher than those of PVAc with same chain length (Figure 2.3). However, it is necessary to point out that although PVMME and PVMEE are not as CO₂ soluble as PVAc, they indeed showed considerable solubility in CO₂.

4.0 PERACEYLATED CELLULOSE TRIACETATE OLIGOMERS

4.1 LITERATURE REVIEW

Many biologically derived materials are highly polar and thus exhibit very low solubility in liquid and supercritical CO₂. Recently, Raveendran and Wallen suggested that acetylation of polyhydroxyl systems such as carbohydrates may be used as an excellent method for making these systems highly CO₂-philic^{105,112}. Guided by these principles, they studied the solubility of three sugar acetates in liquid and supercritical CO₂. β -forms of 1,2,3,4,6-pentacetyl-D-glucose (BGLU) showed a phenomenon analogous to aqueous deliquescence in gaseous CO₂ around 55.9 bar and 296 K, which indicating a strong affinity between the solvent CO₂ and the solute BGLU. α -forms of 1,2,3,4,6-pentacetyl-D-glucose (AGLU) exhibited a lower deliquescence point than that of BGLU by approximate 6-7 bar, while the third sugar, 1,2,3,4,6-pentacetyl β -D-galactose (BGAL), does not show the deliquescence in dense CO₂. All the sugar derivatives completely dissolve in liquid and supercritical CO₂ at a high concentration up to 30 wt% under a relative mild pressure (< 110 bar). The phase behavior data was shown in Figure 4.1.

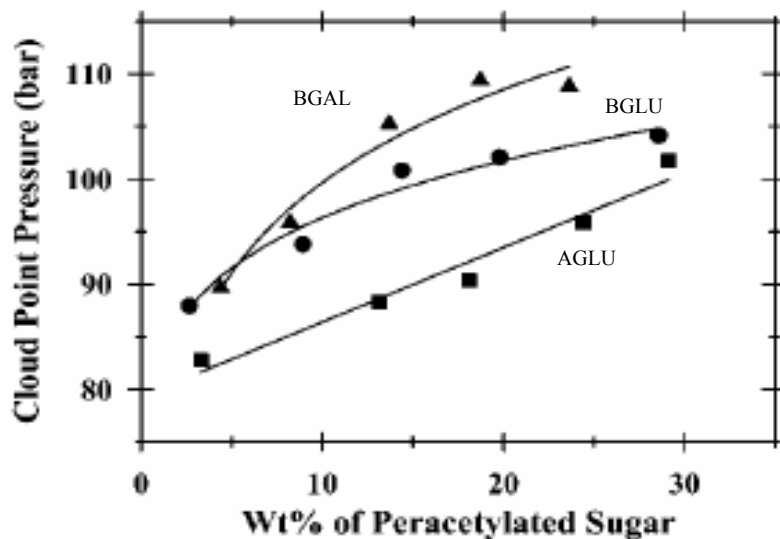


Figure 4.1 Pressure-composition phase diagram for the CO₂+AGLU/BGLU/BGAL at 313K¹¹²

Our group has extensively studied the phase behaviors of various peracetylated sugar derivatives in CO₂. The solubility of β-D-galactose pentaacetate in CO₂ was measured at 298 and 313 K, which showed very low bubble points, e.g. 6.34 MPa at 298K and 5 wt%. β-cyclodextrin heneicosacetate showed outstanding solubility in liquid and supercritical CO₂ over a very broad range of concentration (up to 30 wt%). Without surprise, the bubble point of β-cyclodextrin heneicosacetate was reported at higher pressures compared to the per-acetylated monosaccharide, β-D-galactose pentaacetate, because of the substantial increase in molecular weight. Per-acetylated amides also were observed CO₂ solubility at elevated temperature.¹²⁴ A class of acetylated cyclodextrins exhibited high solubility in dense CO₂. Similar as observed in BGLU + CO₂ system, the cyclodextrins also showed melting point depression at low pressure before completely miscibility. The two phase equilibrium curves of the cyclodextrins demonstrated a dramatic leap before 5 wt% and tended to be flat at higher pressure especially

larger than 15 wt%. All these results suggested that the per-acetylated cyclodextrins are highly accessible for favorable Lewis acid:Lewis base interactions with CO₂.¹²³ Our group also reported a global phase behavior for a binary mixture of the CO₂-philic solid β -D-maltose octaacetate (MOA) with carbon dioxide. MOA is a representative for CO₂-philic materials that exhibit melting point depression in dense CO₂. Both critical end points (LCEP and UCEP) and pressure vs. composition isotherms at 283, 298, and 323 K were measured. A global pressure vs. temperature phase behavior was identified for this system. A detailed description of this work will be reviewed in the following chapter.¹¹³

For the first time, Chandrika, et al. utilized high pressure NMR to study the solution structure of a carbohydrate, sucrose octaacetate (SOA), and CO₂ system. The author assumed that SOA is very CO₂-soluble, but they did not demonstrate the phase behavior study of SOA. Our study showed that the solubility of SOA in CO₂ is very low, less than 1wt%, comparing to its isomers such as maltose octaacetate, as discussed in Chapter 2.3. However, this solubility is high enough for NMR study. The studies can contribute a wealth of fundamental understanding on the structure and dynamics of molecules in liquid and supercritical CO₂. The NMR spectra of SOA in supercritical CO₂ revealed that the average solution-state conformation of the glucopyranosyl ring of SOA in supercritical CO₂ is consistent with the ⁴C₁ chair form. However, the fructofuranosyl ring adopts an envelope conformation in supercritical CO₂ medium. The authors also argued that the NMR spectrum was a strong evidence of the existence of C—H \cdots O hydrogen bonding interaction between the methyl proton of the acetate moiety and one the negatively charged CO₂ oxygen atoms.¹⁰⁷

The results showed that acetylation is a highly effective technique to design CO₂ philic materials. In contrast to the conventional view of the non-polar solvent properties of CO₂,

relative polar sugar-acetates can be highly soluble in supercritical CO₂, revealing the polar nature of CO₂ as a solvent which provides very important clue for designing CO₂-philes. Sugar acetates are renewable, inexpensive and environmentally benign materials which have extensive biomedical engineering and pharmaceutical applications. For instance, cyclodextrins and their derivatives have recently been recognized as useful pharmaceutical excipients which are able to be used in different areas of drug delivery, particularly in protein and peptide delivery and gene delivery.¹⁴⁹⁻¹⁵¹ The high solubility of the per-acetylated sugars in CO₂ point toward the utilization of supercritical CO₂ as a promising “green” solvent for cleaning, separations, and reactions in a wide range of molecular systems, especially in the biomaterial applications.

4.2 CELLULOSE TRIACETATE OLIGOMERS

4.2.1 Design of Cellulose Triacetate Oligomers

Although cellulose triacetate (CTA) (M_w≈103,000 g/mol) can be plasticized in the presence of dense CO₂, the per-acetylated polysaccharide was observed to be insoluble in CO₂ over a range of temperatures from 298-448 K and pressure up to 52 MPa.¹²⁴ This could be attributed to the high crystallinity of the high molecular weight CTA. We carried out a new degradation method, pivaloylysis as shown in Figure 4.2,¹⁵² to prepare cellulose triacetate oligomers. The technique avoids the presence of aggressive acid catalysts which could lead to more or less undesired degradation products. More importantly, the pivaloylysis products would have pivalate as the end group rather than a hydroxyl end group that is always CO₂-phobic. Based on the empirical heuristics (Chapter 2.3.2), pivalate group should be more CO₂ philic than hydroxyl group.

Figure 4.3 shows the distribution of every CTA oligomer during a period of 240 h. The compositions of monomer and dimer increase in the whole recording period, while larger molecular weight CTAs (trimer, tetramer and pentamer) show a maximum yield after a specific time, around 50-75 h, and then slip down. Therefore, we ran the cleavage process about 36 h.

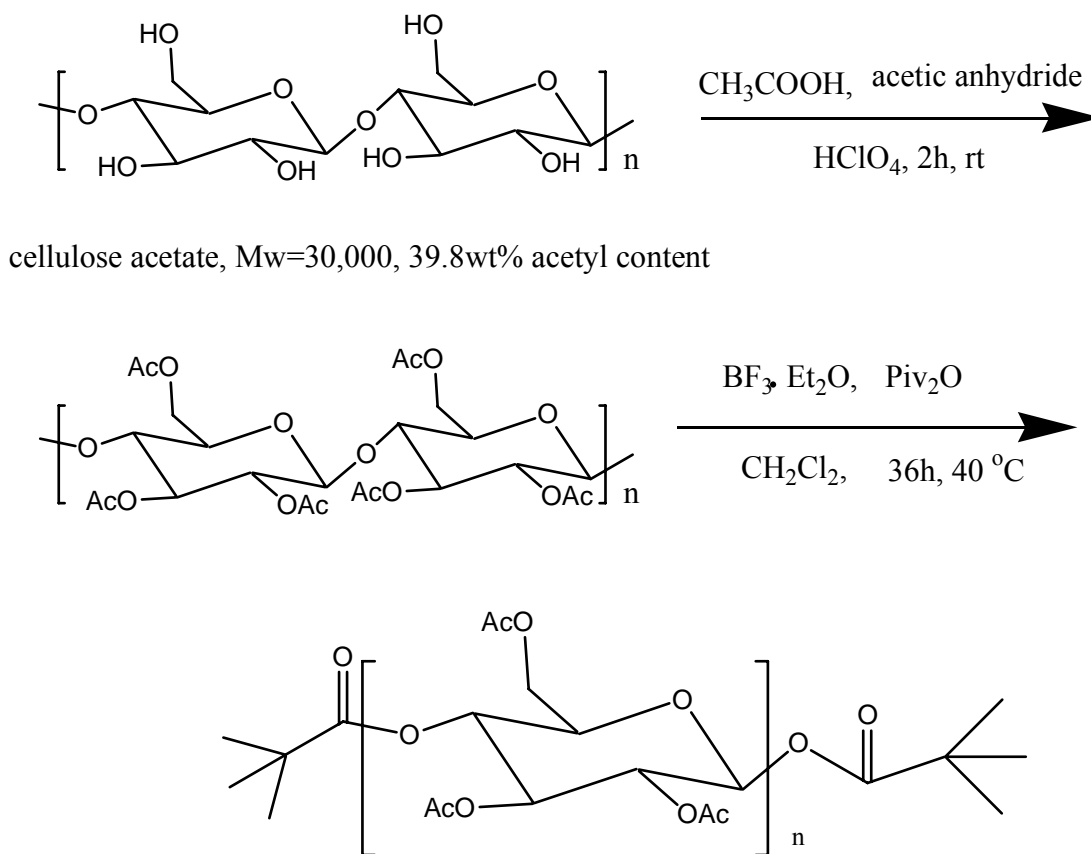


Figure 4.2 Pivaloyl cleavage of cellulose triacetate ¹⁵²

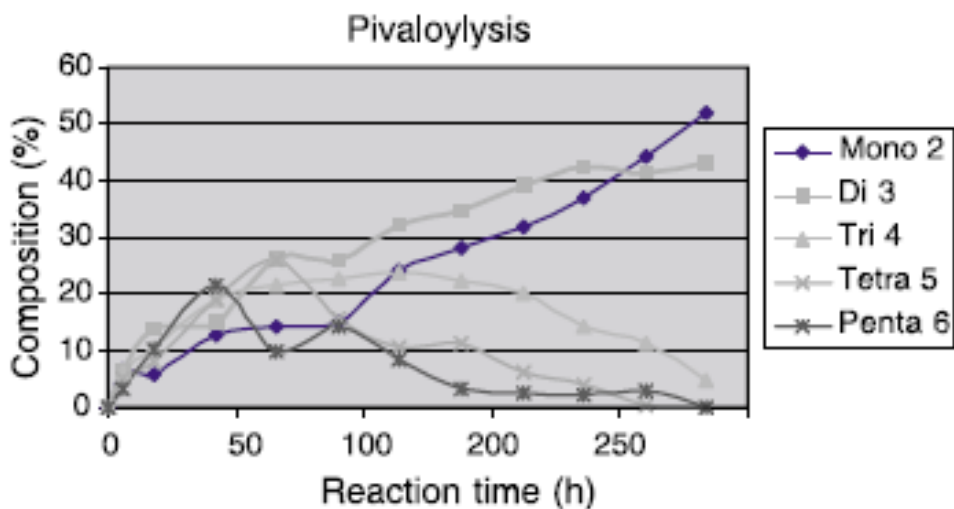


Figure 4.3 Composition tracking of every CTA oligomer during pivaloylysis¹⁵²

4.2.2 Synthesis

4.2.2.1 Materials

Cellulose acetate (39.8 wt% acetyl content, average $M_n=30,000$ (GPC)), anhydrous dichloromethane, boron trifluoride etherate, and pivalic anhydride were obtained from Aldrich. Acetic acid, perchloric acid, sodium bicarbonate, and silica gel (60-200 mesh) were purchased from J.T. Baker. Acetic anhydride and cyclohexane were obtained from Fisher Scientific. Ethyl acetate was purchased from EMD Chemicals Inc. All the chemicals were used as received without further processing.

4.2.2.2 Synthesis Procedure^{152,153}

2,3,6-tri-O-acetyl-cellulose Before the reaction, cellulose acetate was dried at 100 °C overnight. To a 500 mL, three necked, round-bottomed flask equipped with a magnetic stirring bar, 10 g cellulose acetate was charged in 270 mL acetic acid under stirring. 20 mL acetic

anhydride and 0.7 mL 72% perchloric acid were added into the solution sequentially. The reaction mixture was allowed to stir for 2 h and then slowly poured into 1 L of water. After aggressive mixing, the per-acetylated cellulose triacetate was collected by vacuum filtration. The product was alternately washed by saturated sodium bicarbonate aqueous solution and pure water until the filtrate was neutral determined by pH testing paper. 9.7 g white polymer was then obtained after drying at 50 – 60 °C under vacuum overnight. ¹H-NMR is given in Figure A. 14. ¹H-NMR (300MHz, CDCl₃), δ_H: 1.95, 2.02, 2.14 (s, 3×3H, -OCOCH₃), 3.55 (br, 1H, H-5), 3.72 (t, 1H, J=9.0, H-4), 4.08 (br, 1H, H-6'), 4.41 (br, 2H, H-1/H-6), 4.80 (br, 1H, J=9.0, H-2), 5.08 (t, 1H, J=9.0, H-3).

Pivaloylysis of 2,3,6-tri-O-acetyl-cellulose A 500 mL, three-necked, round-bottomed flask was equipped with a magnetic mixer. The dried 2,3,6-tri-O-acetyl-cellulose (3g, 10.4 mmol) and 250 mL anhydrous dichloromethane were charged into the flask. Pivalic anhydride (99.5 mL, 490 mmol, 47 eq.) was added dropwise over 30 min. Then 20 mL (156 mmol, 15 eq) boron trifluoride etherate was charged. The solution was placed into an oil bath and warmed to 40 °C. After 36 h the reaction mixture was quenched with 500 mL saturated sodium bicarbonate solution. Aggressive mixing the solution for at least half hour, separate the organic phase (bottom) from the aqueous phase (top) by a 500 mL separatory funnel. Wash the aqueous phase with 100 mL dichloromethane three times (100 mL × 3). The combined organic solutions were dried over sodium sulfate and filtered. The dried solution was then dried at high temperature (>90 °C) under high vacuum. A dark brown solid mixture was obtained. Figure A. 15 shows a distribution of different compounds in the reaction mixture measured by MALDI.

The oligomers with different chain length were purified by wet-column chromatography using combination of cyclohexane and ethyl acetate as an eluent system. The silica gel column

was packed by cyclohexane. And the eluent systems, R_f , developing system for each oligomer, and yield were listed in Table 4.1. The oligomers were characterized by ESI, as shown in Figure A. 16, Figure A. 17, Figure A. 18, and Figure A. 19.

Table 4.1 Parameters of wet-column separation

Oligomer	Mw (g/mol)	Eluent System (cyclohexane/ethyl acetate)	Developing System for TLC (cyclohexane/ethyl acetate)	R_f	Yield (%)
Monomer	497	5:1	1:1	0.55	11.4
Dimmer	785	3:1	1:1	0.45	13.0
Trimer	1073	2:1	1:1	0.3	6.2
Tetramer	1361	1:1	1:1 1:2	0.15 0.4	4.1

4.2.3 Phase Behavior Study

A pressure-composition phase diagram of CTA oligomers, monomer, dimmer, trimer, and tetramer, is presented in Figure 4.4. For CO_2 + monomer system, only bubble point was observed at a very low pressure within 1-5 wt%. A three-phase VL_2S equilibrium line was identified while VL_1L_2 equilibrium line was not observed. The general nature of the corresponding pressure-composition (P-x) diagram for such systems is illustrated in Figure 4.5 as a classic P-x diagram for heavy solid-supercritical fluid system depicted by McHugh and Krukonis.⁷ The small box A within Figure 4.5 presents the region where the bubble point loci were measured. Phase behaviors of CO_2 + CTA dimer/trimer/tetramer system are consistent with the novel type of phase behavior of heavy solid-supercritical fluid system identified by Hong and his

coworkers.¹¹³ The new type phase diagrams are identified by two three-phase equilibrium lines, VL_1L_2 and VL_2S , shown in Figure 4.6 and Figure 4.7. The dotted-line box B within Figure 4.6 presents the region where the CO_2 +dimer system was measured. The experimental data are located on the phase transition locus. The small VL_1 region approximately ends at 3.5wt%, hence, the experimental data were observed as bubble points. However, when the concentration increases, phase behavior turns to be L_1L_2 equilibrium region. As a result, under higher concentration such as 4 and 5wt% the experimental data were dew points. For CO_2 + trimer/tetramer system, the VL_1 region shrinks further, less than 1 wt%. Therefore, only dew points were observed for these two systems in our measured range, 1-5wt%, shown in Figure 4.7. The VL_1L_2 three-phase lines reveal a strong affinity between CO_2 and the CTA oligomers.

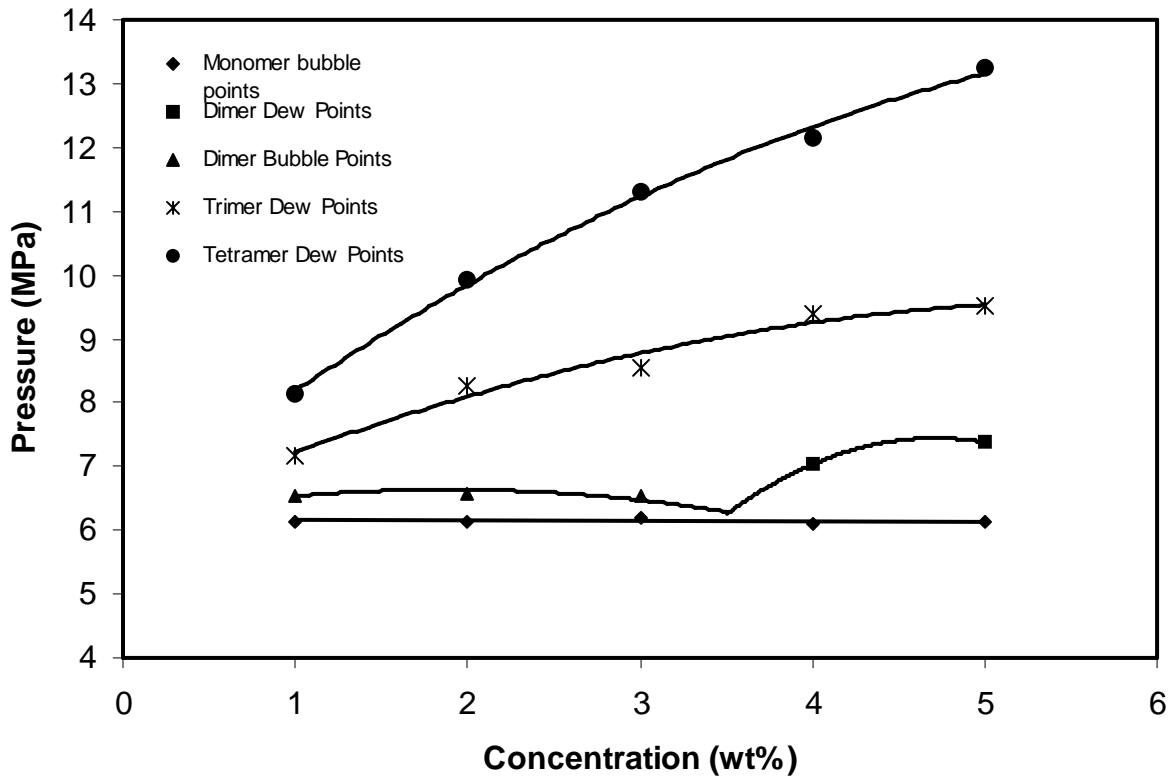


Figure 4.4 Pressure-composition diagram for CO₂ + CTA oligomer system at 298 K

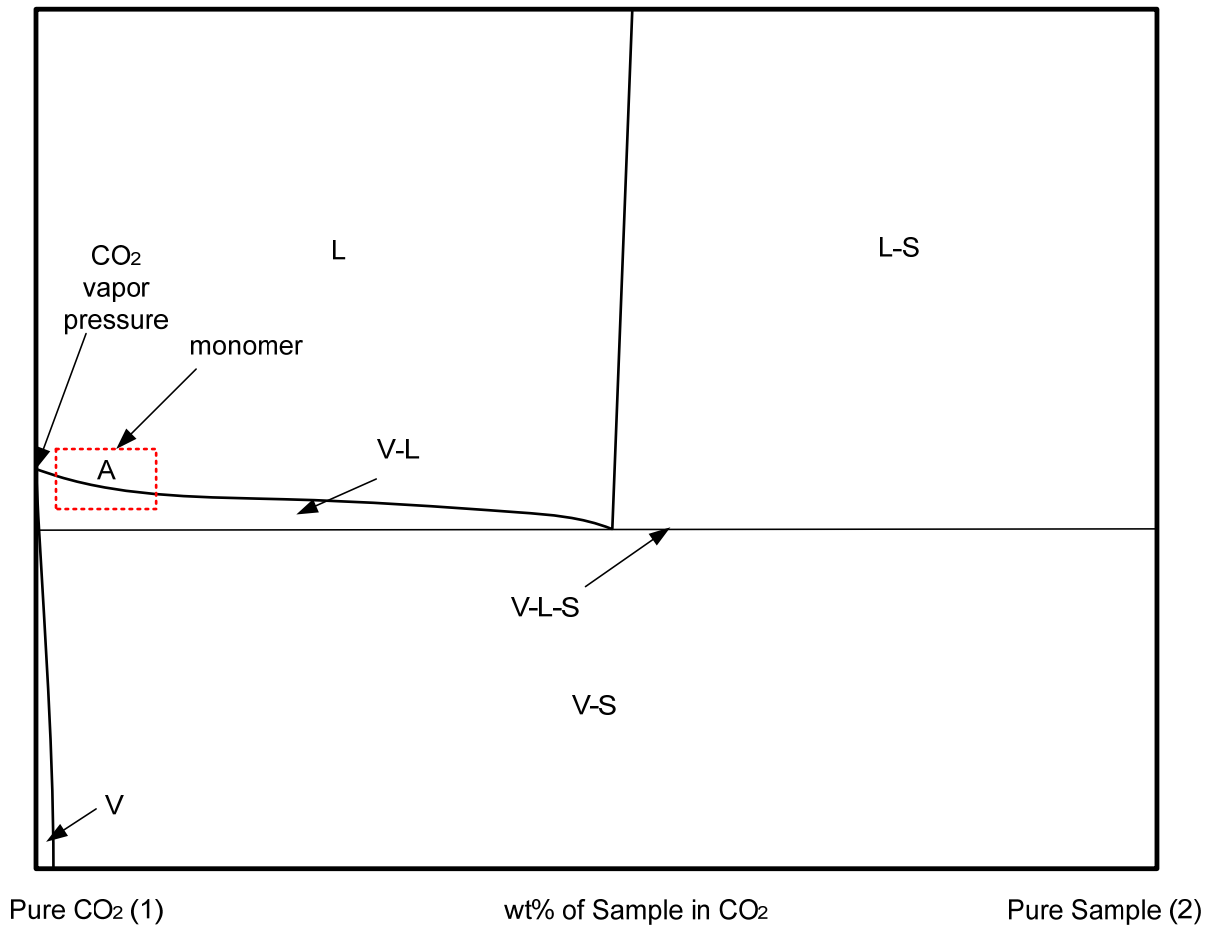


Figure 4.5 General pressure-composition (P-x) phase diagram for classic sub/supercritical CO₂ + heavy solid system⁷

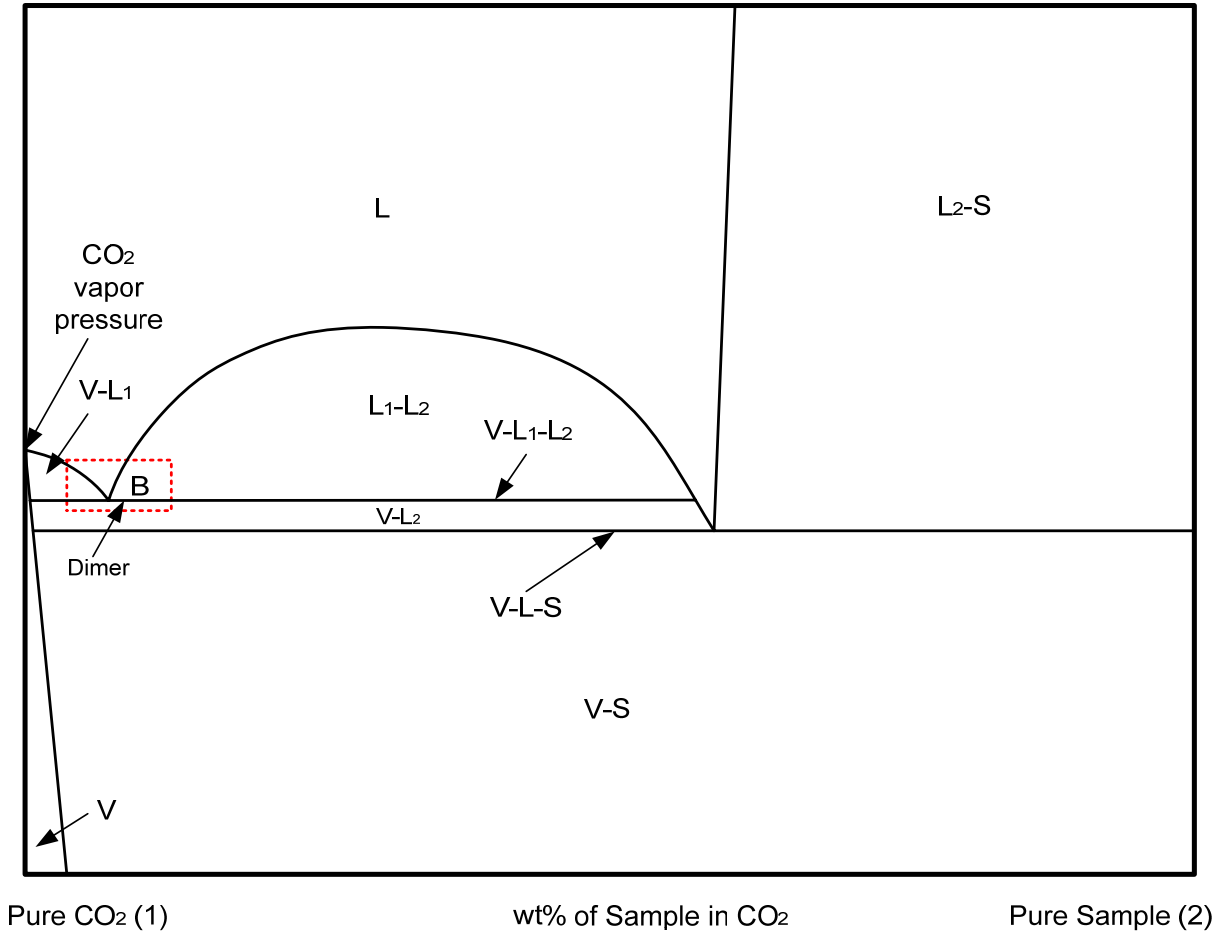


Figure 4.6 General pressure-composition (P-x) phase diagram for the novel sub/supercritical CO₂ + heavy solid system¹¹³

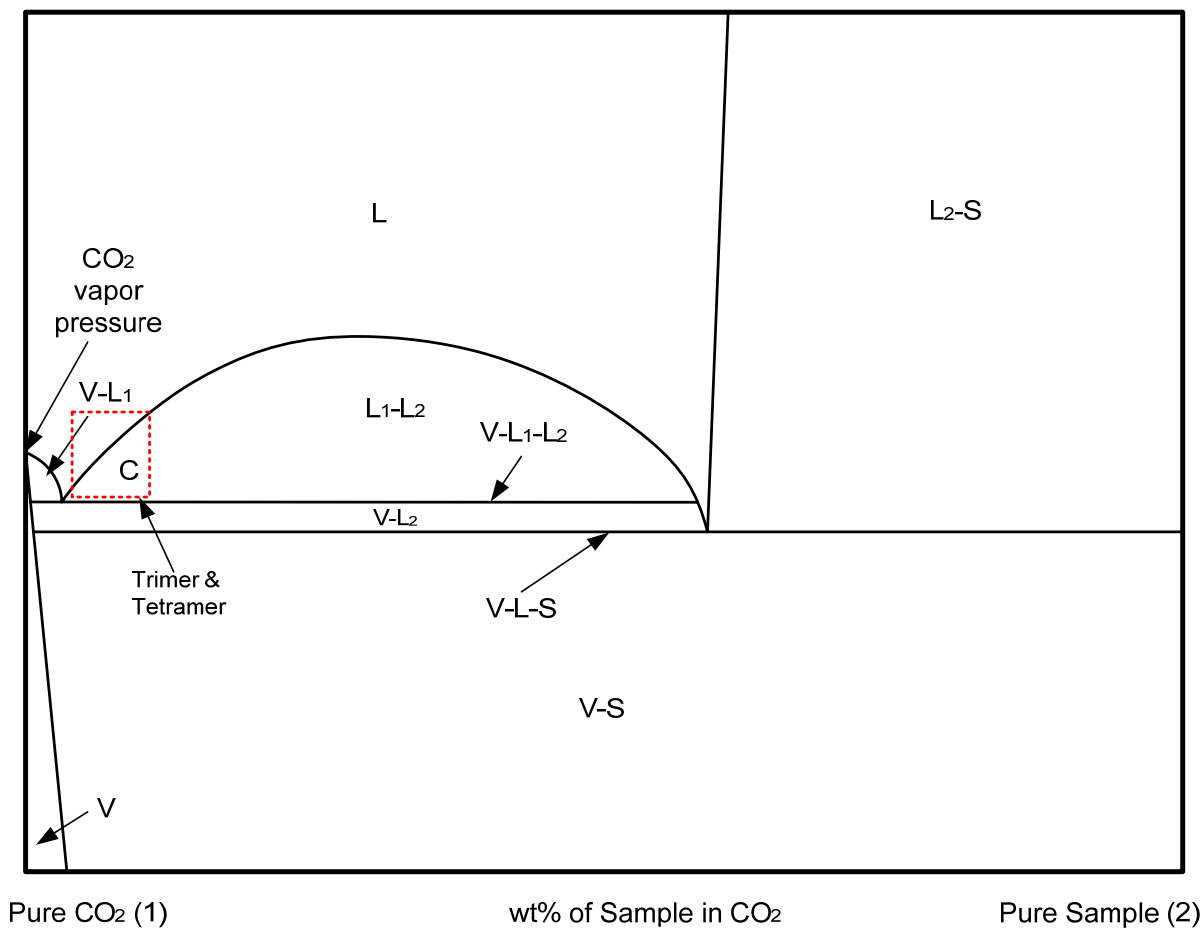


Figure 4.7 General pressure-composition (P-x) phase diagram for the novel sub/supercritical CO₂ + heavy solid system¹¹³

4.3 CONCLUSIONS

CTA oligomers were prepared by a new degradation method, pivaloylysis. Oligomers with as many as four repeat units were separated and characterized. All the oligomers exhibited remarkably high CO₂ solubility. With the increase of the number of repeat units, the miscible

pressures increase. In the studied concentration range (1-5 wt%), the phase transition points evolved from bubble points to dew point with the increasing of the repeat units. When the number of repeat units is greater than two, the phase diagrams are characterized by a VL₁L₂ equilibrium lines which have been identified for binary systems of CO₂ and CO₂-philic solids.¹¹³

5.0 PHASE BEHAVIOR STUDY

5.1 GLOBAL PHASE BEHAVIOR FOR CO₂-PHILIC SOLIDS

5.1.1 Introduction

The identification and synthesis of so-called “CO₂-philic” materials, that is, those that exhibit significant mutual solubilities with dense sub- and supercritical carbon dioxide, are of increasing interest to the “green” chemical processing community. These CO₂-philes are being considered for a wide range of applications, including copolymers, surfactants, chelating agents, and viscosity enhancers for CO₂. Examples of CO₂-philic polymers include poly(fluoroalkyl acrylate),^{26,89} poly(perfluoroether),¹³³ and poly(dimethyl siloxane).^{131,154} More recently, hydrocarbon-based CO₂-philes, such as poly(propylene oxide)¹³¹, branched alkyls¹²⁹, poly(ether-carbonate),¹⁵⁵ sugar acetates,^{112,123,124} and poly(vinyl acetate),^{118,119} have also been investigated.

Many of these compounds are solids at temperatures well above the critical point of carbon dioxide; furthermore, many exhibit regions of liquid-liquid equilibrium with CO₂. Thus, their binary phase behavior with CO₂ might be expected to be relatively complex. And, as Beckman states in his recent commentary,¹⁵⁶ we still are not able to predict the phase behavior of complex molecules in CO₂. Unfortunately, phase behavior measurements for these new CO₂-

philic materials are very limited, and those studies that do exist have focused only on limited portions of the liquid-liquid region. For example, cloud-point pressures were measured for mixtures of CO₂ with several CO₂-philic sugar acetates^{112,123,124} at temperatures of 298 and/or 313 K. Liquid-liquid cloud points were also reported for mixtures of CO₂ with solid poly(vinyl acetate) oligomers at 298 K¹¹⁹ and for the CO₂ + poly(heptadecafluorodecyl acrylate) binary at temperatures from 298 to 373 K.²⁰ Thus, in none of the above cases was the scope of measurements adequate for determining the global pressure-temperature phase behavior of the binary system of interest.^{7,115,157}

An important long-term goal in the design and synthesis of CO₂-philes is the prediction of their mutual solubilities with carbon dioxide only from molecular structure information. However, the first step in such a plan will have to be the experimental determination of the global CO₂ + CO₂-phile phase behavior for a number of well-defined systems. In this study, measurements are reported for the per-acetylated disaccharide, β -D-maltose octaacetate whose structure is shown in Figure 5.1, because of the high degree of CO₂ solubility previously reported for sugar acetates. Of particular interest to us in this work were (1) the temperature range of the three-phase liquid-liquid-vapor line and (2) whether the solid-liquid-vapor three-phase line would interrupt fluid-phase boundaries at higher pressures.

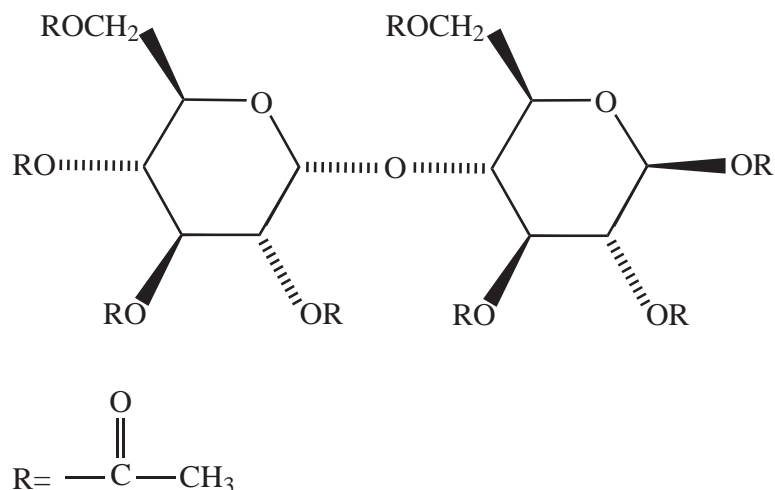


Figure 5.1 Structure of β -D-maltose octaacetate

5.1.2 Results and Discussion

Results for the $\text{CO}_2 + \text{MOA}$ system at 283, 298, and 323 K are presented in the form of pressure vs. composition isotherms in Figure 5.2, Figure 5.3, and Figure 5.4, respectively. A distinguishing feature of this system is the unusually high solubility (i.e., ~ 0.5 wt fraction) of MOA in liquid CO_2 at moderate (< 20 MPa) pressures. These results lie in vivid contrast to the low solubilities of high-melting, non- CO_2 -philic solids that are well-represented in the literature.⁷ Of the three phase diagrams presented, Figure 5.3 is the most complex, being characterized by five two-phase regions and two three-phase pressures within which exist four separate phases. Thus, this figure is discussed in more detail below. Here, L_1 refers to the CO_2 -rich and L_2 to the MOA-rich liquid phases; S refers to solid MOA.

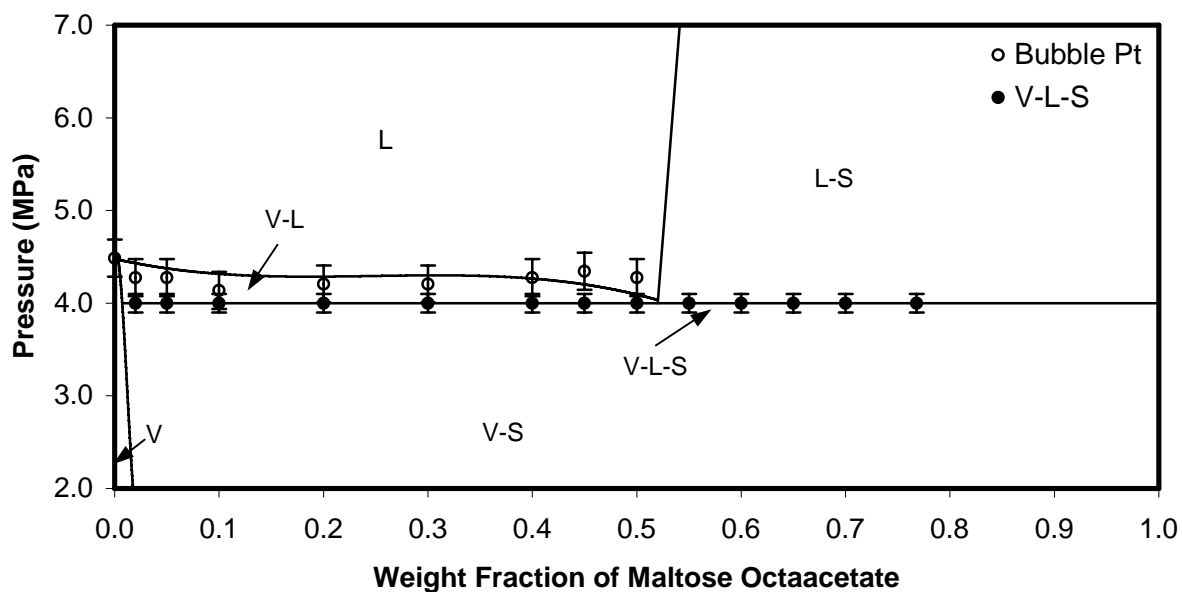


Figure 5.2 Pressure-composition diagram for the carbon dioxide (1) + maltose octaacetate (2) system at 283 K

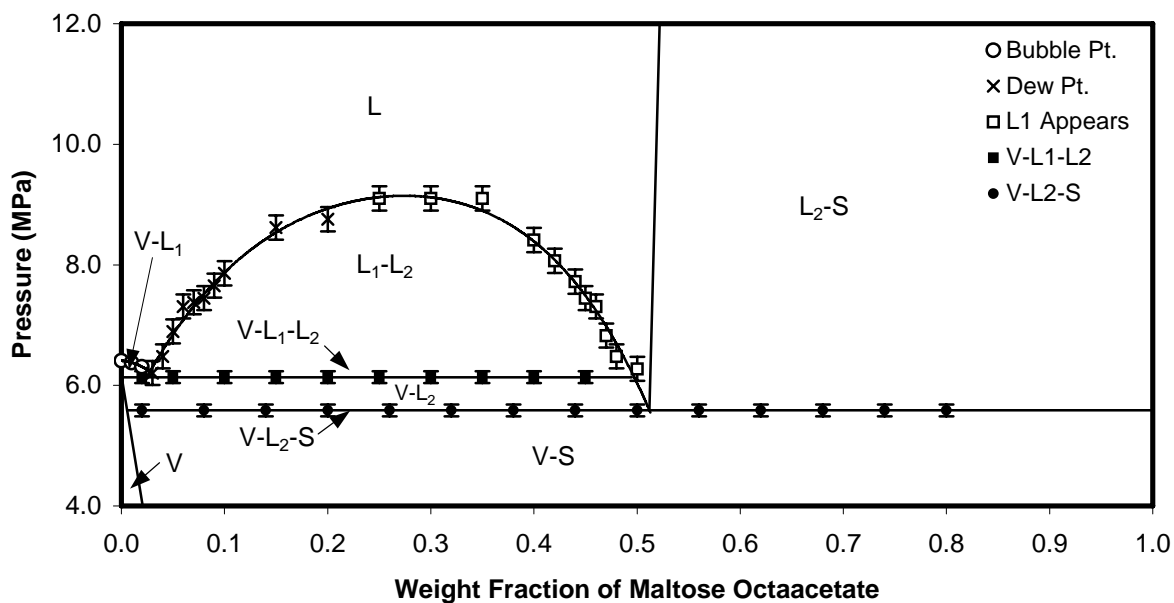


Figure 5.3 Pressure-composition diagram for the carbon dioxide (1) + maltose octaacetate (2) system at 298 K

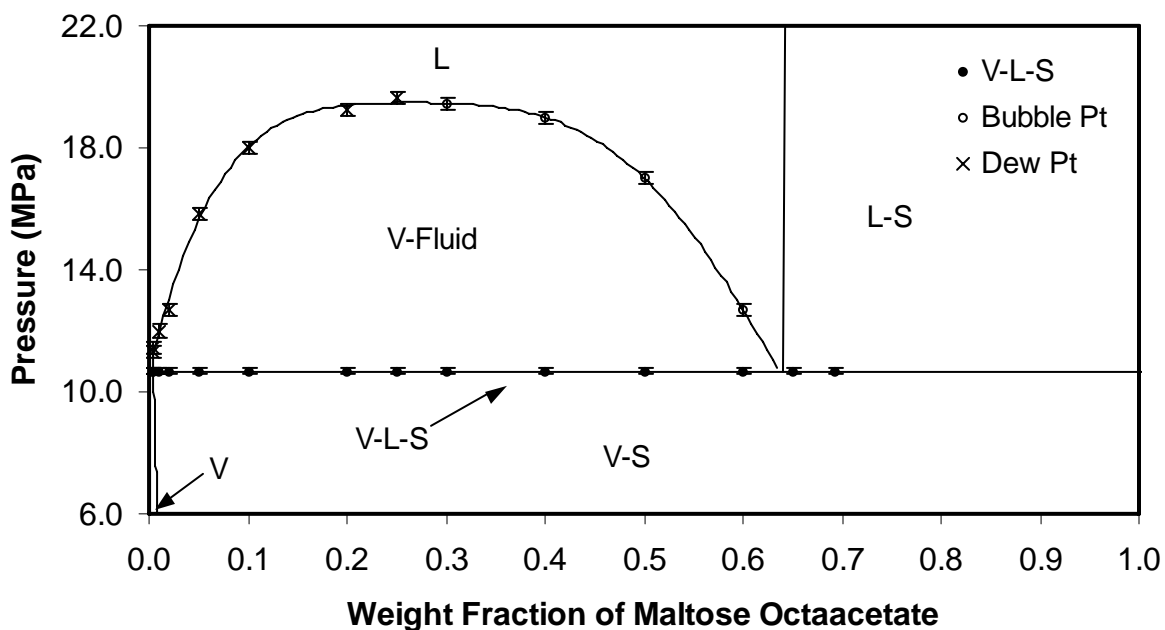


Figure 5.4 Pressure-composition diagram for the carbon dioxide (1) + maltose octaacetate (2) system at 323 K

5.1.2.1 Pressure – Composition Diagram at 298K

VL_1 Expansion of the CO_2 -rich liquid L_1 resulted in VL_1 equilibrium. The small VL_1 region (0.03 wt fraction MOA and less) is bounded by the CO_2 vapor pressure, the VL_1 bubble-point locus, a VL_1 dew-point locus (but no dew-point data was measured for this region), and the three-phase VL_1L_2 line.

L_1L_2 Expansion of single-phase liquids that contained higher concentrations of MOA (0.03-0.52 wt fraction) resulted in the dew point appearance of more dense, sugar acetate-rich liquid (0.25-0.52 wt fraction) or the appearance of the less dense, CO_2 -rich liquid (L_1) (0.03-0.24 wt fraction) of an L_1L_2 liquid-liquid region. The red color of the fluid phases (associated with critical opalescence) and slow phase segregation of the liquid phases associated with the 0.25 wt

fraction mixture bubble point indicate that this composition is close to the critical-point composition. The L_1L_2 region is bounded by the binodal curve and by the VL_1L_2 line.

L_2S Solid-liquid (L_2) equilibrium was observed at MOA concentrations greater than ~ 0.5 wt fraction and pressures above the three-phase VL_2S line. Expansion of these two-phase mixtures resulted in the formation of CO_2 -rich vapor bubbles at the VL_2S three-phase pressure. The L_2S region is bounded by a steep cloud-point curve (but no data were collected along this boundary), the neat MOA boundary, and the VL_2S line.

VL_2 Isobaric expansion of the three-phase VL_1L_2 mixture resulted in the depletion of the CO_2 -rich L_1 phase and the growth of the V and L_2 phases. Pressure decreased upon expansion when the L_1 phase was no longer present and the mixture entered the VL_2 two-phase region. The pressure range of the VL_2 region was narrow, with further expansion leading to the occurrence of the S phase. The VL_2 two-phase region is bounded by the VL_1L_2 and VL_2S three-phase loci, and the VL_2 bubble- and dew-point loci (however, no data were collected on these two short two-phase boundaries).

VS Isobaric expansion of three-phase VL_2S mixtures resulted in depletion of the MOA-rich L_2 phase and growth of the V and S phases. The system pressure began to decrease only when the L_2 phase was no longer present, leaving the vapor and solid phases behind. The VS region is bounded by the VL_2S three-phase line, the neat MOA boundary, the vapor pressure of solid MOA at 298 K, and the VS dew-point locus.

VL_1L_2 and VL_2S Three-Phase Lines The pressure difference between these two lines is only 0.6 MPa, so isothermal expansions must be conducted slowly and carefully in order to obtain two-phase VL_2 equilibria.

To our knowledge, CO₂ + MOA is the first binary mixture with CO₂ for which the pressure-composition diagram illustrated by Figure 5.3 has been observed.

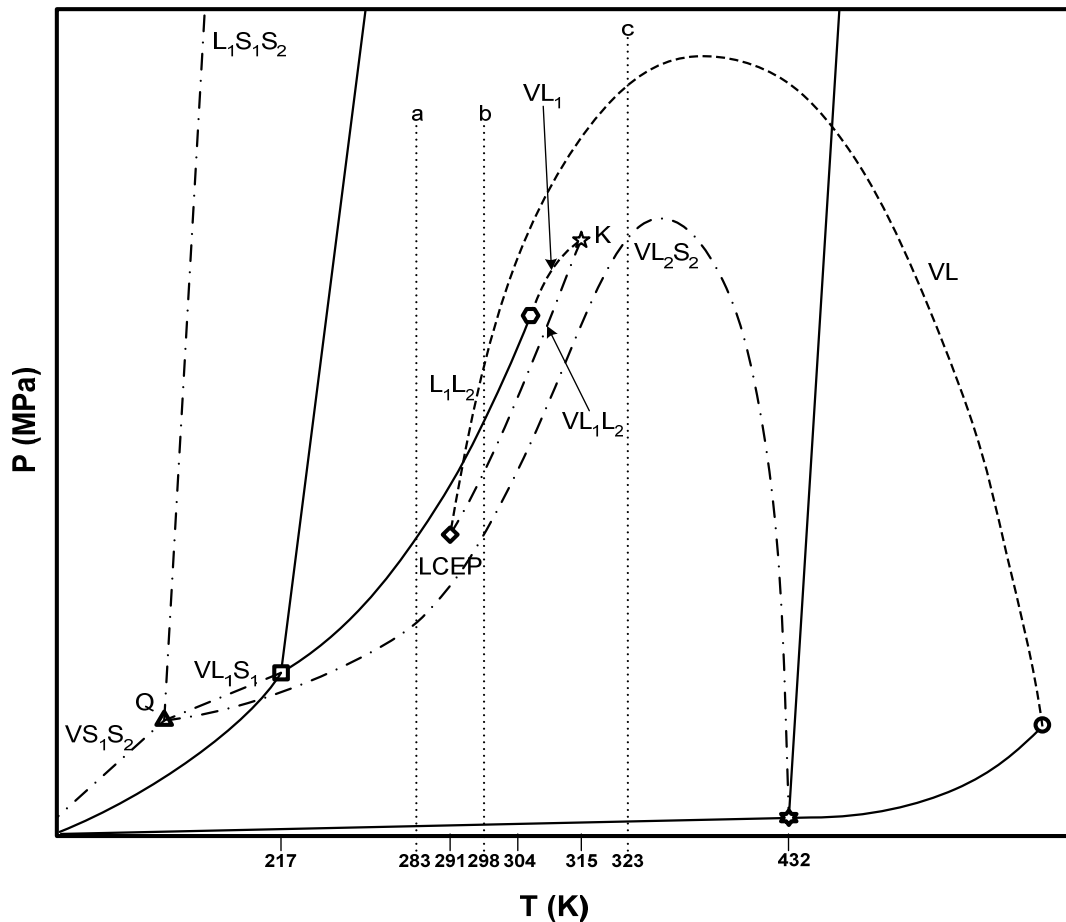


Figure 5.5 P-T Projection for the carbon dioxide (1) + maltose octaacetate (2) system. Solid lines represent pure-component saturation curves, dashed lines represent critical curves, and dotted-dashed lines represent three-phase lines. □ is the triple point and ○ is the critical point of CO₂; ☆ is the triple point and ○ is the critical point of MOA.

5.1.2.2 Pressure-Temperature (P-T) Projection

The pressure-composition isotherms of Figure 5.2, Figure 5.3, and Figure 5.4, along with the experimentally determined K point and lower critical end point (LCEP), were used to generate a P-T projection for the CO₂ + MOA system (Figure 5.5). The axes of the figure are not drawn to

scale in order to make the figure more legible. All pure-component vapor pressure, melting point, and sublimation curves are included for clarity and should only be regarded as qualitatively correct, as they were not measured. Similarly, the low-temperature part of the phase diagram, from the triple point of CO₂ and lower, is included for illustrative purposes only. Finally, solid MOA is represented by S₂ in order to distinguish it from the solid CO₂ phase S₁.

Because of both the CO₂-philic nature and the relatively high melting point of the solute, CO₂ + MOA exhibits a combination of fluid-phase and solid-fluid equilibria previously unreported for CO₂ + solute systems. The fluid-phase behavior is Type V according to the classification system of Scott and Van Konynenburg.^{158,159} Type V behavior is characterized by a short VL₁ critical locus that originates at the critical point of CO₂ and ends at an upper critical end point (UCEP), also referred to as the K point. A VL₁L₂ three-phase line begins at the K point and extends to lower temperatures, ending at the LCEP. Beginning at the LCEP, the lower critical solution temperature (LCST) curve extends to higher temperatures and pressures and transitions to a vapor-liquid critical curve above the critical temperature of CO₂.

The LCEP (291 K and 5.17 MPa) was estimated by cooling 0.025 and 0.05 wt fraction MOA solutions to sub-ambient temperatures until no evidence of VL₁L₂ phase equilibrium was observed. Further cooling to 253 K did not result in the re-occurrence of either L₁L₂ or VL₁L₂ equilibrium; thus, we believe that the system is Type V and not Type IV.^{158,159} A similar procedure was used to locate the K-point (312 K and 7.37 MPa), but in this case the mixtures were heated until no three-phase equilibrium was observed.

Because the solubility of CO₂ in the solute-rich L₂ phase is high, the VL₂S₂ three-phase line is continuous. It does not intersect any fluid-phase boundaries at higher pressures, but instead reaches a pressure maximum and then decreases in pressure as the temperature is

decreased, running parallel and just below the VL_1L_2 line before finally terminating at a $VL_1S_1S_2$ quadruple (Q) point. A similar type of solid-fluid equilibrium, albeit with Type I fluid-phase behavior, was measured by Donnelly and Katz.¹⁶⁰

The pressure-composition diagrams illustrated in Figure 5.2, Figure 5.3, and Figure 5.4 correspond to the three dashed-line isotherms *a*, *b*, and *c* in Figure 5.5 at 283, 298, and 323 K, respectively. For example, we can follow isotherm *b* in Figure 5.5 from the one-phase region to lower pressures, intersecting in order the L_1L_2 critical curve, the CO_2 vapor pressure curve, the VL_1L_2 three-phase line, the VL_2S_2 three-phase line, and the solid MOA sublimation curve.

The combination of fluid-phase and solid-fluid behavior observed herein has been measured for only a few systems, for example, water + salt and ammonia + salt¹⁶¹ mixtures. A distinguishing feature of our system, however, is the long three-phase VL_1L_2 line, which begins at temperatures well below the critical temperature of CO_2 and extends over a range of more than 20 K. For most Type V systems, this line is short, no more than a few degrees long.¹⁵⁹

5.1.3 Conclusions

The global phase behavior for the binary system $CO_2 + MOA$ has been determined. The pressure-temperature projection of the binary has the fluid-phase features of a Scott and Van Konynenburg Type V system, but also includes a continuous VL_2S_2 line that extends from the triple point of the MOA, goes through a pressure maximum, and then runs just below the VL_1L_2 line before ending in a $VL_1S_1S_2$ quadruple point at very low temperatures. This type of phase behavior, which is relatively rare, is likely to be observed for other high-melting CO_2 -philic solids, including poly(vinyl acetate), poly(fluoroalkyl acrylate), and other sugar acetates. The

solubility of MOA in CO₂ can be explained by the interaction between a Lewis base (carbonyl groups of MOA) and Lewis acid (CO₂). This same mechanism was previously illustrated by Sarbu¹⁵⁵ and Raveendran.¹⁰⁵

5.2 SOLUBILITY OF LINEAR POLY(TETRAFLUOROETHYLENE-CO-VINYL ACETATE) IN DENSE CARBON DIOXIDE

5.2.1 Introduction

Poly(tetrafluoroethylene-co-vinyl acetate) (poly(TFE-co-VAc)) is a fluoropolymer with potential applications in the coatings, optical and biomedical fields.¹⁶²⁻¹⁶⁴ (Although most of the polymers in this study were intended to be completely non-fluorous, this novel copolymer was of interest to Soichet and co-workers; so we agreed to help them understand its behavior in CO₂). Further, fundamentally understanding the high miscibility of fluorinated materials with CO₂ enables us the success of designing novel non-fluorinated hydrocarbon based CO₂ soluble materials.

Poly(TFE-co-VAc) can be synthesized via free radical copolymerization of tetrafluoroethylene (TFE) and vinyl acetate (VAc) in dense carbon dioxide, with the composition of the TFE-VAc copolymer being controlled by the ratio of monomers in the feed.¹⁶⁵ Although a small concentration of fluorosurfactant is added to the monomers and CO₂ in an initial study of this polymerization, subsequent trials without surfactant yielded copolymers of similar polydispersity and greater molar mass, implying that the surfactant is not necessary for solubility of the macroradical chains.¹⁶⁶ Based on reactivity ratios, poly(TFE-co-VAc) is a random copolymer because TFE cross-propagates with VAc, and VAc propagates in such a manner that

the sequence of VAc and TFE units in the polymer backbone is randomly ordered (i.e. these polymers are not di-block copolymers composed of a long chain of perfluoroethylene joined to a long chain of poly(vinyl acetate)) Hydrolysis of VAc to vinyl alcohol (VA) yields the predicted decrease in copolymer molar mass to form poly(TFE-co-VAc-co-VA), suggesting that the copolymer was linear^{165,166}. This is in contrast to poly(TFE-co-VAc) prepared by emulsion, where a precipitous drop in molar mass is observed upon hydrolysis due to ester groups in the backbone. The high yield and high molar mass of the TFE-VAc copolymers provides indirect evidence that poly(TFE-co-VAc) is CO₂-soluble at reaction conditions of 45 °C and 20-to-23 MPa and loadings of 20% w/v. Because the polymerization was conducted in a vessel that did not permit detection of the phase behavior, the actual CO₂ solubility of these polymers was not determined.

The phase behaviors of the homopolymers of each monomer have been previously established. PVAc is a non-crystalline, low T_g (glass transition temperature) polymer that exhibits the greatest degree of CO₂ solubility associated with any high molecular weight oxygenated hydrocarbon homopolymer that has yet been identified, although it is far less CO₂-philic than fluoroacrylate or siloxane-based polymers.^{118,119} This high degree of CO₂ solubility has been attributed to a weak complex that forms between CO₂ and the readily accessible acetate group.^{118,119} PTFE is a crystalline polymer that is insoluble in CO₂ and organic solvents, although it does dissolve at high temperatures in high molecular weight fluorocarbon solvents.¹⁶⁷ Poly(tetrafluoroethylene-co-19.3 mol% hexafluoropropylene) (FEP₁₉) is a nonpolar fluorocopolymer that has similar properties to PTFE, but FEP₁₉ is highly branched and therefore has normal melting point at ~145°C, whereas PTFE has a melting point in excess of 300°C. It has been demonstrated that FEP₁₉ can dissolve in supercritical CO₂ at temperatures in excess of

185°C and pressures of approximately 100 MPa.^{115,167,168} If the TFE segments in FEP₁₉ are replaced with vinylidene fluoride (VF), this VF-HFP copolymer remains in solution to very low temperatures since the polar character of the VF group interacts with the quadrupole of CO₂.¹⁶⁹ These phase-behavior results suggested that perfluorination does not impart polymers high solubility in CO₂. This argument had also been made by Raveendran et al. through molecular simulation; i.e. partially fluorinated molecules provide more favorable binding sites for CO₂ than perfluorinated analogs.¹¹⁰

The objective of this study is to experimentally establish whether random copolymers of TFE and VAc are indeed CO₂-soluble at levels in excess of those exhibited by PVAc homopolymer containing a comparable number of repeat units. Poly(TFE-co-VAc) samples are prepared by radical copolymerization in supercritical CO₂ without surfactants, and the phase behavior of the copolymers is measured using non-sampling techniques in windowed, variable-volume cells. If the TFE-VAc copolymers are indeed more CO₂-soluble than homopolymers of VAc, then molecular modeling will be used to characterize the CO₂-polymer interactions in the CO₂-PVAc and CO₂-poly(TFE-co-VAc) systems.

5.2.2 Results and Discussion

A series of TFE-co-VAc copolymers was synthesized in supercritical CO₂ as described by Baradie and her colleagues.¹⁶⁶ The results of yield, bulk composition, molar mass, and T_g are summarized in Table 5.1. As shown, a series of copolymer compositions was prepared where monomer feed composition influenced polymer composition, from 11.6-to-63.3 mol% TFE. The yield (based on mass) was high for all compositions, between 78 and 86%. The T_g was similar for all samples, between 36°C and 38°C, which is similar to that of PVAc (38 °C). Since we

were interested in comparing solubility in CO₂ as a function of copolymer composition, the samples were synthesized in such a manner to yield similar molecular weight characteristics, with M_w between 140 and 180 kg/mol and the polydispersity index (PDI) between 2.7 and 3.1. For 63.3 mol% TFE copolymer, however, M_w was higher and PDI lower than the other samples.

Table 5.1 Bulk Analysis of TFE-VAc copolymers

TFE in feed (mol%)	Yield (wt%)	TFE in the Copolymers (mol%)^a	T_g (°C)	Mw/Mn/PDI Kg · mol⁻¹
17.6	80	11.6	37.2	140/42/3.2
23.6	80	19.3	36.8	156/49/3.1
35.6	86	26.5	36	166/61/2.7
53.7	78	46.7	37	180/55/3.1
67.7	79	63.3	37	290/157/1.84 ^b

^a Determined from %C analysis. ^b Measured using ethyl acetate as mobile phase. For entries 1-4, THF was used as the mobile phase for the measurement of molar masses.

It is important to note that this sample was measured by GPC in ethyl acetate whereas the other polymers were measured in THF. Ethyl acetate may have affected the hydrodynamic radius of the copolymer differently from THF, thereby accounting for the greater M_w and smaller PDI.

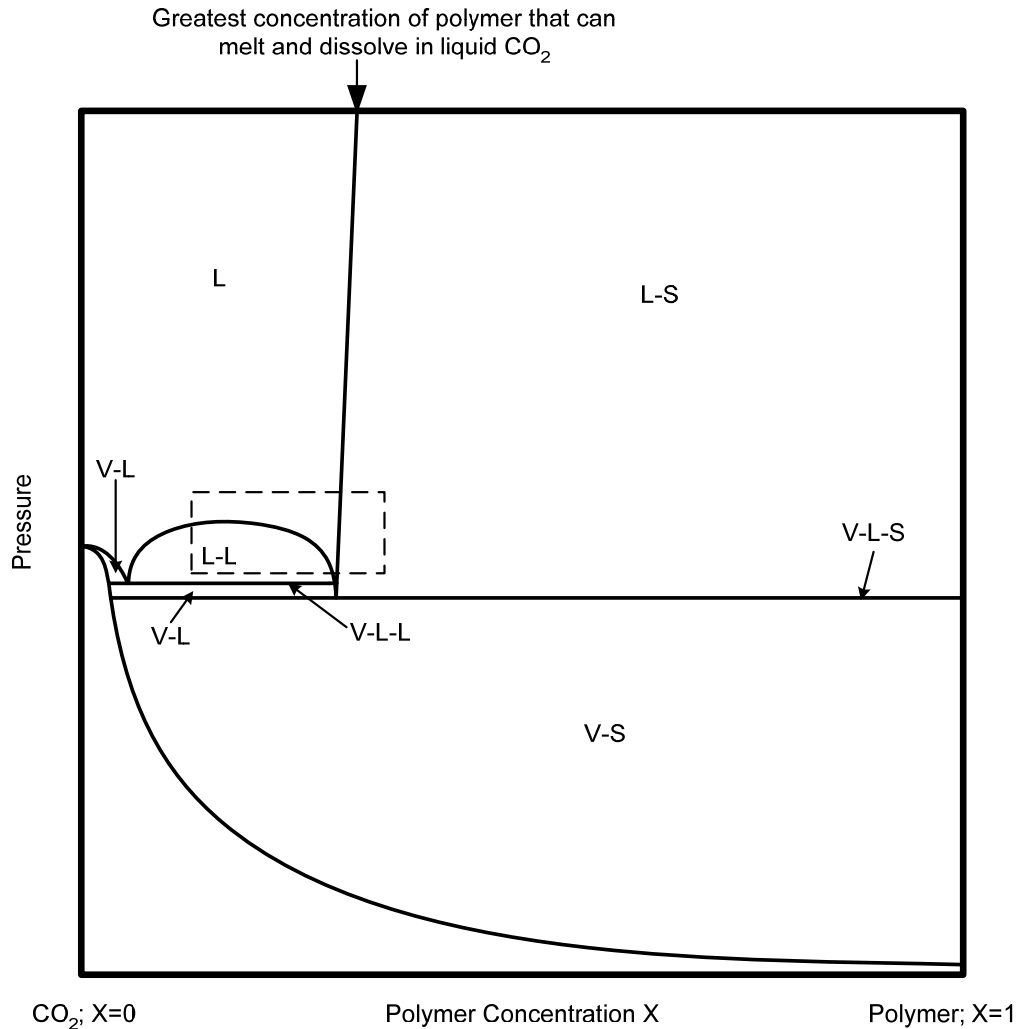


Figure 5.6 General pressure-composition (P-x) phase diagram for CO₂ and solid CO₂-philic compounds or polymers

The phase behavior of poly(TFE-co-VAc) – CO₂ mixtures was strongly influenced by the copolymer composition. (The copolymer will hereafter be designated as TFE-co-VAc, with the value of the TFE subscript corresponding to the mol fraction of that monomer.) The three copolymers with the smallest proportion of TFE, TFE_{11.6}-co-VAc, TFE_{19.3}-co-VAc and TFE_{26.5}-co-VAc, melt-flowed in CO₂ when heated above their T_g's, as did the PVAc homopolymer (these are amorphous polymers). Like PVAc, these copolymers dissolved in the presence of liquid CO₂,

and the general nature of the corresponding pressure-composition (P-x) diagram for such systems is illustrated in Figure 5.6¹¹³ (Although this figure strictly applies to binary systems in which no CO₂ dissolves in a monodisperse crystalline polymer, the region bounded by the dashed line in Figure 5.6 illustrates the qualitative features of the mixtures of CO₂ with the polymers used in this study.) The small box within Figure 5.6 illustrates the region where the CO₂-rich liquid – polymer-rich liquid data were measured. The results, shown in Figure 5.7, indicate that these three TFE-VAc copolymers are more CO₂-soluble than PVAc as evidenced by the cloud-point curves of these copolymers being comparable to one another and being 10 MPa lower than the PVAc cloud-point curve. Furthermore, a single phase could not be achieved at a PVAc concentration of 6 wt% at the pressure limit of 67 MPa. The greatest concentrations of the (TFE-co-VAc) polymers that could be attained in liquid CO₂ at the same pressure limit of 67 MPa were 7.5 wt%, 10 wt% and 8 wt% for the TFE_{11.6}-co-VAc, TFE_{19.3}-co-VAc and TFE_{26.5}-co-VAc polymers, respectively. These results indicate that TFE_{19.3}-co-VAc is close to the optimal composition for CO₂-solubility. These results also suggest that copolymers with a small proportion of TFE are not as likely to form TFE crystalline segments of TFE that are likely to inhibit solubility in CO₂. Because of the relatively low TFE content and copolymerization technique, the probability of lengthy block segments of TFE is low in these copolymers, and hence the propensity to crystallize and form CO₂-insoluble polymers is low.

The copolymers with higher concentrations of TFE, TFE_{46.7}-co-VAc and TFE_{63.3}-VAc, were markedly less CO₂-soluble. TFE_{46.7}-co-VAc was insoluble in CO₂ at temperatures below 75 °C, which is notably less CO₂ soluble than the three copolymers with lower TFE concentrations; however, the copolymer did dissolve at elevated temperatures. At a copolymer concentration of 5 wt% in CO₂, a representative mixture composition that typically yields a cloud point pressure

at or near the maximum cloud-point pressure of this portion of the phase diagram — cloud-point pressures were observed at higher temperatures. The cloud point pressure was found to be 74 MPa at 75 °C and 91 MPa at 128 °C (see Figure 5.8). However, TFE_{63.3}-co-VAc does not dissolve in CO₂ even at 144 °C and 210 MPa. This may be due in part to the increased crystallinity of the copolymer associated with TFE-rich regions or blocks.

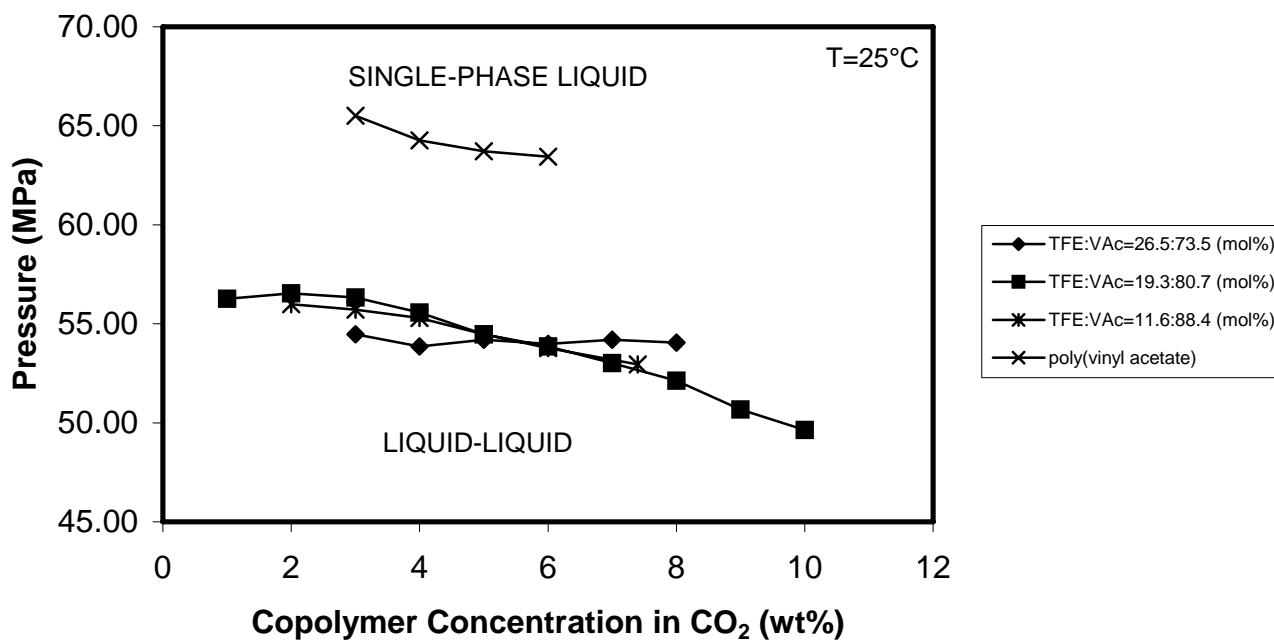


Figure 5.7 Pressure-composition phase diagram for CO₂ + TFE-VAc copolymer system at 25 °C

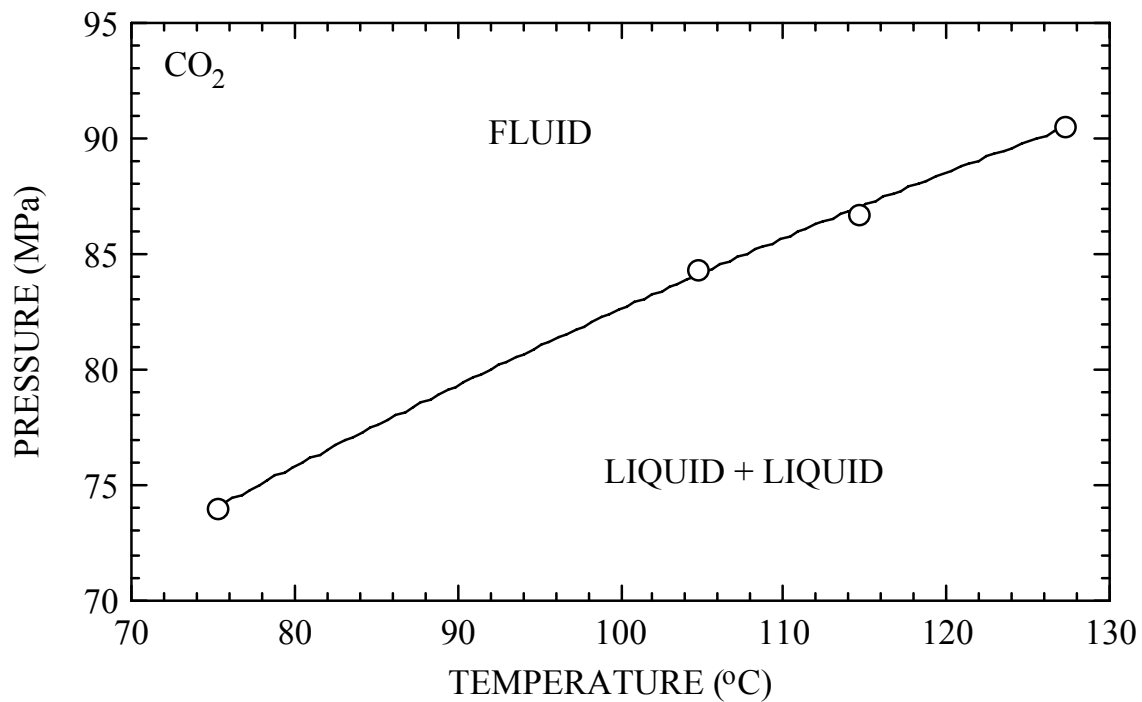


Figure 5.8 Cloud-point curve for ~5 wt% CO₂ + TFE_{46.7}-co-VAc system¹⁷⁰

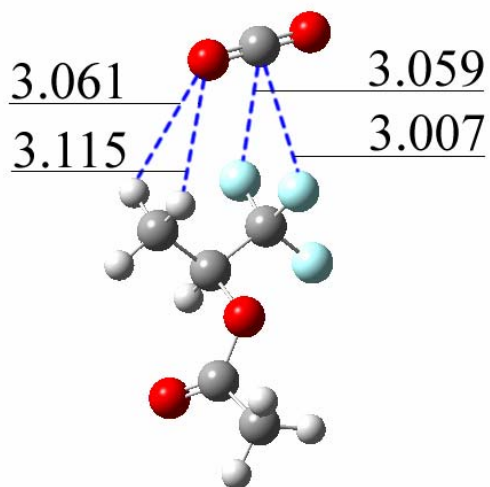


Figure 5.9 Quadridentate binding configuration for CO₂ + TFE-VAc dyad using MP2/6-31+g(d) level of theory

Ab initio molecular modeling was employed to identify reasons for the enhanced solubility of TFE-co-VAc relative to the PVAc homopolymer.¹⁷⁰ A CO₂ molecule can act simultaneously as both a Lewis acid and as a Lewis base if the molecule with which it is interacting has both Lewis base and acid groups. Our molecular modeling results show that this is precisely the case for semi-fluorinated polymers such as TFE-VAc. Not surprisingly, calculations made on the geometry and strength of the interactions between CO₂ and various dyads (TFE-VAc, VAc-VAc, etc.) in the copolymer showed that the presence of the fluorine in the backbone render neighboring protons more acidic. This neighbor effect allows quadridentate binding between CO₂ and the TFE-VAc dyad (Shown in Figure 5.9). The carbon of the CO₂ interacts with the two fluorine atoms while one oxygen of the CO₂ interacts with two hydrogens. However, perfluorinated polymers lack Lewis acid sites and also exhibit very high melting points. Furthermore, O-F interactions are only weakly attractive since both oxygens in CO₂ and the fluorine in the polymer are electron-rich¹⁷¹. This is one of the major reasons that partially fluorinated polymers are more CO₂-philic than perfluorinated ones. Raveendran et al.¹¹⁰ have also observed enhanced binding of CO₂ with partially fluorinated molecules. They performed *ab initio* calculations on CO₂-CF_nH_{4-n} for n=0 to 4. They concluded that there may be an optimal density of fluorine atoms in a molecule leading to maximum CO₂-phicity.¹¹⁰ They attribute this optimal density to the competition among the individual electronegative fluorine atoms. In other words, fluorine atoms in highly fluorinated molecules are less effective electron donors. We believe this effect to be of minor importance compared with the requirement for a molecule to have both Lewis acid and base sites present in the correct geometry to interact simultaneously with CO₂. This is difficult to achieve in a small molecule like CF_nH_{4-n}. We note that Fried and Hu have also studied the binding of CO₂ on semi-fluorinated small molecules using *ab initio*

calculations.¹⁷² They found that quadrupole-dipole interactions between CO₂ and the partially fluorinated molecules contribute significantly to the total interaction energy.¹⁷² Their results are in agreement with our calculations, showing that partially fluorinated molecules should be more soluble than per-fluorinated species.

Another important consideration is that fluorination of methane makes the hydrogen atoms become less acidic compared with hydrogen atoms in methane.¹¹⁰ This is not the case for larger molecules. The hydrogen atoms on the carbon β to the fluorine atom are more acidic than the hydrogens on n-butane. NBO charges for hydrogens on FB and butane are about 0.26 and 0.23, respectively. The enhancement of H-atom acidity relative to the hydrocarbon cannot be observed by studying semi-fluorinated methane.

Binding of CO₂ to carbonyl functional groups is virtually unaffected by the fluorination according to the modeling calculation. In contrast, Raveendran et al. noted that fluorination decreases the carbonyl CO₂-philicity of partially fluorinated acetaldehyde.¹¹² Separation of the fluorine atoms from the carbonyl group by more than one carbon atom mitigates the effect of the fluorine on carbonyl-CO₂ binding, however.

5.2.3 Conclusions

High molecular weight poly(TFE-co-VAc) with TFE content ranging between 11.6-26.5 mol% required lower pressure for dissolution in CO₂ at 25 °C and at low concentrations (<6 wt%) than PVAc homopolymer. Further, these poly(TFE-co-VAc) copolymers were soluble to higher concentrations in CO₂ (7.4-10 wt%) than PVAc (6 wt%). The copolymer composed of 46.7 mol% TFE was not soluble in CO₂ at 25 °C, but was CO₂-soluble at temperatures greater than 75

°C. The copolymer with 63.3 mol% TFE was insoluble in CO₂ at all conditions, possibly due to the presence of TFE blocks, which may be crystalline and thereby reduce solubility. Introduction of hexafluoropropylene units may disrupt this apparent crystallinity while maintaining the fluorocarbon content and enhancing CO₂-solubility.

Ab initio calculations have revealed the following reasons for the increased solubility of poly(TFE-co-VAc) relative to PVAc. (1) The specific geometry and functionality of the polymer gives rise to “quadridentate” binding of CO₂ to the polymer, having interaction energy about 2.5 kJ/mol more favorable than the nonfluorinated analogue. (2) The interaction of CO₂ with the partially fluorinated backbone is 3.7 kJ/mol more favorable than with the hydrocarbon analogue. (3) The electron withdrawing effects of the F atoms on the backbone renders nearby H atoms slightly more acidic, promoting stronger hydrogen bonding with the O atoms in CO₂. Finally, we note that CO₂ acts simultaneously as both a Lewis acid and a Lewis base for many of the binding geometries identified through molecular modeling.

5.3 PHASE BEHAVIOR OF POLYPROPYLENE GLYCOL IN DENSE CARBON DIOXIDE

5.3.1 Introduction

Although the CO₂-philicity of methyl acetate group has been well known for a long time,^{103,105,113,123} Kilic and coworkers suggested ether oxygens are expected as important as carbonyl oxygens in facilitating CO₂ solubility.¹²⁵ The molecular modeling calculation demonstrated that the bonding energy between CO₂ and ether oxygen is comparable with the

energy that CO₂ interacts with the oxygen in carbonyl group. Propyl ethyl ether-functionized siloxane copolymer exhibited a lower cloud point pressure in CO₂ than poly(dimethylsiloxane) of similar molecular weight did. Meanwhile an optimum miscibility pressure was observed in terms of the number of ether side substitutions as a result of the balance between favor and disfavor factor for the dissolution. The flexible ether group on the side chain enhances the entropy of mixing. In addition, the specific interactions between ethers and CO₂ favor the dissolution. However, addition of ether segments improved molecular weight of the copolymer and unfavorable specific interactions between the methylene groups and CO₂, which detracts from the CO₂-philicity of ether side chains.¹²⁵

Besides the ether group was introduced as a side chain in polymer, the CO₂-philicity of the ether groups in backbones on has been extensively studied.^{119,121,131,155} Previous authors have showed that poly(propylene oxide) (PPO) is much more soluble than poly(ethylene oxide) (PEO) in carbon dioxide for a given molecular weight.^{121,131} The pendent methyl group on each monomer unit in poly(propylene oxide) led to a lower cohesive energy density and surface tension that reduces the intermolecular interaction between polymer segments, resulting in a higher solubility of PPO versus PEO in CO₂. However, the solubility of poly(butylene oxide), an ethyl-substituted PEO, and poly(tetrahydrofuran) with respect to PPO were smaller as demonstrated by higher cloud point pressures at a given temperature. The solubility reduction for the first polymer could be explained by the fact that the ethyl substitution adds a larger surface tension increment than the methyl substitution.¹³¹ In the case of poly(tetrahydrofuran), the addition of methylene units in the backbone diluted the effect of the CO₂-philic ether oxygen versus PPO.¹²¹ The phase behavior of a variety of polyether block copolymers was also studied. Without surprise, the solubilities of the block polymers decreased with an increase in the

PEO/PPO ratio for a given molecular weight.¹³¹ Sarbu et al. proposed a design principle which can be used to create a wide range of low-cost CO₂-philes based on oxygenated hydrocarbon polymers, rendering a variety of CO₂-based processes economically favorable and commercially available. Guided by this principle, they synthesized a poly(ether-carbonate) copolymer from PPO and CO₂, in which ethers provided high flexibility and high free volume to enhance the entropy mixing, and the carbonyl groups in carbonate segments which formed Lewis acid – Lewis base interaction with CO₂ favored the enthalpy mixing. The phase behavior study showed that the poly(ether-carbonate) copolymer was even more soluble than those of fluoroether polymer with equivalent chain length by demonstrating a lower miscibility pressure in CO₂.¹⁵⁵ This particular compound is very well suited to the design and synthesis of amphiphilic compounds. Most recently, the poly(propylene glycol) monobutyl ether (PPGMBE) -based surfactants has been successfully developed by our group.¹⁰⁰ The cloud point pressure of PPGMBE 340 (Mn=340 g/mol) pyridinium sulfate exceeded the equipment limit even at concentration of 0.1wt% while the limiting solubility of PPGMBE 340 sodium sulfate is approximately 54 MPa at 0.5 wt%. It was concluded that sodium counterion is less CO₂-phobic than pyridinium counterion. However, it was interesting to observe that PPGMBE 1000 (Mn=1000g/mol) pyridinium sulfate can dissolve in CO₂ at a lower miscible pressure with respects to PPGMBE 340 sodium sulfate at a given concentration, which implied that CO₂-philicity of a longer PPG segment could offset the CO₂-phobicity introduced by pyridinium counterion. More interestingly, the twin-tailed sodium bis(PPGMBE 340) sulfosuccinate has been proved to be the most CO₂-soluble surfactants in the series of PPGMBE-based surfactants.¹⁰⁰ The current work in our group showed that the surfactants are able to form long-

term steady foam in the system of CO₂ and water, which could have potential application in Enhanced Oil Recovery.

PPOs are very important commercial polymers that are used as chemical intermediates in a wide range of industries. The solubility of PPO in water decreases drastically as the molecular weight increases. Generally, PPOs with molecular weight of above 700 g/mol are insoluble in water. On the contrary, their solubilities in hydrocarbons improve with increasing molecular weights. The vast majority of uses of PPO are in preparation of polyurethanes. Their characteristic properties arising from the nature of the polymer backbone suit them to a large variety of applications such as lubricants, surfactants, dispersants, foam control agents, and solubilizers.^{173,174} Taking advantage of the unique physical properties associated with liquid/supercritical CO₂, material chemists and engineers are given rise to a wide range of intriguing opportunities, not only producing novel polymeric materials, but also developing “greener” processing technologies for polymers which could eliminate or avoid the use of hazardous solvents. In order to exploit the CO₂-based technologies for PPO synthesis and processing, it is required to understand the underlying physics and chemistry of PPO + CO₂ solution behavior. Although limited understanding of the physics and chemistry of PPO + CO₂ mixtures has been reported in the previous study as discussed above, significant challenges for exploring phase behavior in a wide scope are urgently driven to be resolved due to the dramatic increase in the public demanding on sustainable products and technologies. The objective of this research was to identify the phase behavior of PPGMBE, whose structure is depicted in Figure 5.10, with different molecular weight in CO₂. The data were compared with the ones in the previous publications.

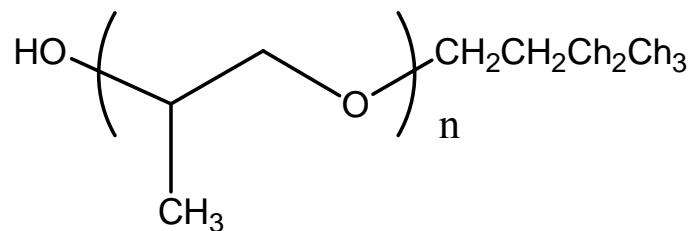


Figure 5.10 Structure of poly(propylene glycol) monobutyl ethers

5.3.2 Results and Discussion

As shown in Figure 5.11, the cloud point pressures obtained in this work are in very good agreement with previously reported results at low concentration by our group. The slight difference between the data is mainly due to the improvement of stirring systems.¹²¹ Instead of a mixing-ball and rocking mixing method used before, the solution mixing is currently achieved by an energetic magnetic mixer with a maximum stirring speed of 2500 RPM. The solution could be fully mixing using this new mixer.

The cloud point result of PPGMBE with various molecular weights at 298 K is shown in Figure 5.12. A global range of concentration, from 0-80 wt%, has been studied. For polymer with $M_n=1000$ and 1200 g/mol, expansion of single-phase solutions resulted in liquid-liquid cloud point. However, vapor-liquid equilibrium was observed when expanding the CO_2 solution of PPGMBE with $M_n=340$ g/mol. When the concentration of solution is close to 0 wt%, all the curves will converge into the vapor pressure of CO_2 at 6.41 MPa. The cloud point pressures dramatically elevate with the increase of the polymers' concentration and molecular weight. According to the thermodynamic principle of mixing, the spontaneous mixing condition is $\Delta G_{\text{mix}} < 0$, which is represented by $\Delta G_{\text{mix}} = \Delta H_{\text{mix}} - T \cdot \Delta S_{\text{mix}}$. Increase of system pressure would balance the unfavorable effects being arisen from increasing concentration towards to

enthalpy of mixing and increasing molecular weight towards to entropy of mixing. These trends have been confirmed by numerous publications.^{115,119,121} At higher concentration, especially above 60 wt%, all the curves converge together again. In this range, the solutions obey Henry's Law. Ideally, all these curves will end up at 0 MPa and 100 wt%.

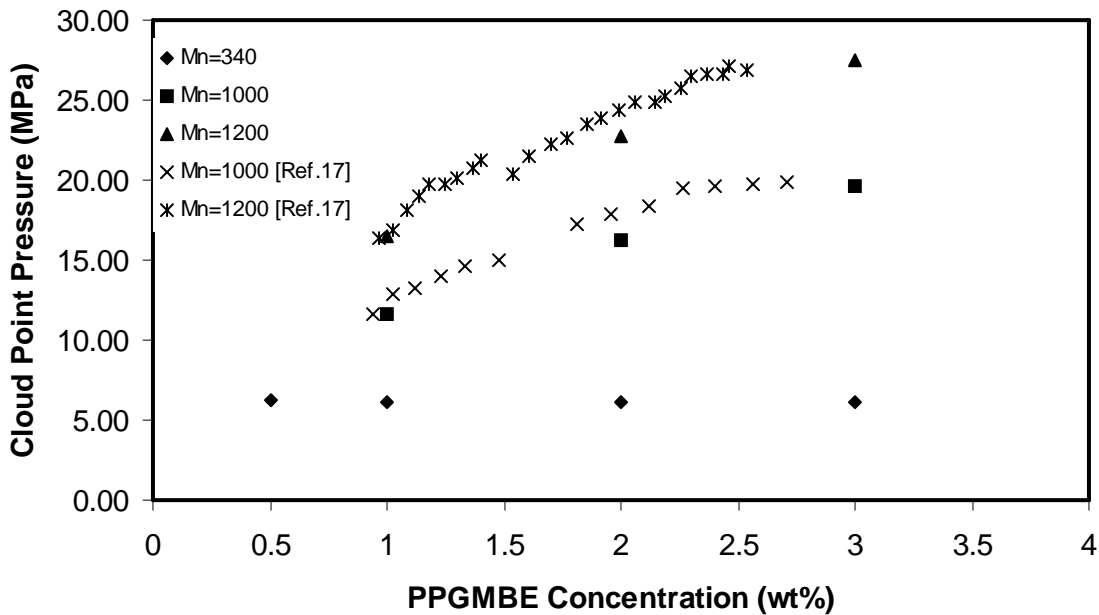


Figure 5.11 The comparison of the cloud point pressures with the published data ¹²¹

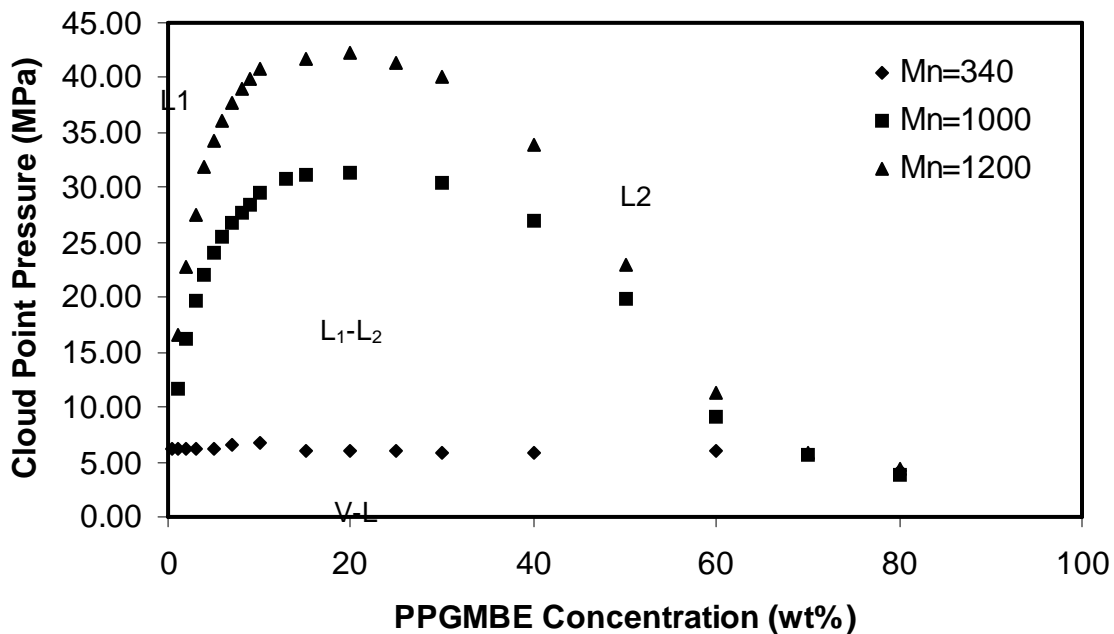


Figure 5.12 Pressure-composition isotherm at 298 K for binary mixture of carbon dioxide with Poly(propylene glycol) monobutyl ethers

Once again, our work, shown in Figure 5.13, confirms that the cloud point pressure is strongly related to the end group. Replacing the hydroxyl end group with ionic groups, sodium sulfate and pyridium sulfate, dramatically decreases the miscibility pressure due to the sharp increase in the intra- and intermolecular interactions by ionic interaction.

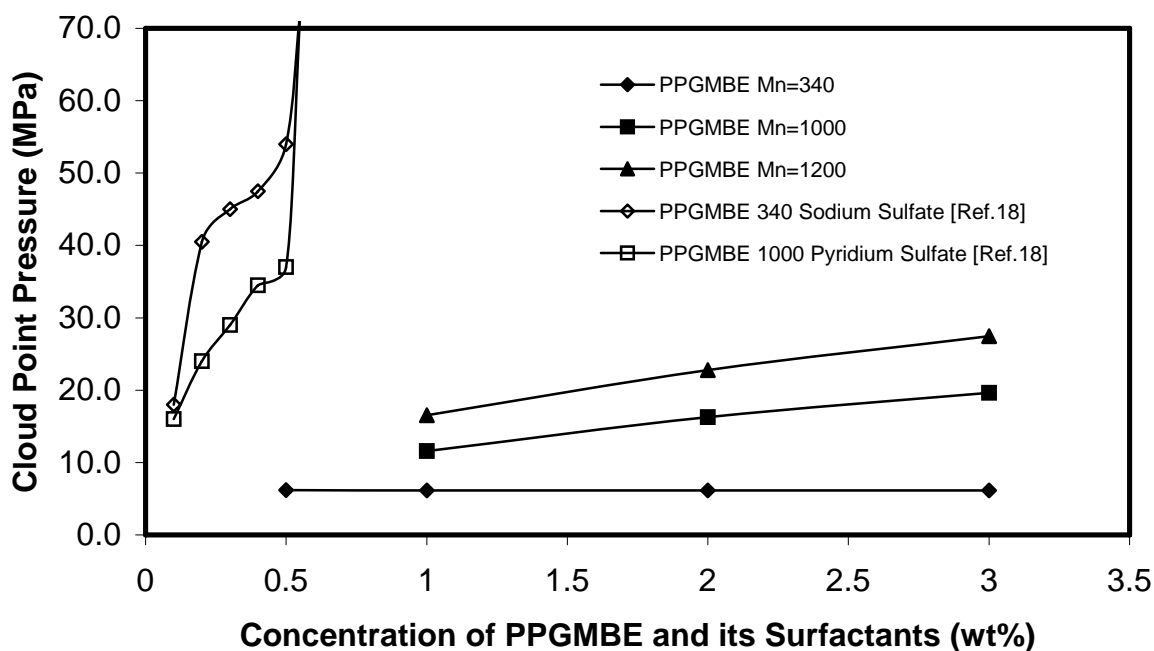


Figure 5.13 The comparison of the phase behavior of PPGMBE with the PPGMBE surfactants ¹⁰⁰

5.3.3 Conclusions

A global pressure-composition phase behavior of PPGMBE has been reported. The data showed high consistence with published data. The effects of molecular weight, concentration, and end group on phase behavior have also been discussed. The phase behavior study demonstrated that the PPGMBE is CO₂-philic. With a wise design, the PPGMBE can be used as construction blocks for CO₂-soluble surfactants, copolymers, thickeners, and dispersants, which would significantly enhance the CO₂ applications in chemical and pharmaceutical industries.

5.4 SOLUBILITY OF TERT-BUTYLATED AROMATICS IN DENSE CARBON DIOXIDE

5.4.1 Introduction

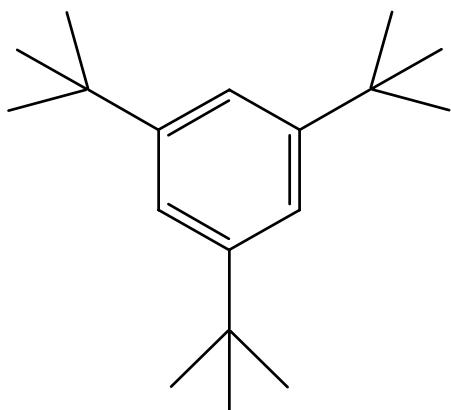
In the design of CO₂-philes, researchers paid tremendous attention on fluorine- and oxygen-contained compounds. That fluorinated compounds were labeled as CO₂-phile could track back to 1992, when DeSimone and colleagues published the first report of a truly “CO₂-philic” material, poly(perfluoroalkyl acrylate) (Poly(FOA)).²⁶ Further study showed that partially fluorinated molecules should be more soluble than perfluorinated species based on both experimental^{115,118,169} and modeling results.^{110,170,172} Modeling simulation presented the hydrogen atoms in some specific positions could be more acidic than typical hydrocarbon ones. When a semifluorinated compound forms CO₂ solution, a CO₂ molecule can act simultaneously as both a Lewis acid (the acidic H and one CO₂ oxygen) and Lewis base (fluorine and CO₂ carbon). Hydrocarbons that show highly CO₂ philic properties always contain oxygens forming either carbonyl or ether. Kazarian et al. proved that carbonyl groups in polymers exhibit specific interactions with CO₂ using FT-IR spectroscopy.¹⁰³ Raveendran and Wallen argued that, besides the well-known Lewis acid-Lewis Base interaction, cooperative C-H···O hydrogen bonding is an additional stabilizing interaction in the solvation of polycarbonyl moieties in CO₂.¹⁰⁵ Our group suggested that ether oxygen atoms are just as important as carbonyl oxygen atoms in facilitating CO₂ solubility of the CO₂-philes.

Besides the extensive study on the interaction between CO₂ and the functional groups, however, some researchers also suggested that high flexibility and high free volume could enhance the entropy of mixing, resulting in a high CO₂ solubility.^{129,175} O’Neill and colleagues

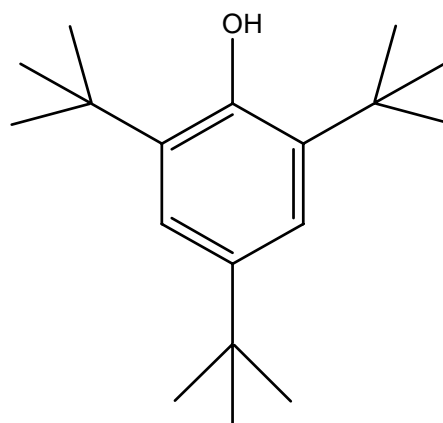
previously noted that most of the CO₂-philes known exhibit relatively weak self-interactions, as evidenced by low cohesive energy density. Many of the identified CO₂-philic materials, such as fluoroacrylates, fluoroethers, and silicones, exhibit a low cohesive density. After studying the CO₂-philicity of a series of poly(ethyleneimine)s, Kilic concluded that the stronger self-interaction of the amine-containing compounds actually elevates their miscibility pressures in CO₂ comparing with those of oxygen-containing analogs, although tertiary amines interact more strongly with CO₂ than do carbonyls.⁸⁷

The objective of our research is to evaluate the effects of molecular structure of hydrocarbon-based compounds (rather than fluorinated or oxygenated hydrocarbon) on CO₂-philicity. Hydrocarbon-based groups should, in general, be the least expensive and most stable moiety for generating CO₂-soluble compounds, especially at low molecular weight. The phase behavior of 1,3,5-tri-tert-butylbenzene (TTBB) and, particularly, 2,4,6-tri-tert-butylphenol (TTBP) (shown in Figure 5.14) were extensively studied. It is well known that butylated phenols, such as butylated hydroxyl toluene (BHT) and butylated hydroxyanisole (BHA), are used as antioxidants in rubbers, plastics, foods, and oils to inhibit or slow oxidative processes, while being it oxidized. Phenolic antioxidants function as free radical terminators and sometimes also as metal chelators.¹⁷⁶ BHT and BHA are used as an antioxidant in plastics, elastomers and petroleum (lubes, greases and waxes), practically bigger market size than food field. BHT is also used as a stabilizer to inhibit the auto-polymerization of organic peroxides^{177,178}. Moreover, TTBP is actually available in railroad car lots at \$3/lb. Therefore Manke, Gulari, Marentis and Enick have proposed CO₂ as a recyclable sand-binding agent, in place of current non-recyclable binders.¹⁷⁹

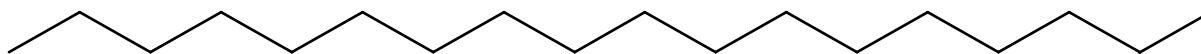
1,3,5-tri-tert-butylbenzene (97%) was purchased from Aldrich and used as received. 2,4,6-tri-tert-butylphenol (96%) were obtained from TCI and recrystallized by a methanol and water mixture before using.



1,3,5-Tri-tert-butylbenzene, TTBB



2,4,6-Tri-tert-butylphenol, TTBP



n-Octadecane

Figure 5.14 Structures of 1,3,5-tri-tert-butylbenzene, 2,4,6-tri-tert-butylphenol, and n-octadecane

Table 5.2 Physical properties of butylated compounds and linear compound (Aldrich)

	Molecular Weight (g/mol)	Boiling Point (°C)
1,3,5-tri-tert-butylbenzene (TTBB)	246.3	121-122
2,4,6-tri-tert-butylphenol (TTBP)	262.43	277
n-octadecane	254.49	317

5.4.2 Results and Discussion

With same number of carbon, molecule with branching groups, TTBB, was observed a much higher solubility than the linear one, n-octadecane (Figure 5.15). Long chain n-alkanes shows orientational order among molecules, which does not exist among more nearly spherical branched alkanes. Upon mixing with CO₂, short-range orientational order is destroyed and hence the mixing process requires more energy with linear alkane than with the branched alkane.

Intermolecular force depends not only on the center-to-center distance but also on the relative orientation of the molecules¹¹⁴. With branching, the shape of a molecule tends to approach that of a sphere and then the surface area per molecule decreases. As a consequence, intermolecular attraction per pair of molecules becomes weaker and a lower kinetic energy is sufficient to overcome that attraction. As shown in Table 5.2, boiling point of n-octadecane is approximately 200 °C higher than TTBB. Hydrogen binding could contribute a higher boiling point for TTBP than TTBB, while is still lower than n-octadecane. Weak self-interactions facilitate branching molecules dissolve in CO₂ comparing with linear ones.¹⁷⁵ It is noted that both TTBP and n-octadecane are hydrocarbons without oxygen, indicating that there is no specific interactions involved as TTBB showed lower CO₂ solubility than n-octadecane did. Therefore, the study implied that, besides consideration of the specific interactions between the solute molecules and CO₂, the design of efficient three-dimensional molecular structure should also be taken significant account of.

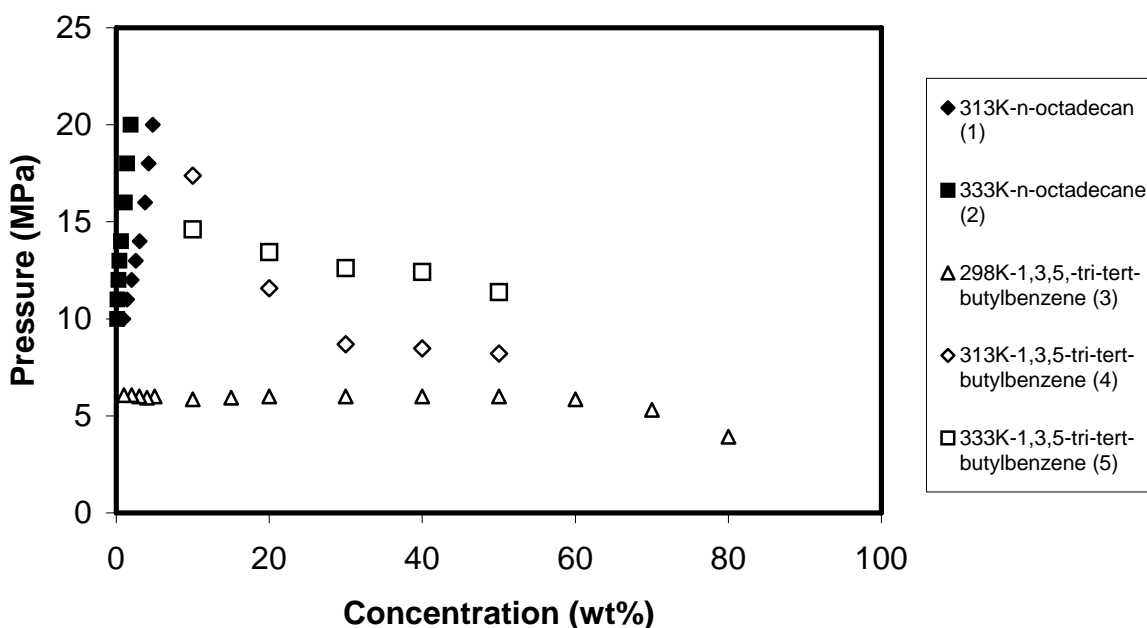
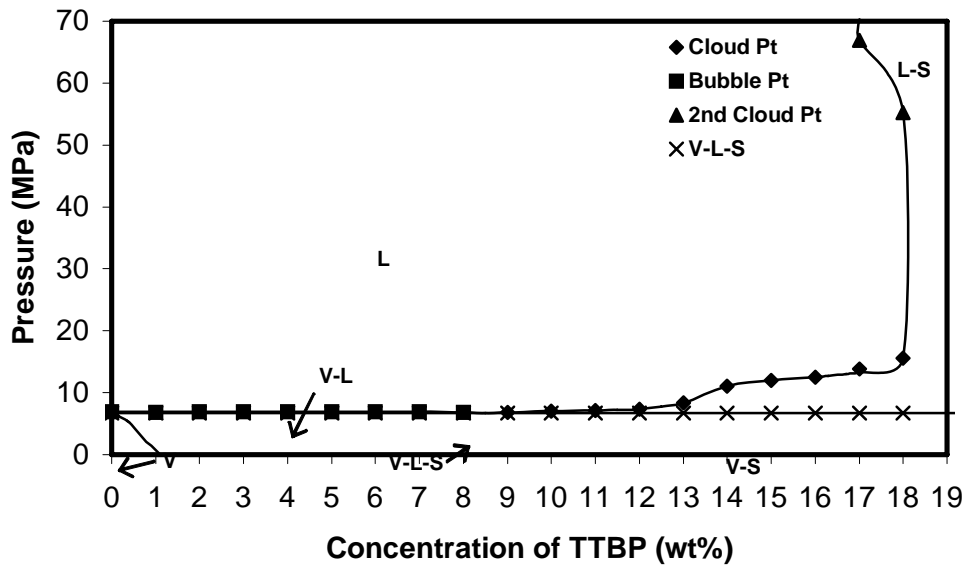


Figure 5.15 Phase behaviors of n-octadecane¹⁸⁰ and 1,3,5-tri-tert-butylbenzene in CO₂

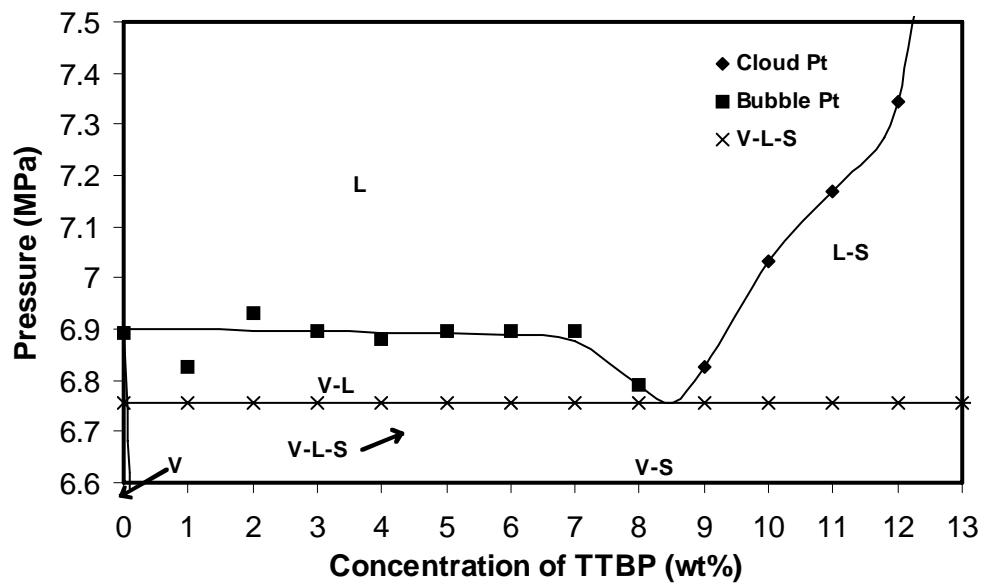
Results for CO₂+TTBP system at 301K, 328K, and 343K are presented in the form of pressure versus composition isotherms in Figure 5.16, Figure 5.17, and Figure 5.18. In the following descriptions, the designations liquid (L) and fluid (F) are used interchangeable. A homogenous phase is denoted as a liquid phase (L) when the temperature is less than critical temperature; otherwise, it is denoted as a fluid phase (F). When the temperature is less than the critical temperature of CO₂, the VL region is bounded by the CO₂ vapor pressure, the VL bubble point locus, a VL dew point locus (but no dew point data was measured for this region), and the three-phase VLS line, as illustrated in a clear vision of Figure 5.16 (b). If the temperatures are greater than the critical temperature of CO₂, the VL envelopes no longer contacts the pressure axis and their areas are much larger than that at 301 K (shown in Figure 5.17 and Figure 5.18). The VL envelope at 301K ends at around 8.5wt%, while the VL envelopes reach 52wt% and

70wt% at 328K and 343K, respectively. The vapor-liquid mixture critical point occurs between 20-25wt% for both at 328K and 343K.

When the isothermal phase diagrams with multiple phases are projected onto a two-dimensional P-T plane, their geometrical representations are simplified because pressure and temperature are field variables, i.e. they are the same in each of the equilibrium phases. A P-T projection for CO₂+TTBP system, presented in Figure 5.19, is proposed according to the pressure-composition isotherms. Curves AC1 and MC2 are the pure component vapor pressure curves of CO₂ and TTBP, respectively. Curve MN is the TTBP melting curve, and curve DM the TTBP sublimation curve. Points C1 and C2 represent critical points for CO₂ and TTBP, respectively. M is the melting point of TTBP. The three pressure-composition isotherms shown in Figure 5.16, Figure 5.17, and Figure 5.18 correspond to the three dashed-line a, b, and c in Figure 5.19 at 301K, 328K, and 343K, respectively. From the one-phase region to lower pressures, isotherm “a” in Figure 5.19 intersects in order the CO₂ vapor pressure curve and VLS three-phase line. Similarly, isotherm “b” and “c” have intersections with the critical mixture curve, DH, and VLS three-phase line. At 328K three-phase VLS line is observed 9.76 MPa which is higher than the VLS equilibrium of 9.24 MPa at 343 K. Nonetheless, the mixture critical point (~16.5 MPa) at 343 K is higher than that (~12.7 MPa) at 328 K.



(a)



(b)

Figure 5.16 Pressure –composition diagram for CO₂ + TTBP system at 301K, (a) a overall view, (b) a close view for low concentration

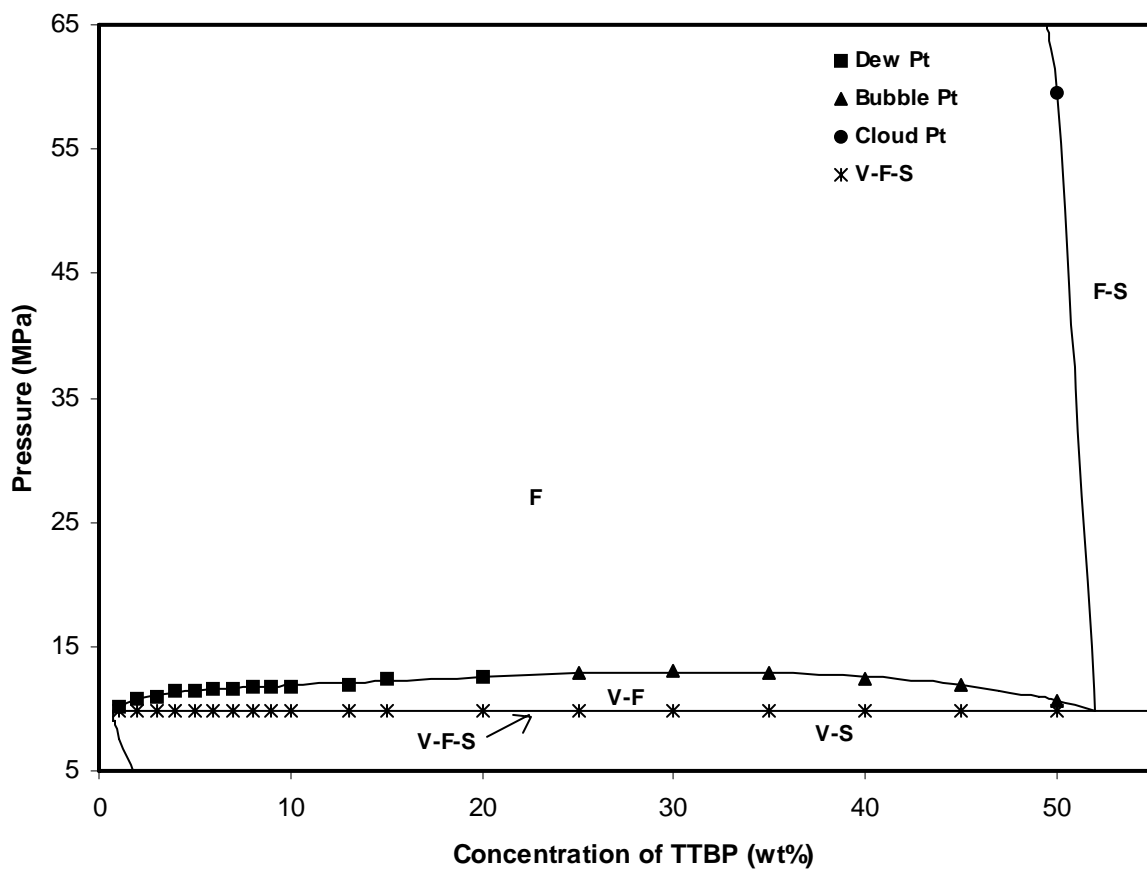


Figure 5.17 Pressure –composition diagram for CO₂ +TTBP system at 328K

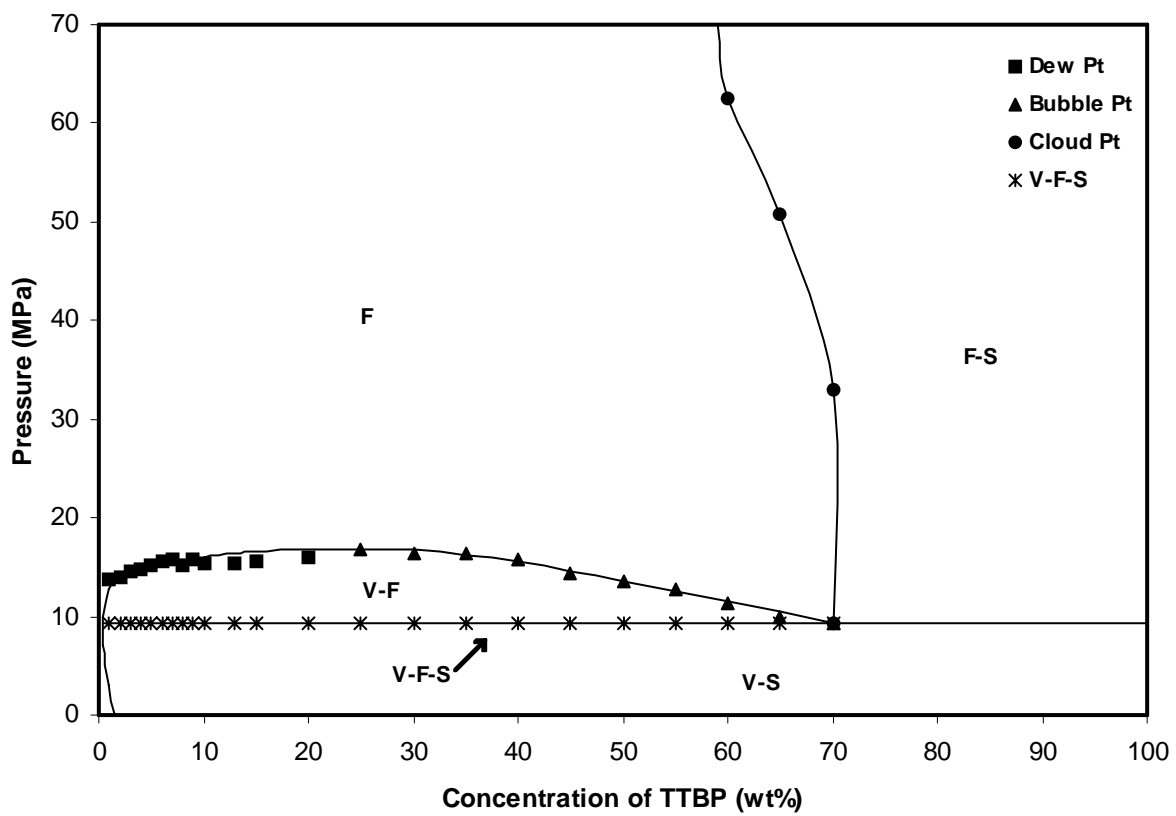


Figure 5.18 Pressure –composition diagram for CO₂ +TTBP system at 343K

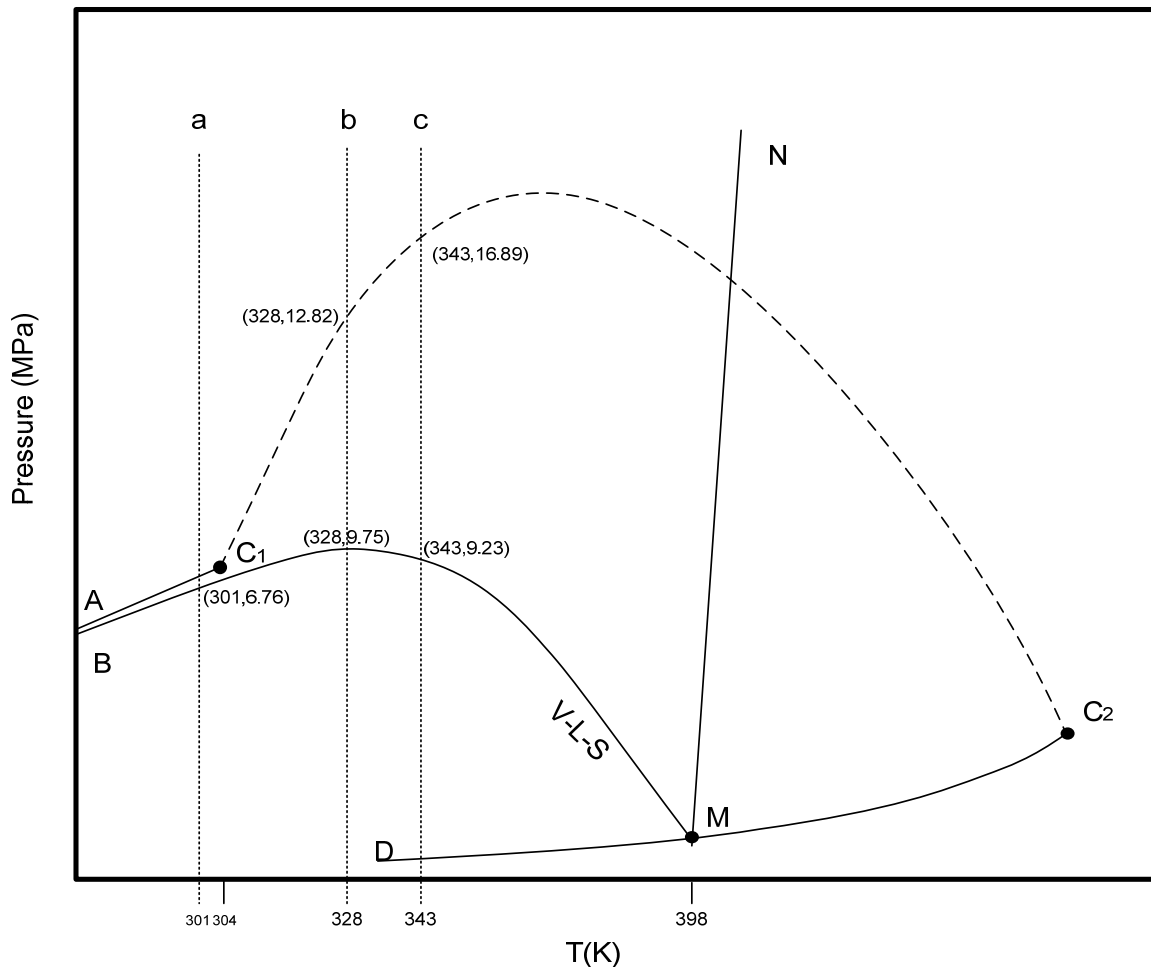


Figure 5.19 P-T diagram for CO₂+TTBP system; C₁ and C₂ represent critical points of CO₂ and TTBP, respectively; M is melting point of TTBP; AC₁ is CO₂ vapor pressure curve; MN and DM are TTBP melting curve and sublimation curve, respectively; BM is three-phase solid-liquid-vapor line; C₁C₂ is the mixture critical curve.

5.4.3 Conclusions

The phase behaviors of tert-butylated benzene and phenol in dense CO₂ were extensively investigated. Without the presence of functional groups such as acetate and ether, branched structure is able to enhance the CO₂ solubility though weakening the interaction forces among solute molecules. These results strongly suggest that molecular structure, exactly like the

functional groups (acetate, ether, etc.), should play significant role in designing hydrocarbon-based highly CO₂ soluble materials.

6.0 VISCOSITY STUDY

6.1 SAMPLES FROM AIR PRODUCTS AND CHEMICALS

The viscosity of three experimental products provided by Air Products and Chemicals were evaluated in CO₂ at room temperature using falling cylinder viscometry. In our experiments, two aluminum cylinders were used, O.D. of 0.0312 (1.228 inch) and 0.0316 m (1.244 inch). Both of them are put in the in the glass tube (ID = 1.250 in) simultaneously in the order of small one on the top of large one. After the tube is turned down, small cylinder falls faster than the large one.

Viscosities of Sample 1 and Sample 2 in CO₂ solution were evaluated at the suggested conditions, 10 wt%, room temperature, and 29.99 MPa (4350 psi). Viscosity of Sample 3 was evaluated at 46.89 MPa (6800 psi) at room temperature and 10wt% because the miscible pressure is determined at 5870 psi at 10wt% and room temperature.

Before sample measurement, viscosities of neat CO₂ were first studied at 4350 and 6800 psi. The results were list in Table 6.1. Increasing the aluminum cylinder's diameter could significantly lower the relative error of the measurement.

Table 6.1* Comparison of neat CO₂ viscosity obtained by falling cylinder viscometer with reference data¹⁸¹

	Aluminum Cylinders	Terminal Velocity (m/s)	Shear Rate (s ⁻¹)	Viscosity (cP)	Viscosity (cP), reference data	Rel. err. (%)
4350psi	r _{cl} =0.0156m	1.14×10 ⁻²	6.38×10 ³	3.85×10 ⁻¹	1.19×10 ⁻¹ (4350psi)	246.85
	r _{cl} =0.0158m	1.14×10 ⁻³	6.87×10 ³	1.09×10 ⁻¹	1.19×10 ⁻¹ (4350psi)	1.27
6300psi	r _{cl} =0.0156m	1.34×10 ⁻²	7.48×10 ³	3.17×10 ⁻¹	1.32×10 ⁻¹ (6300psi)	139.94
	r _{cl} =0.0158m	1.50×10 ⁻³	9.07×10 ³	8.02×10 ⁻²	1.32×10 ⁻¹ (6300psi)	39.39

* The experimental data present in Table B.1.

The results are shown in Table 6.2. Comparing all the viscosities of three sample solutions with the viscosity of neat CO₂ at same conditions, there is no significant enhancement in the carbon dioxide viscosity observed. Inversely, the viscosities of S1 and S2 are smaller than those of neat carbon dioxide.

Table 6.2* Viscosities of neat CO₂ and S1, S2, and S3 in CO₂ at 298 K and 10 wt%.

	Aluminum Cylinders	Terminal Velocity (m/s)	Shear Rate (s ⁻¹)	Viscosity (cP)	Viscosity of Neat CO ₂ (cP)
S1 (29.99 MPa)	I (r _{cl} =0.0156m)	1.57×10 ⁻²	8.76×10 ³	2.80×10 ⁻¹	3.85×10 ⁻¹ (29.99MPa)
	II (r _{cl} =0.0158m)	1.56×10 ⁻³	9.43×10 ³	7.96×10 ⁻²	1.09×10 ⁻¹ (29.99MPa)
S2 (29.99 MPa)	I (r _{cl} =0.0156m)	1.64×10 ⁻²	9.15×10 ³	2.68×10 ⁻¹	3.85×10 ⁻¹ (29.99MPa)
	II (r _{cl} =0.0158m)	1.55×10 ⁻³	9.36×10 ³	8.02×10 ⁻²	1.09×10 ⁻¹ (29.99MPa)
S3 (46.89 MPa)	I (r _{cl} =0.0156m)	1.29×10 ⁻²	7.20×10 ³	3.29×10 ⁻¹	3.17×10 ⁻¹ (46.89MPa)
	II (r _{cl} =0.0158m)	1.29×10 ⁻³	7.79×10 ³	9.32×10 ⁻²	8.01×10 ⁻² (46.89MPa)

* The experimental data present in Table B.2.

6.2 VISCOSITY OF SUGAR ACETATE IN CO₂

Viscosity of β -D-galactose pentaacetate, whose structure is shown in Figure 6.1, in CO₂ was determined at 313 K and 17.23 MPa (2500 psi) using the cylinder with a radius of 0.0158 m. Galactose pentaacetate exhibited very high CO₂-philicity. 25 wt% sugar acetate showed solubility in CO₂ under 11 MPa at 313 K.¹¹² The viscosity data are collected in Table 6.3 and relative viscosity versus concentration is plotted in Figure 6.2. It is noted that the viscosity of CO₂ at same condition is 0.0738 cp from reference,¹⁸¹ which has a relative error of 11.83%. Even at 25wt%, the viscosity of mixture of sugar acetate and CO₂ did not show significant difference from that of neat CO₂. This is attributed to that sugar acetate does not form effective intermolecular association in CO₂ solution.

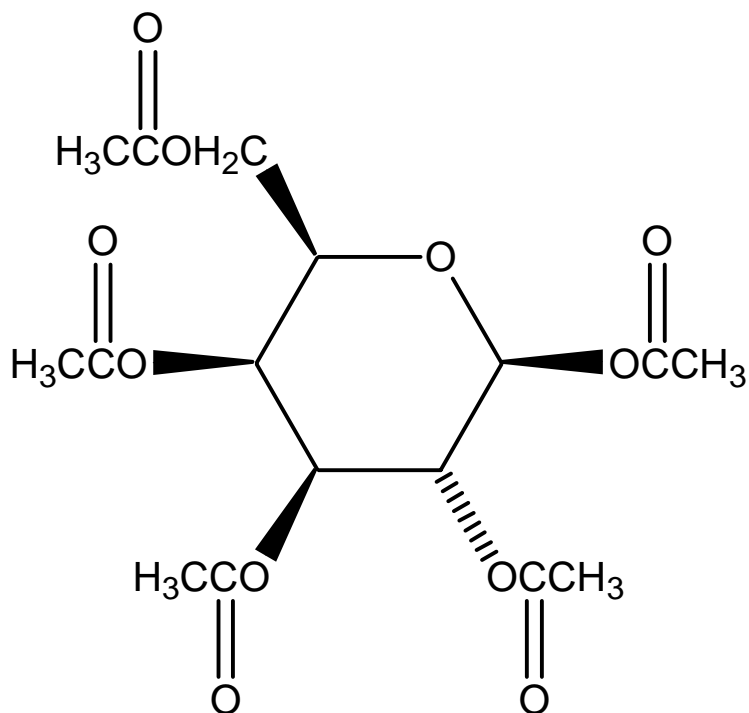


Figure 6.1 Structure of β -D-galactose pentaacetate

Table 6.3* Viscosity of neat CO₂ and galactose pentaacetate solutions at 313 K and 17.24 MPa (2500 psi)

Concentration (wt%)	Viscosity (cp)
0 (neat CO ₂)	0.0825
12	0.1117
18	0.1510
25	0.1707

* The experimental data present in Table B.3.

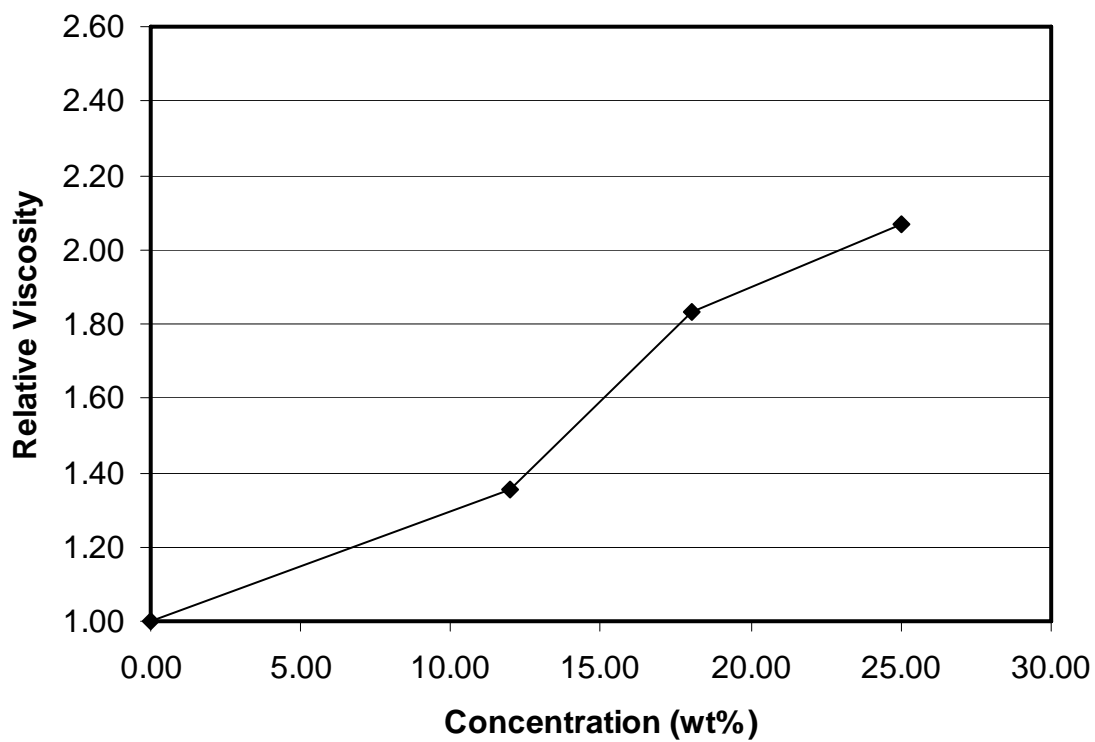


Figure 6.2 Relative viscosity of β -D-galactose pentaacetate solution in CO_2 at 313 K and 17.24 MPa

7.0 SUMMARY

1. PAO was indeed soluble in CO₂, which represents a new addition to the very short list of CO₂-soluble polymers. PAO showed higher cloud point pressure than poly(vinyl acetate) with same chain length, which is not agreement with the modeling prediction. It is believed that the elevation of cloud point pressure is a result of high concentration of CO₂-phobic hydroxyl end groups of PAO with low molecular weights.
2. PVMME and PVMEE were indeed soluble in CO₂, which represents two more new additions to the very short list of CO₂-soluble polymers. Poly(vinyl methoxymethyl ether) (PVMME) was more CO₂ soluble than poly(vinyl 1-methoxyethyl ether) (PVMEE), though, contrary to expectations. Although PVMEE has a higher free volume than PVMME does, the methyl group on the side chain, between the two oxygen atoms would block CO₂ approaching oxygen to form effective interactions. It is believed to be one of the main reasons for the decrease in solubility of PVMEE.
3. CTA oligomers, up to tetramer (Mw=1361.07 g/mol), showed very high CO₂-philicity. In the testing range, 1-5wt%, the phase boundaries evolve from bubble points to dew points as the numbers of repeat units increases. All the phase behaviors of dimer, trimer and tetramer in CO₂ were characterized with a VLL equilibrium lines which are the distinguishing feature of high CO₂-philicity. The unique phase behavior has been comprehensively studied using CO₂+ β -D-maltose octaacetate system as a model.

4. High-pressure phase behavior for a binary mixture of the CO₂-philic solid β-D-maltose octaacetate (T_m = 432 K) with carbon dioxide was determined. Both critical end points (LCEP and UCEP) and pressure-composition isotherms at 283, 298, and 323 K were measured in order to identify the global phase behavior for this system. The pressure-temperature projection of this system has the fluid-phase features of a Scott and Van Konynenburg Type V system. One of the distinguishing features of the CO₂ + maltose octaacetate system is a long VL₁L₂ line, which extends over a range of more than 20 K. The solubility of maltose octaacetate in CO₂ can be explained by the interaction between a Lewis base (the carbonyl groups of maltose octaacetate) and a Lewis acid (CO₂).
5. The solubility of the random copolymers of tetrafluoroethylene (TFE) and vinyl acetate (VAc) at 25 °C in CO₂ reduced after reaching a maximum value at a TFE molar concentration of 19.3 mol%. The 46.7 mol% TFE copolymer only dissolved in CO₂ at elevated temperatures, whereas the 63.3 mol% TFE copolymer did not dissolve in CO₂ even at temperatures in excess of 144 °C and pressures of 210 MPa. The molecular modeling results show that the interaction of CO₂ with acetate side group was not affected by presence of fluorine in the polymer backbone; therefore, the enhanced solubility of the semi-fluorinated copolymers is attributable to the enhanced binding between CO₂ and the semi-fluorinated backbone of the copolymer when the CO₂ molecule can access both the fluorinated (Lewis base) and hydrogenated (Lewis acid) parts of the backbone simultaneously.
6. A global pressure-composition phase behavior of PPGMBE confirmed that ether-CO₂ interactions should receive as much attention as the well-known carbonyl-CO₂ interactions in the design of CO₂-soluble surfactants, copolymers, and thickeners.

7. TTBB and TTBP were very CO₂ soluble solids at room temperature that exhibiting both melting point depression and extremely high solubility in CO₂. Global phase behaviors of TTBP were determined at different temperatures and a pressure-temperature phase diagram was also presented.
8. The viscosities of three company samples and β-D-galactose pentaacetate solutions in high-pressure CO₂ were evaluated using falling cylinder viscometer. No substantial viscosity enhancement was observed in all the samples, indicating that there were no effective intermolecular associations for all the samples.
9. Figure 7.1 showed an upgraded plot for Figure 2.3. So far, this figure is the most throughout collections of the phase behavior results for oxygenated hydrocarbon-based CO₂-soluble polymers.

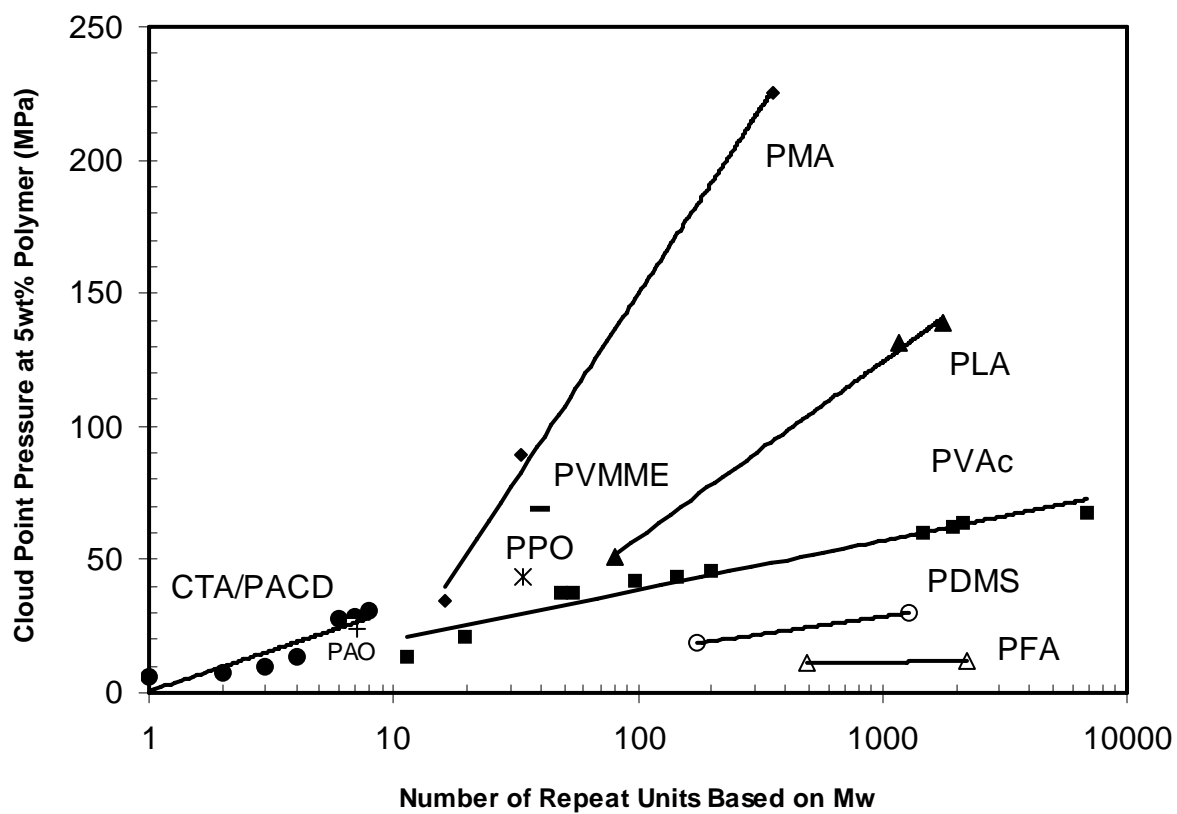


Figure 7.1 Upgraded Figure 2.3

8.0 FUTURE WORK

10. *Ab initio* modeling results showed that PAO is a highly attractive candidate for new generation CO₂-soluble materials because its functional groups exhibit very high binding energies with CO₂ molecules comparing to PVAc does. New synthetic routes are needed to be explored for preparing high molecular weight PAO, and then its CO₂ solubility needs to be evaluated;
11. CTA oligomers with longer repeat units need to be purified and characterized. Their phase behaviors are to be determined in a wider concentration range. New type of surfactants and copolymers can be designed using CTA oligomers as the CO₂-philic segments;
12. Following the synthesis procedure of PVMME, a new poly(vinyl ether), shown in Figure 8.1, will be prepared.

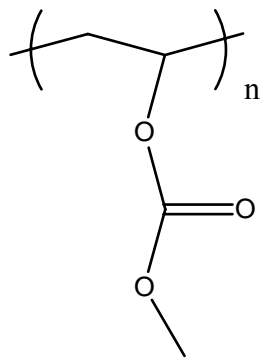


Figure 8.1 Structure of a new poly(vinyl ether) for future work

13. Acylated sugars show very high CO₂-philicity. A new design of CO₂-soluble polymer is to use the acylated sugar as the side chains as shown in Figure 8.2. The polymer can be synthesized by a cationic polymerization described by Yamada and coworkers.¹⁸²

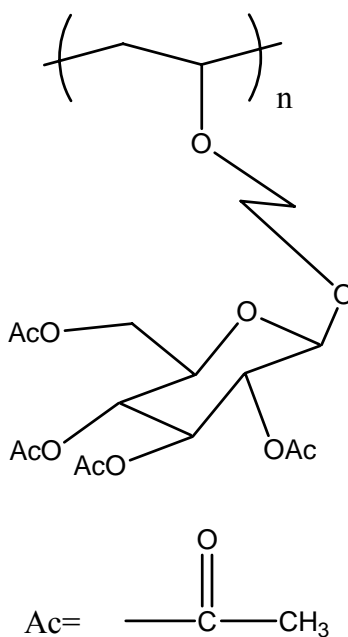
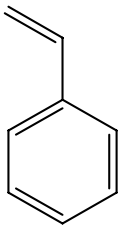
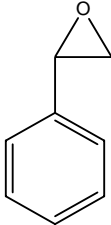
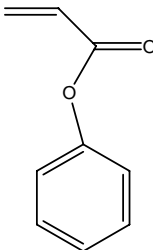
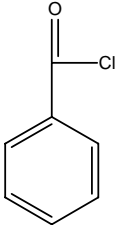


Figure 8.2 Structure of poly(1-O-(vinylloxy)ethyl-2,3,4,6-tetra-O-acetyl-β-D-glucopyranoside) (poly(AcGlcVE))

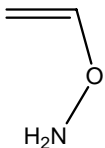
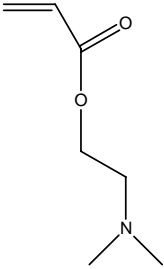
14. To design CO₂-thickeners, intermolecular association groups will incorporate into highly CO₂ soluble polymer chains. Two types of association groups are proposed. Pendant phenyl group can enhance viscosity of CO₂ solution remarkably.⁹¹ The enhancement of viscosity is achieved by the π - π stacking of the phenyl groups. Fortunately, the phenyl groups are only mildly CO₂ phobic relative to ionic or polar associating groups and therefore do not dramatically diminish the thickener solubility in CO₂ when the groups were introduced into the polymers. Structures of phenyl candidate group are summarized in Table 8.1.

Table 8.1 Thickening candidates with phenyl groups

Styrene	Styrene oxide	Phenyl acrylate	Benzoyl chloride
			

Previous work has demonstrated that amines can form organogel with CO₂, in which CO₂ reacts with the amine group to form carbamic acid zwitterinons.¹⁸³ Zwitterions then perform proton exchange with a neighbor amine to form the ion-counterion crosslink. Hence we proposed to incorporate the amine function groups into the highly CO₂ soluble polymers in order to improve viscosity of CO₂ solution. Two proposed structure are shown in Table 8.2. The introduction of ether and acetate groups to the amines is to ensure certain solubility in CO₂ for the thickeners.

Table 8.2 Proposed amino groups for CO₂ thickening groups

Vinyl amino ether	Dimethyl aminoethyl acrylate
 <p>The chemical structure of vinyl amino ether consists of a vinyl group (CH₂=CH-) attached to an oxygen atom, which is in turn bonded to an amino group (-NH₂). The structure is shown as a skeletal formula with a double bond on the left, a single bond to an oxygen atom, and a single bond to an amino group.</p>	 <p>The chemical structure of dimethyl aminoethyl acrylate features an acrylate backbone (CH₂=CH-C(=O)-O-) connected to a two-carbon ethyl chain, which is terminated by a dimethylamino group (-N(CH₃)₂). The structure is shown as a skeletal formula with a double bond on the left, a carbonyl group, an oxygen atom, an ethyl chain, and a nitrogen atom with two methyl groups.</p>

APPENDIX A

¹H NMR SPECTRA OF COMPOUNDS IN CHAPTER 3

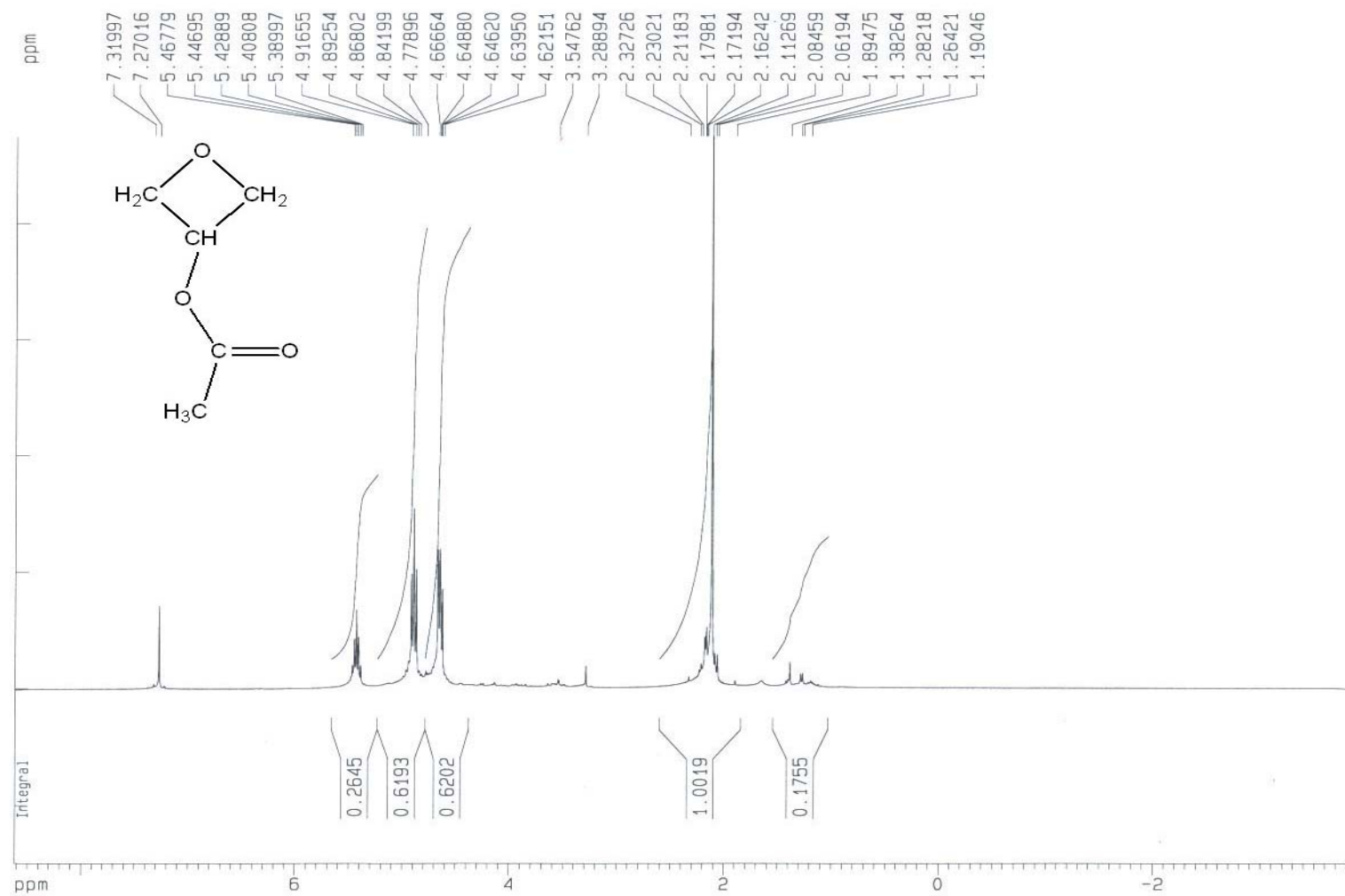


Figure A. ^1H NMR (300 MHz, CDCl_3) spectrum of 3-acetoxy oxetane

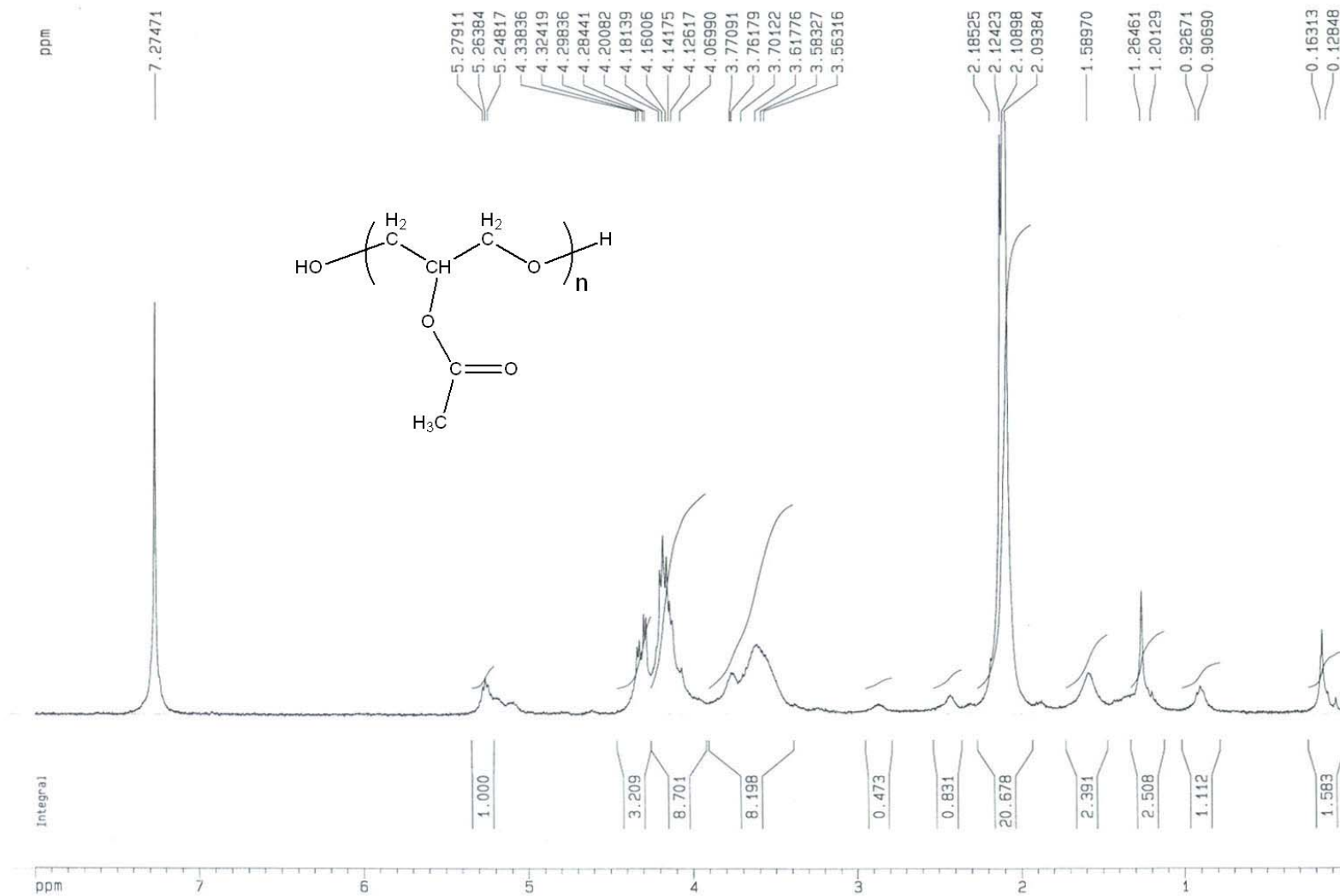


Figure A. 2 ^1H NMR (300 MHz, CDCl_3) spectrum of poly(3-acetoxy oxetane) (polymerization I)

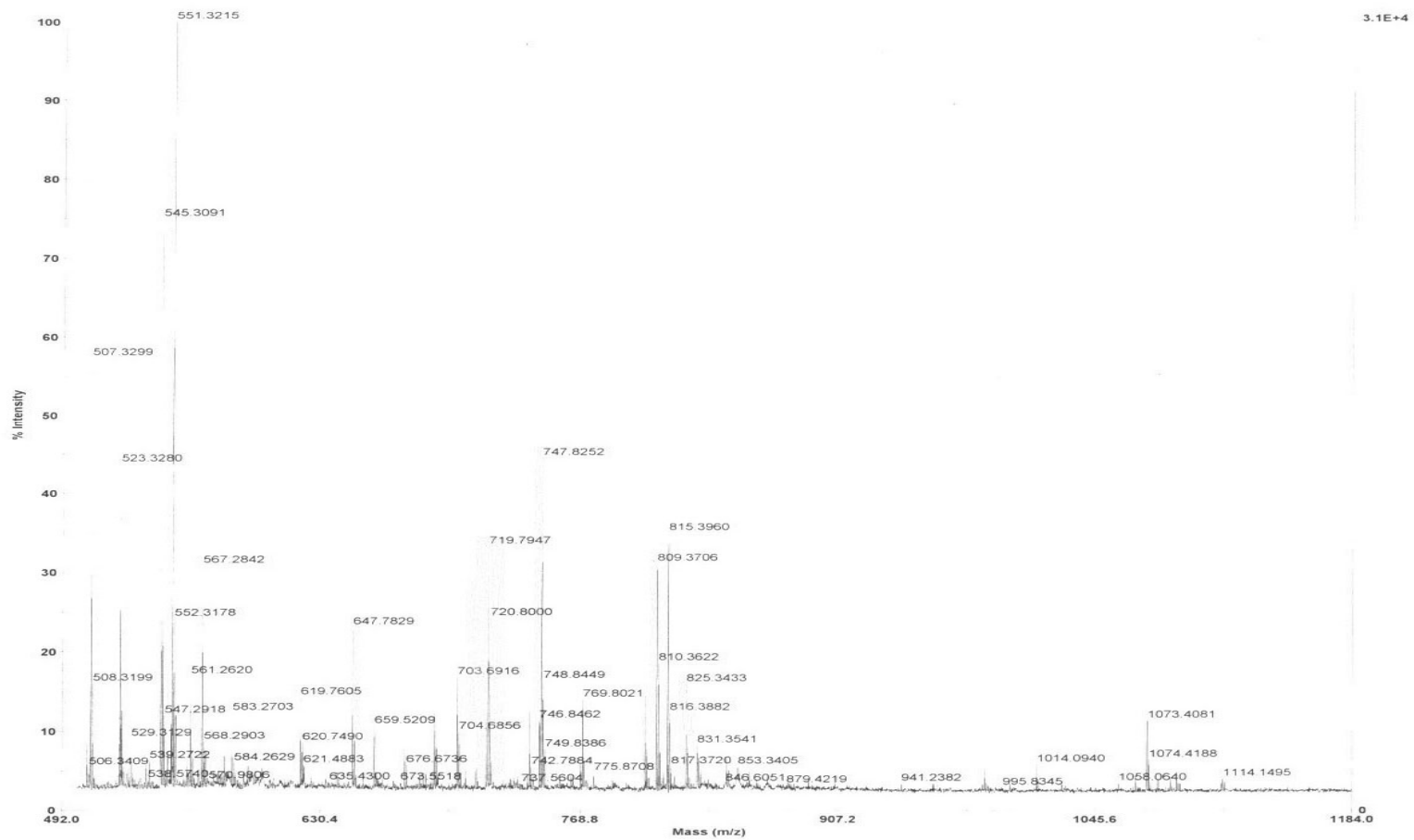


Figure A. 3 MALDI spectrum of poly(3-acetoxy oxetane) (polymerization I)

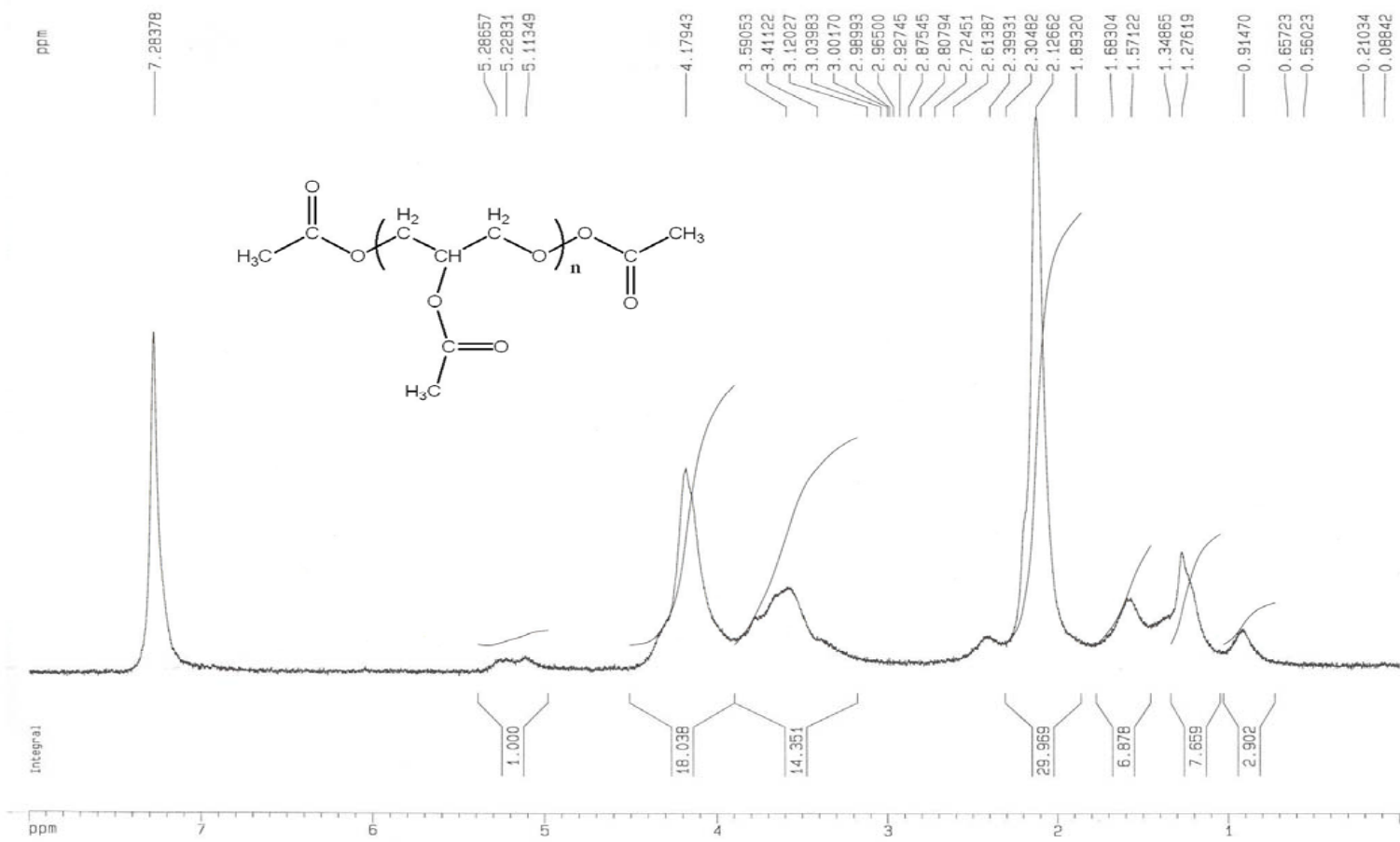


Figure A. 4 ¹H NMR (300 MHz, CDCl₃) spectrum of poly(3-acetoxy oxetane) (polymerization II)

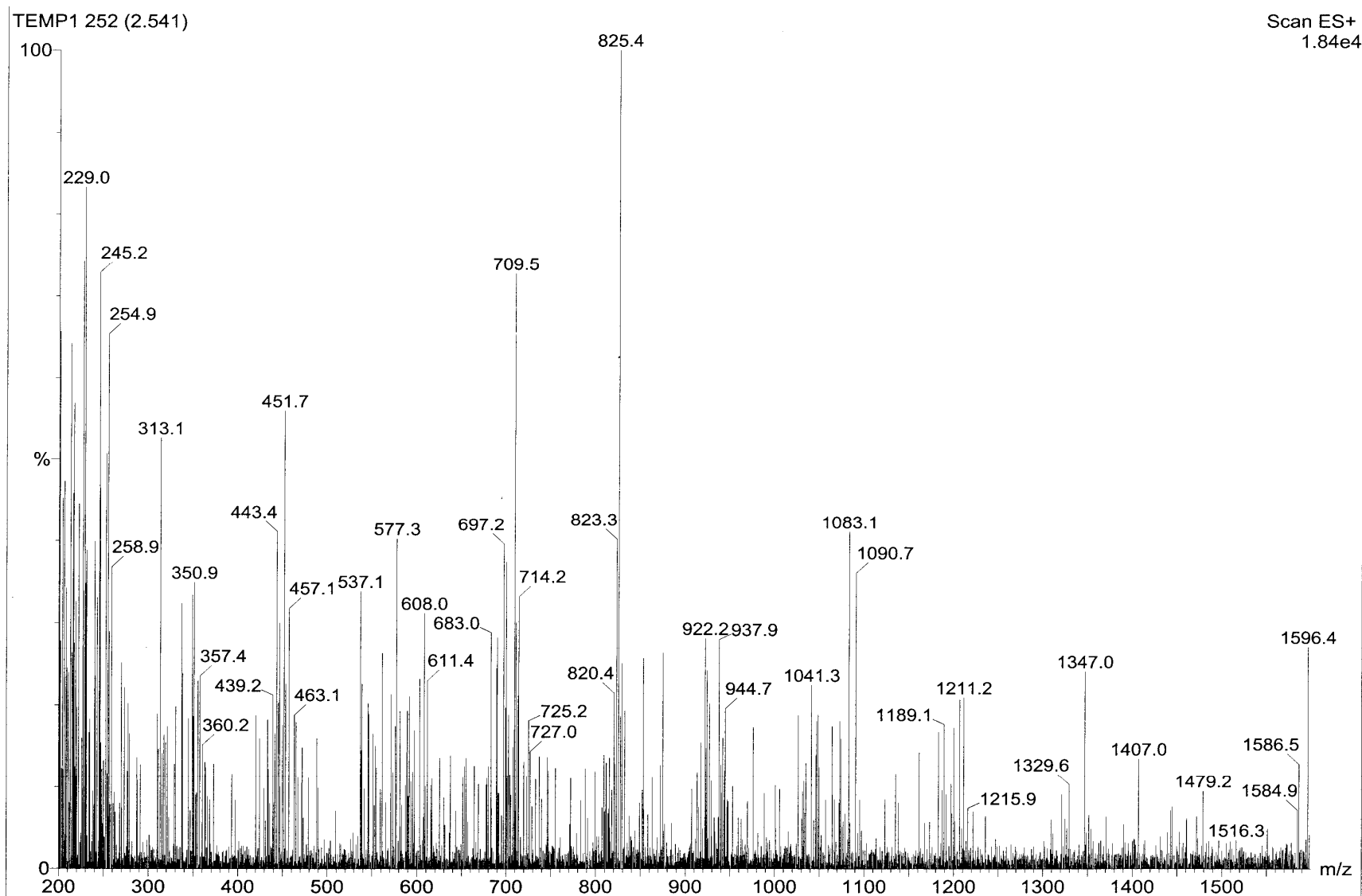


Figure A. 5 MALDI spectrum of poly(3-acetoxy oxetane) (polymerization II)

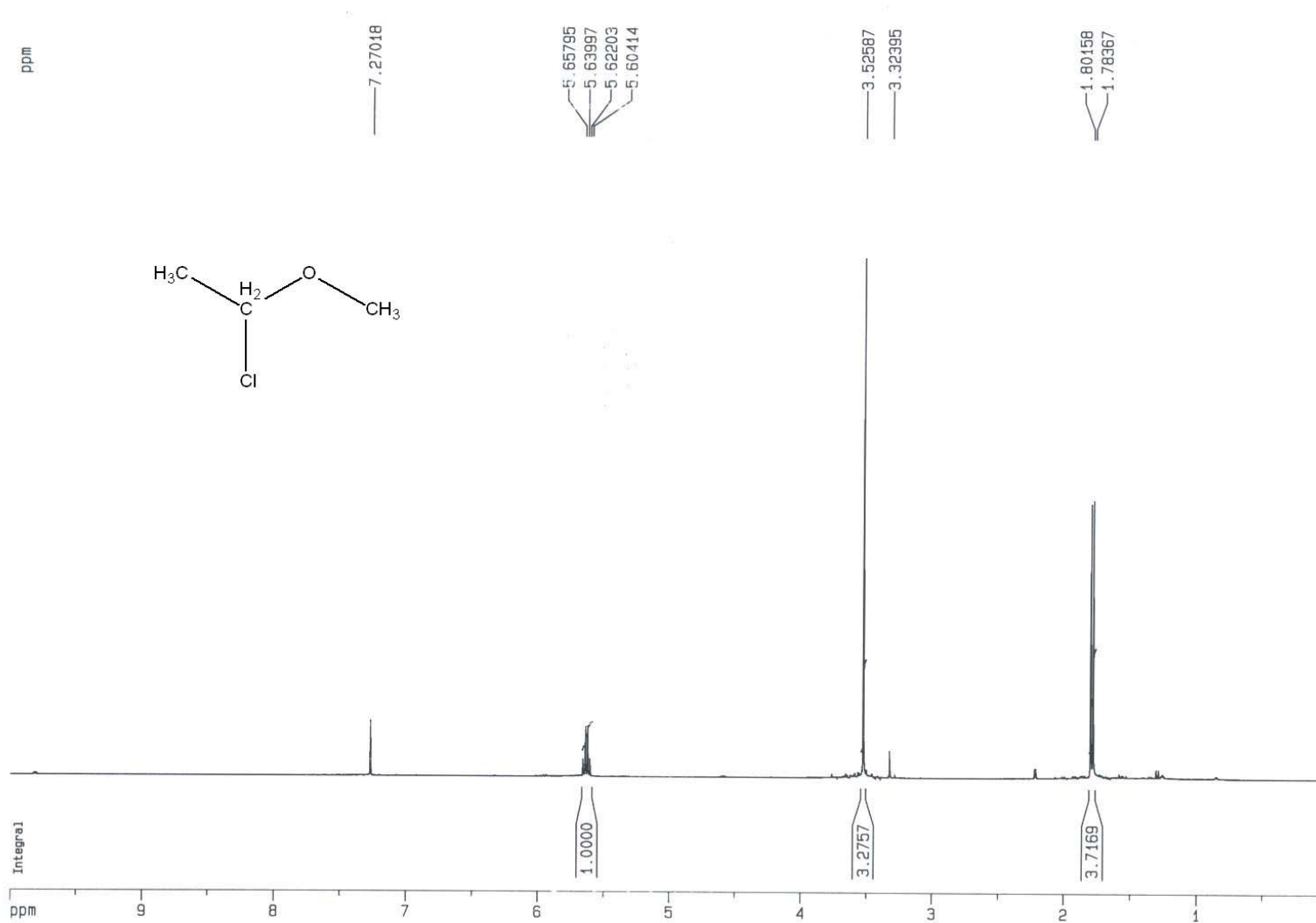


Figure A. ^1H NMR (300 MHz, CDCl_3) spectrum of 1-chloroethyl methyl ether

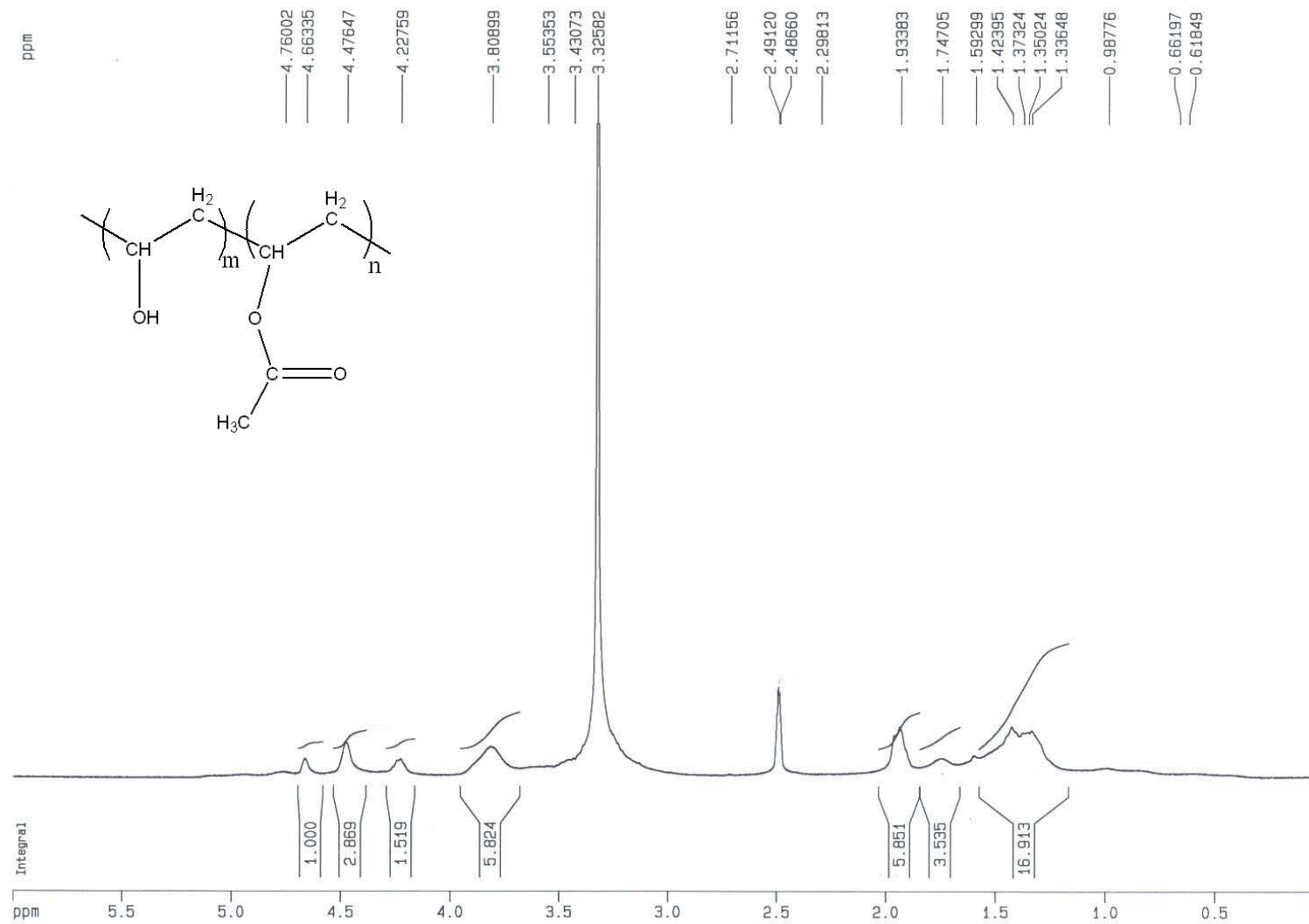


Figure A. 7 ^1H NMR (300 MHz, DMSO-d_6) spectrum of poly(vinyl ether)

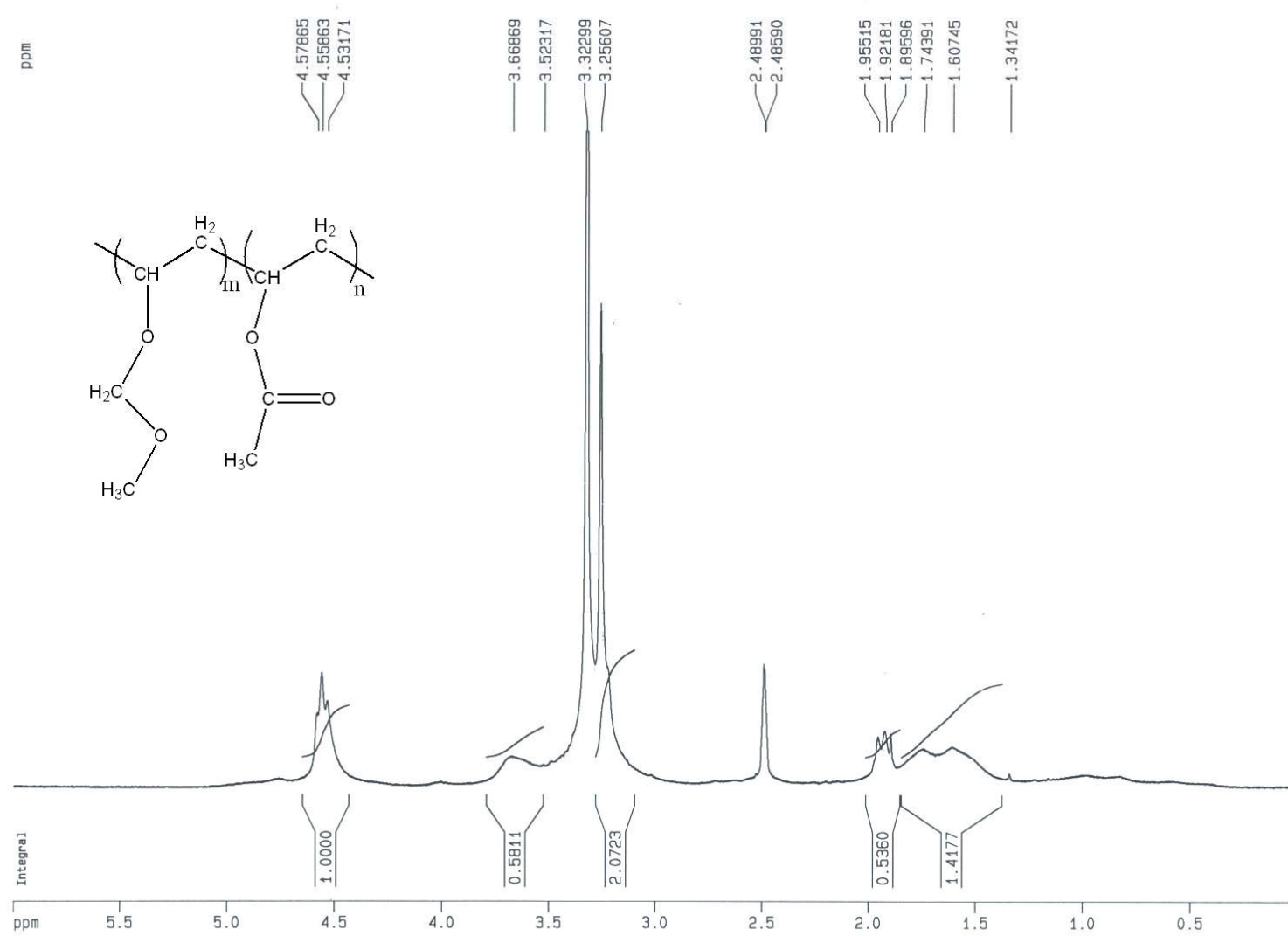


Figure A. 8 ^1H NMR (300 MHz, DMSO-d_6) spectrum of poly(vinyl methoxy methyl ether)

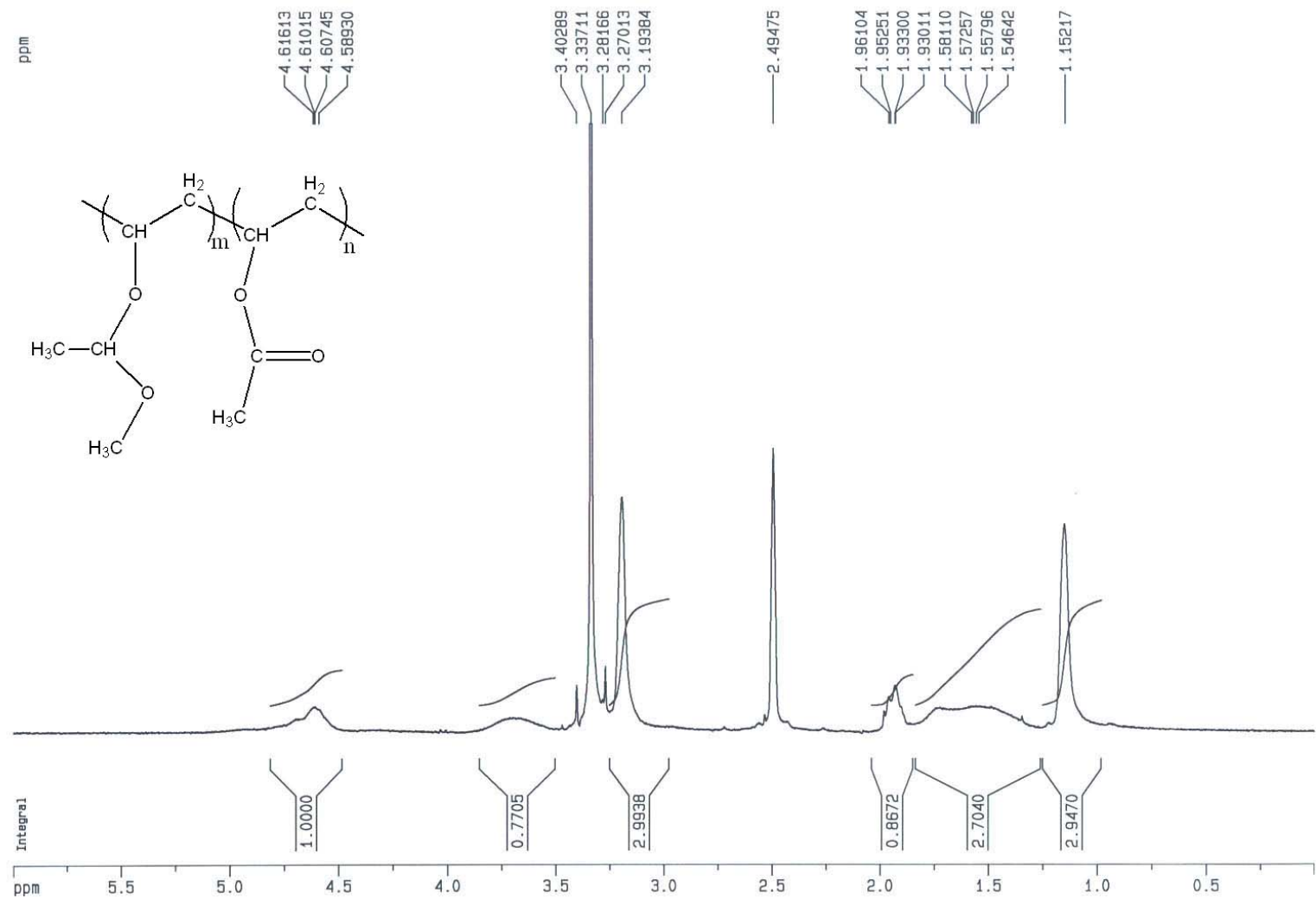


Figure A. 9 ^1H NMR (300 MHz, DMSO-d_6) spectrum of poly(vinyl 1-methoxyethyl ether)

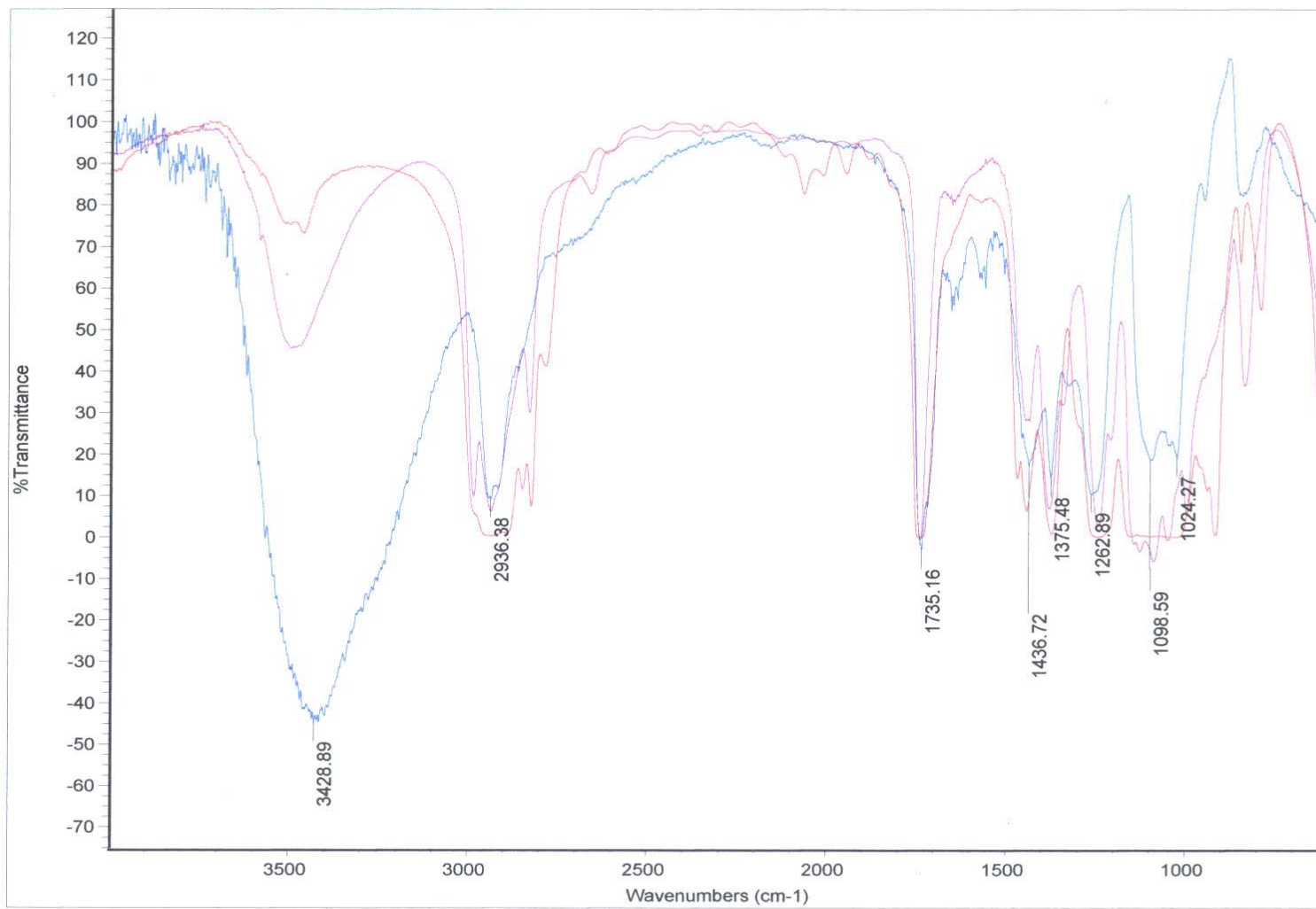


Figure A. 10 IR spectra of PVA, PVMME, and PVMEE

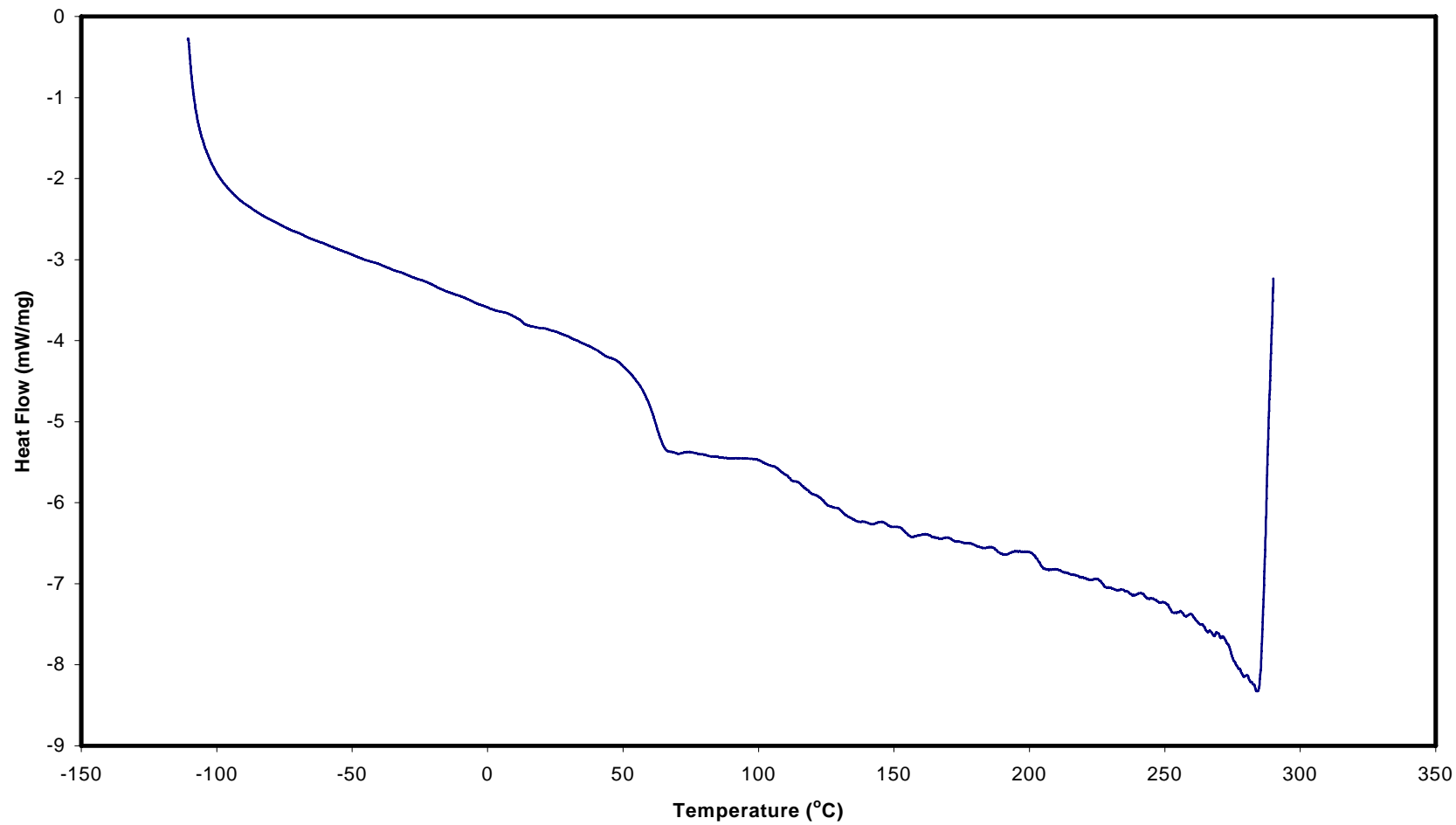


Figure A. 11 DSC for poly(vinyl alcohol)

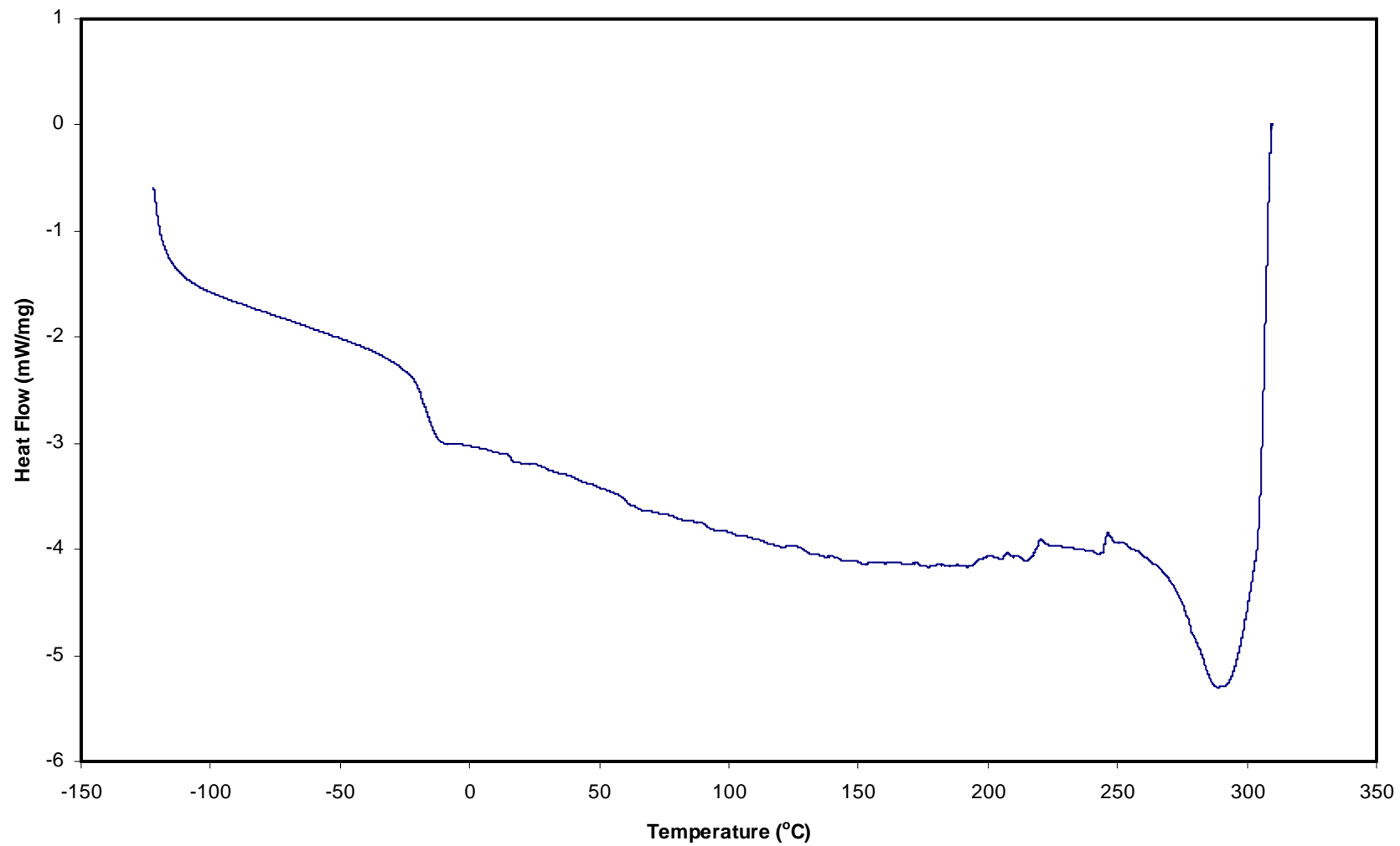


Figure A. 12 DSC for poly(vinyl methoxymethyl ether)

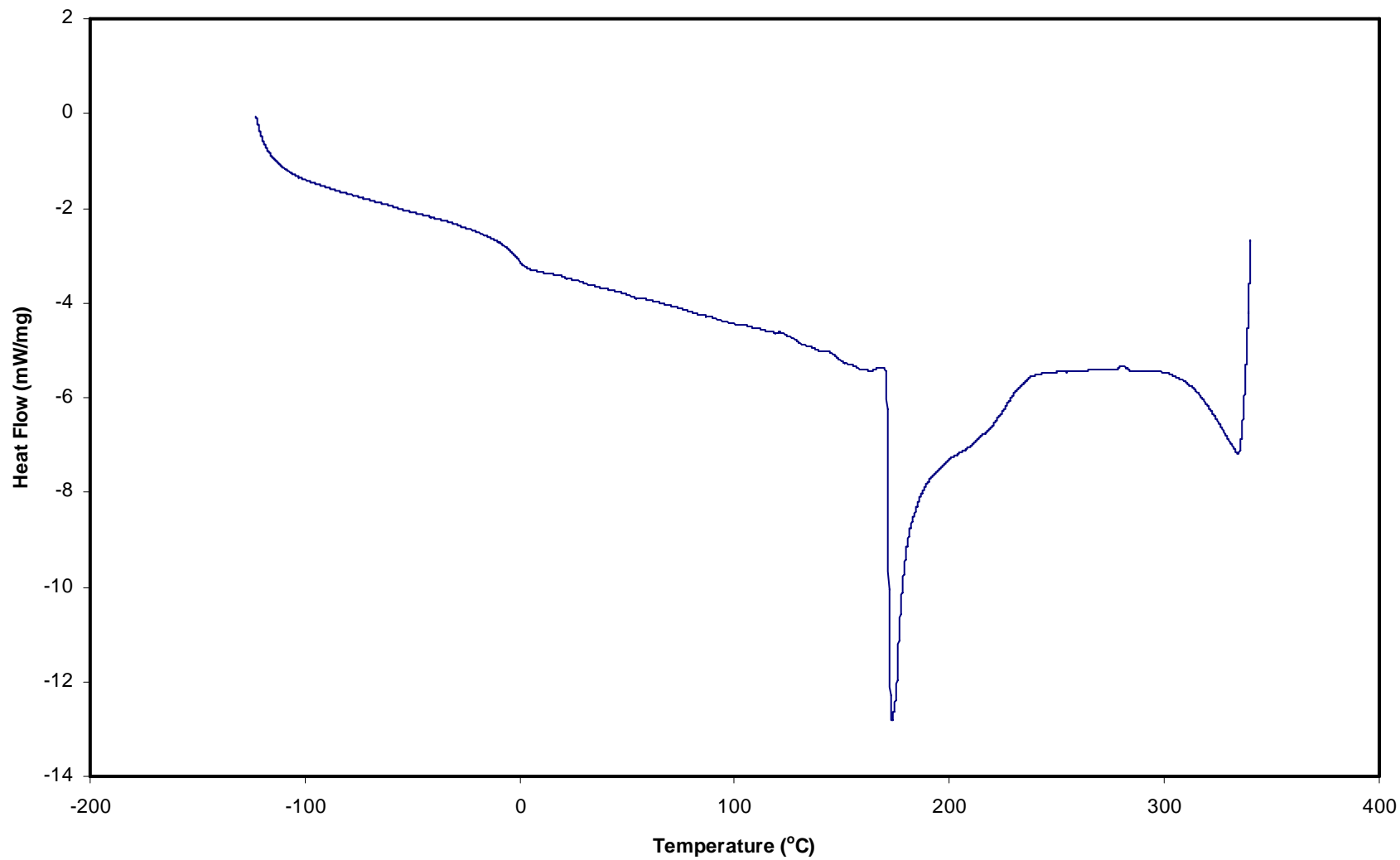


Figure A. 13 DSC for poly(vinyl 1-methoxyethyl ether)

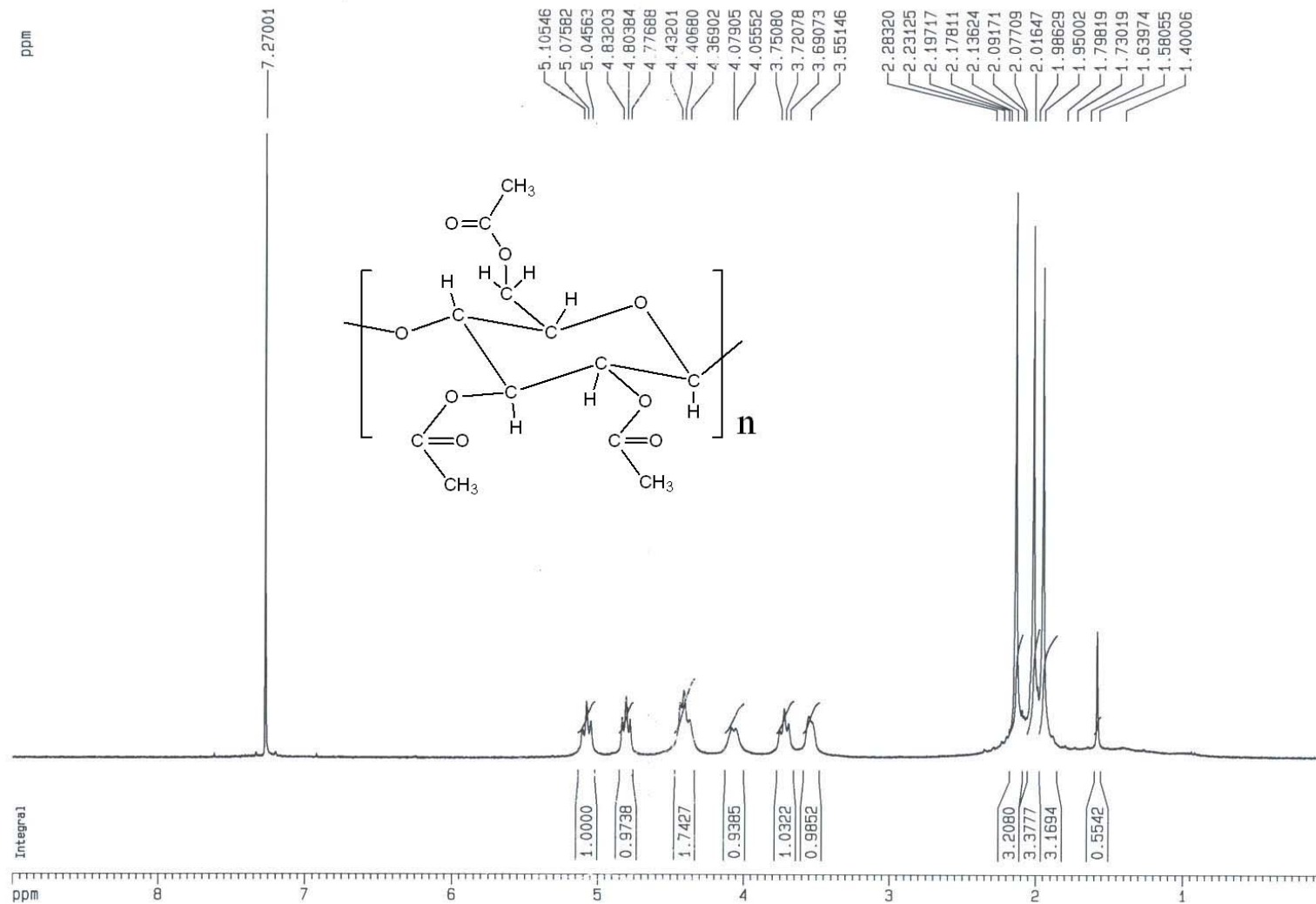


Figure A. 14 ^1H NMR (300 MHz, CDCl_3) spectrum of acetylated cellulose acetate

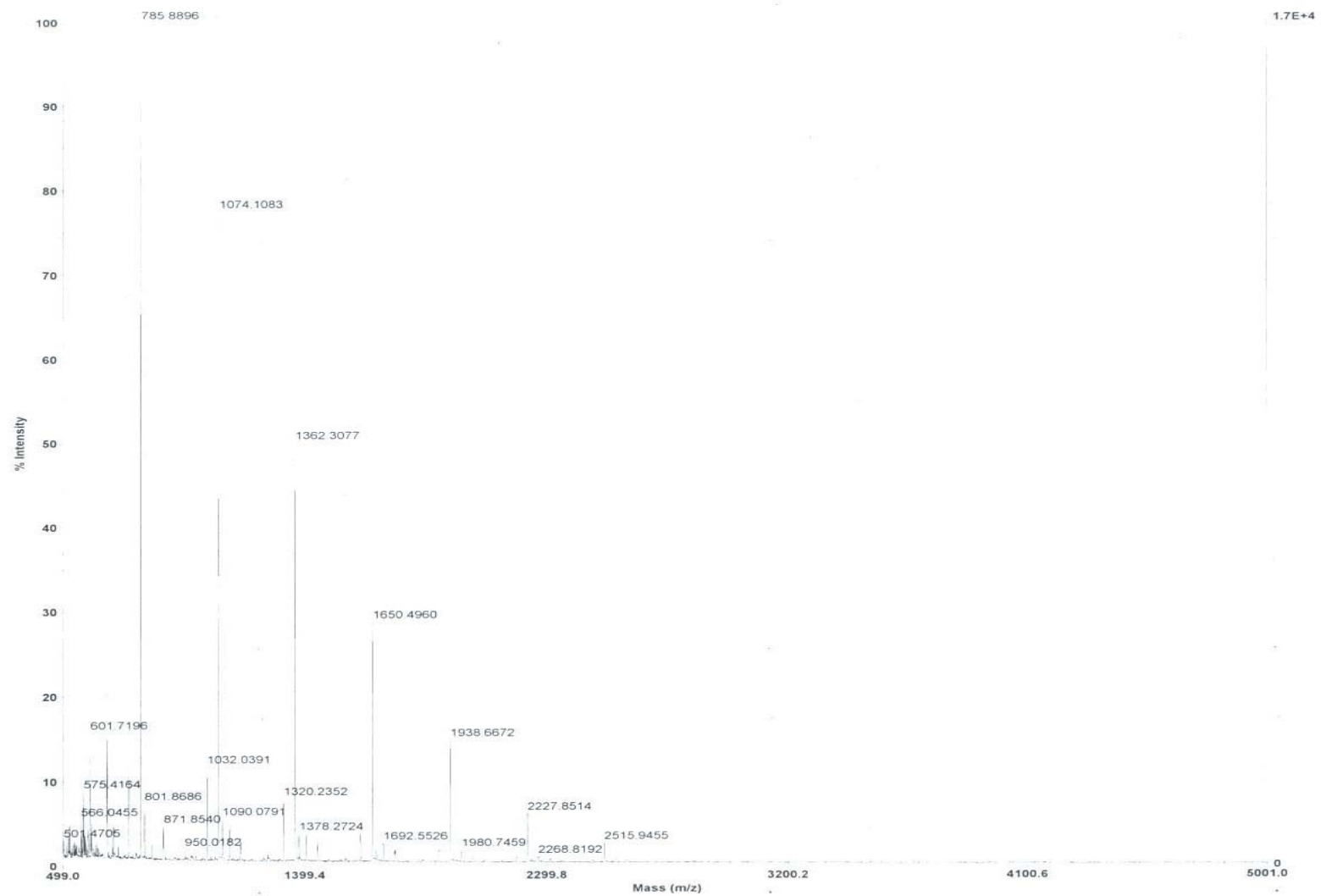


Figure A. 15 MALDI spectrum of pivaloyl products of CTA after 24 hours

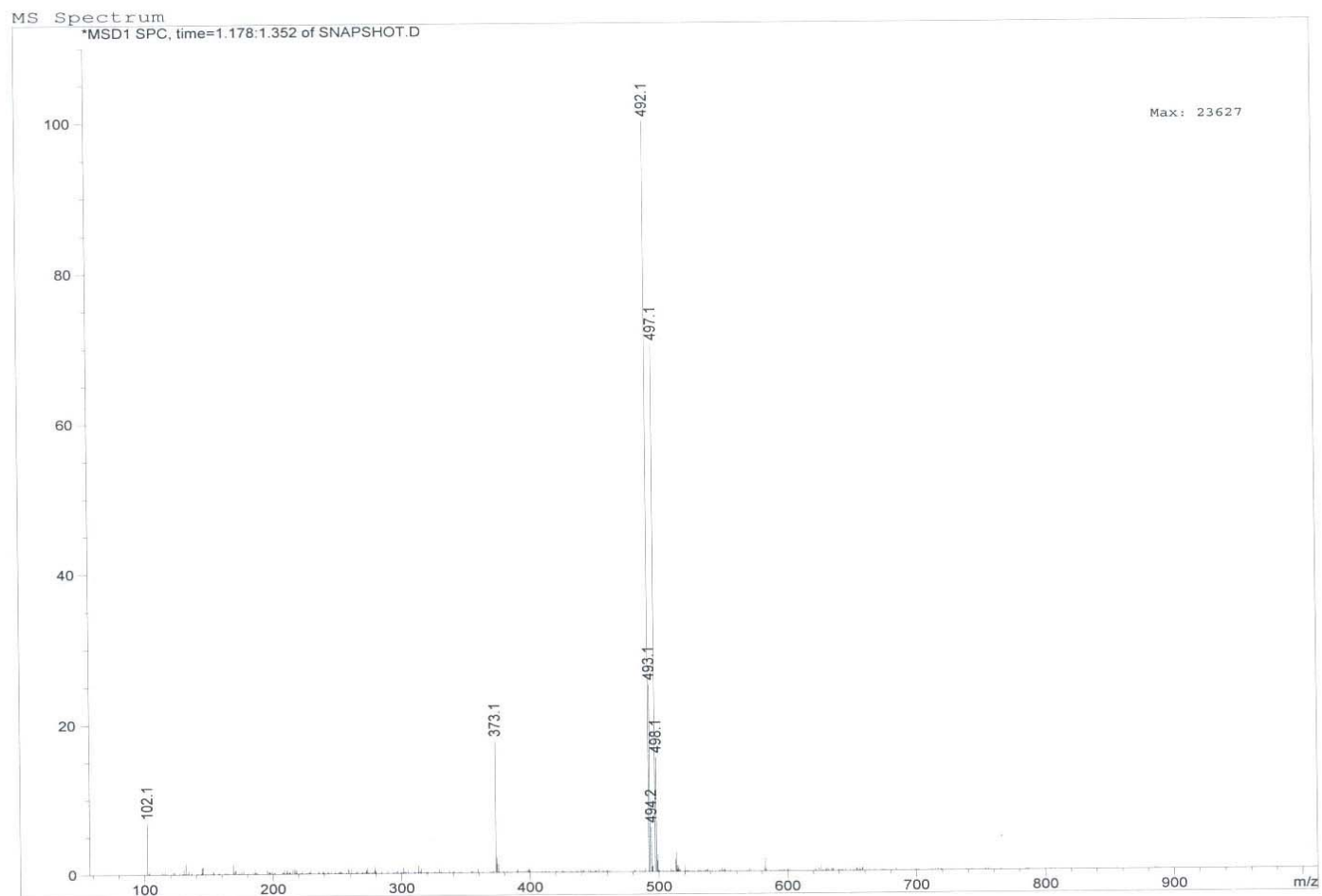


Figure A. 16 Mass spectrum of CTA monomer by ESI

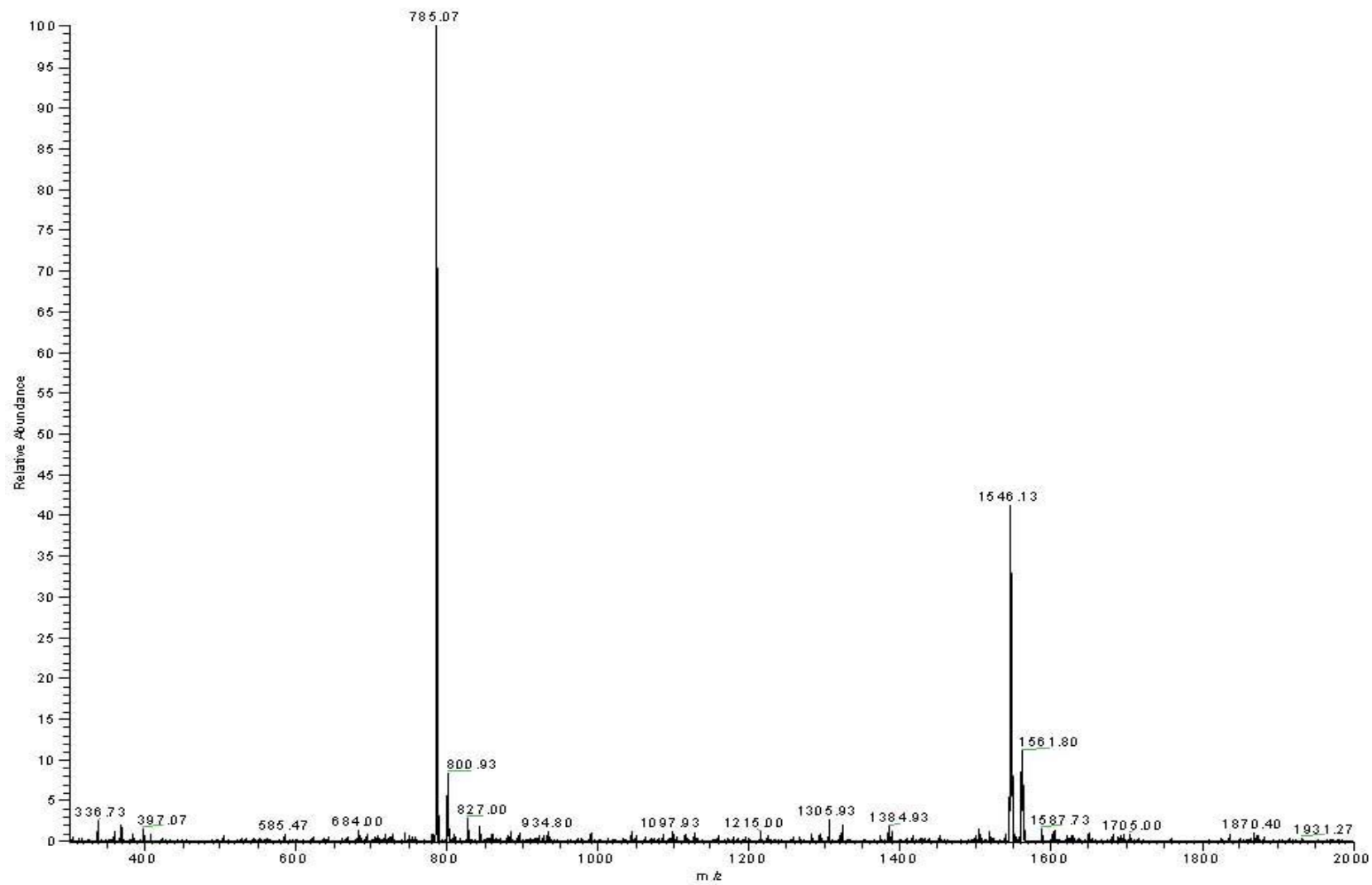


Figure A. 17 Mass spectrum of CTA dimer by ESI

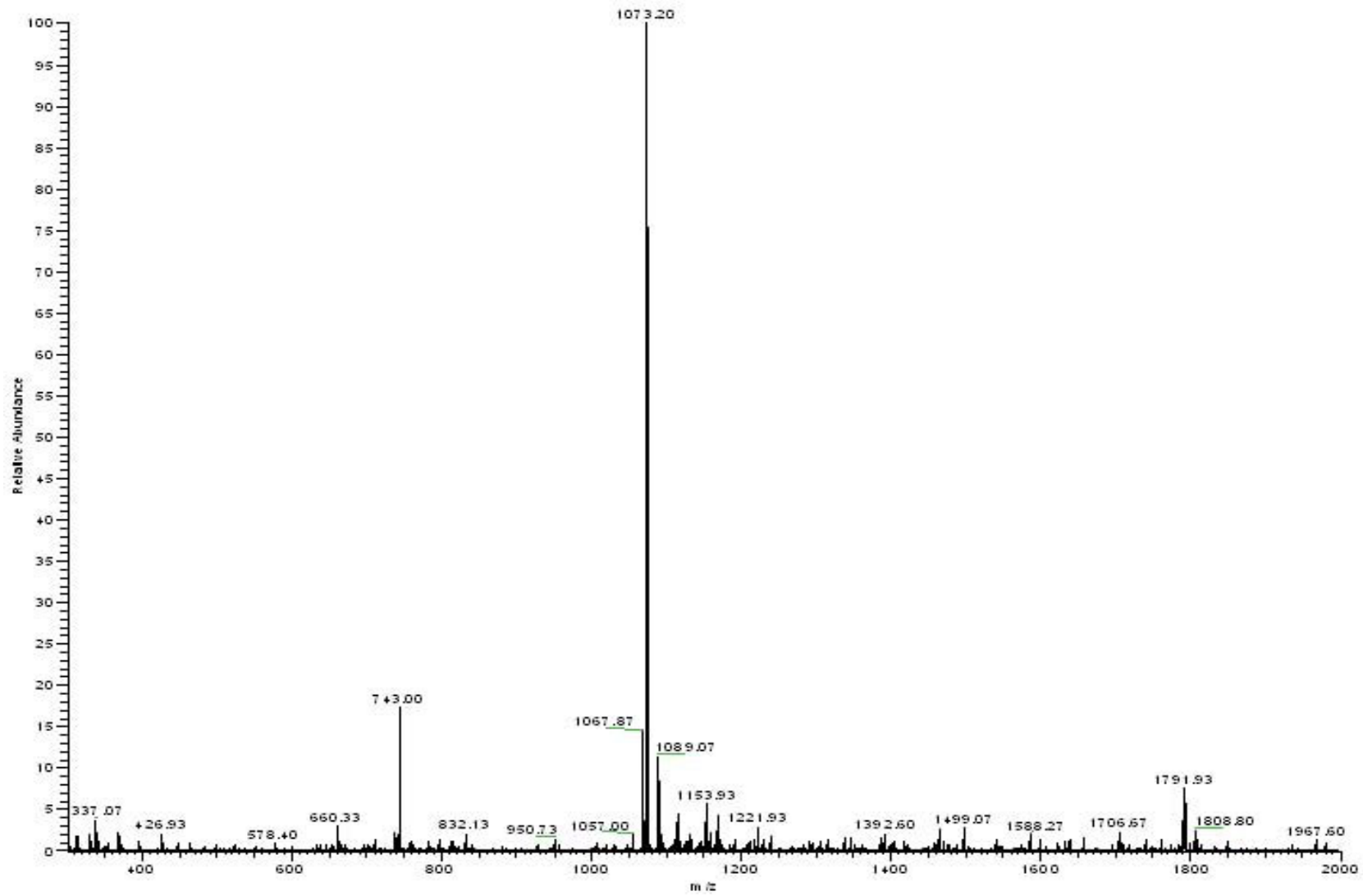


Figure A. 18 Mass spectrum of CTA trimer by ESI

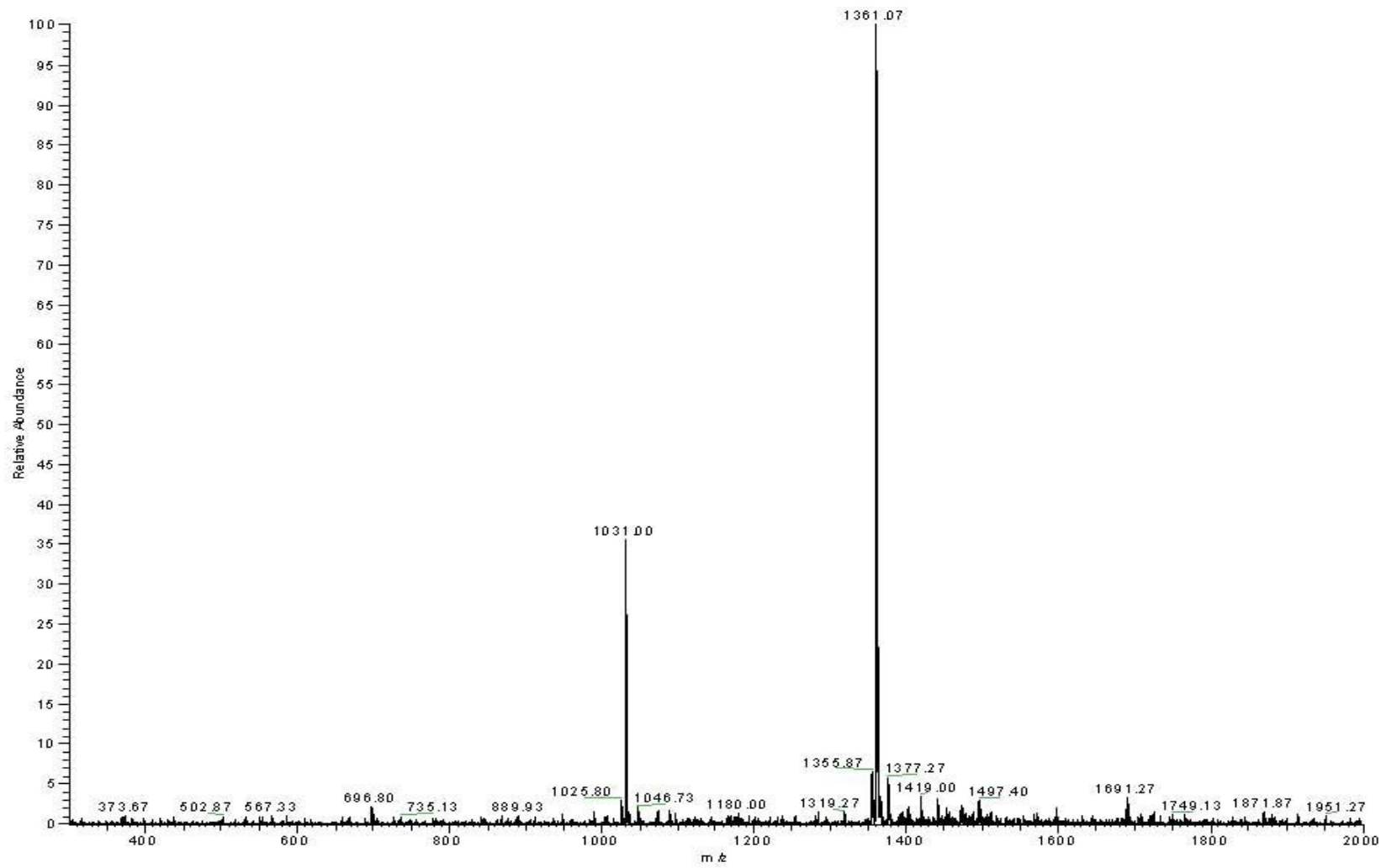


Figure A. 19 Mass spectrum of CTA tetramer by ESI

APPENDIX B

EXPERIMENTAL DATA FOR VISCOSITY MEASUREMENT IN CHAPTER 6

Table B.1 Falling cylinder viscometer experimental data for neat CO₂ at 298 K with a fixed falling distance of 0.05 m

29.99 MPa (4350 Psi)		46.89MPa (6800 psi)	
O.D. cylinder=1.228" K ₁ = 2.54×10 ⁻⁹ m ³ /s ² t (s)	O.D. cylinder=1.244" K ₂ =7.20 × 10 ⁻¹¹ m ³ /s ² t (s)	O.D. cylinder=1.228" K ₁ = 2.54×10 ⁻⁹ m ³ /s ² t (s)	O.D. cylinder=1.244" K ₂ =7.20 × 10 ⁻¹¹ m ³ /s ² t (s)
4.15E+00	3.84E+01	1.42E+00	1.30E+01
4.21E+00	3.84E+01	1.44E+00	1.30E+01
4.21E+00	3.86E+01	1.47E+00	1.30E+01
4.27E+00	3.88E+01	1.47E+00	1.30E+01
4.33E+00	3.89E+01	1.49E+00	1.31E+01
4.34E+00	3.94E+01	1.49E+00	1.31E+01
4.37E+00	4.00E+01	1.50E+00	1.33E+01
4.39E+00	4.02E+01	1.50E+00	1.34E+01
4.50E+00	4.02E+01	1.50E+00	1.35E+01
4.50E+00	4.03E+01	1.54E+00	1.38E+01
4.65E+00	4.04E+01	1.54E+00	1.39E+01
4.77E+00	4.19E+01	1.55E+00	1.48E+01

Table B.2 Experimental data of Air Products and Chemicals' samples at 298 K and 10 wt% with a fixed falling distance of 0.02 m

	Sample 1 (29.99 MPa)		Sample 2 (29.99 MPa)		Sample 3 (46.89MPa)	
	O.D. of	O.D. of	O.D. of	O.D. of	O.D. of	O.D. of
	cylinder=1.228"	cylinder=1.244"	cylinder=1.228"	cylinder=1.24"	cylinder=1.228"	cylinder=1.24"
			"	4	"	4
	1.18E+00	6.60E+00	1.08E+00	1.30E+01	1.50E+00	1.56E+01
	1.19E+00	6.01E+00	1.10E+00	1.22E+01	1.51E+00	1.50E+01
	1.20E+00	6.06E+00	1.12E+00	1.26E+01	1.53E+00	1.53E+01
	1.21E+00	6.25E+00	1.12E+00	1.26E+01	1.54E+00	1.53E+01
	1.23E+00	6.33E+00	1.14E+00	1.26E+01	1.55E+00	1.53E+01
	1.26E+00	6.39E+00	1.15E+00	1.29E+01	1.55E+00	1.54E+01
	1.31E+00	6.40E+00	1.23E+00	1.29E+01	1.56E+00	1.56E+01
	1.33E+00	6.42E+00	1.25E+00	1.31E+01	1.56E+00	1.56E+01
	1.34E+00	6.57E+00	1.32E+00	1.32E+01	1.57E+00	1.57E+01
	1.34E+00	6.65E+00	1.39E+00	1.34E+01	1.57E+00	1.57E+01
	1.34E+00	6.86E+00	1.39E+00	1.35E+01	1.57E+00	1.59E+01
	1.36E+00	6.90E+00	1.40E+00	1.37E+01	1.59E+00	1.60E+01

Table B.3 Experimental data of β -D-galactose pentaacetate at 313K and 17.24 MPa with a fixed falling distance of 0.05 m

	Neat CO ₂	12 wt%	18 wt%	25 wt%
	2.96E+01	3.84E+01	5.13E+01	6.08E+01
Falling time	3.16E+01	3.84E+01	5.17E+01	6.43E+01
of	3.01E+01	3.86E+01	5.28E+01	5.94E+01
cylinder	2.88E+01	3.88E+01	5.54E+01	6.11E+01
(s)	2.77E+01	3.89E+01	5.27E+01	5.84E+01
	2.93E+01	3.94E+01	5.46E+01	5.86E+01

BIBLIOGRAPHY

- (1) Petersen, R. C.; Matson, D. W.; Smith, R. D. *J. Am. Chem. Soc.* **1986**, *108*, 2102-2103.
- (2) Debenedetti, P. G. *AIChE J.* **1990**, *36*, 5507-5515.
- (3) <http://www.kobelco.co.jp/p108/p14/sfe01.htm>.
- (4) <http://ull.chemistry.uakron.edu/chemsep/super/>.
- (5) McHardy, J.; Sawan, S. P., Eds. *Supercritical Fluid Cleaning: Fundamentals, Technology and Applications*; Noyes Publications: Westwood, NJ, USA, 1998.
- (6) <http://sunny.vemt.bme.hu/sfe/angol/supercritical.html>.
- (7) McHugh, M. A.; Krukonis, V. J. *Supercritical Fluid Extraction, Principle and Practice*, 2nd Edition ed.; Butterworth-Heinemann: Boston, 1994.
- (8) Stavroulias, S.; Panayiotou, C. *Chemical and Biochemical Engineering Quarterly* **2005**, *19*, 373-381.
- (9) Zacchi, P.; Daghero, J.; Jaeger, P.; Eggers, R. *Brazilian Journal of Chemical Engineering* **2006**, *23*, 105-110.
- (10) Mongkholkhajornsilp, D.; Douglas, S.; Douglas, P. L.; Elkamel, A.; Teppaitoon, W.; Pongamphai, S. *Journal of Food Engineering* **2005**, *71*, 331-340.
- (11) Yazdi, A.; Beckman, D. E. *J. Ind. Eng. Chem. Res.* **1996**, *35*, 3644-3642.
- (12) Lesellier, E.; West, C.; Tchaplal, A. *Journal of Chromatography A* **2003**, *1018*, 225-232.
- (13) Terfloth, G. *Journal of Chromatography A* **2001**, *906*, 301-307.
- (14) Glaser, R.; Weitkamp, J. *Industrial & Engineering Chemistry Research* **2003**, *42*, 6294-6302.
- (15) Beckman, E. J. *Environmental Science & Technology* **2003**, *37*, 5289-5296.
- (16) Jessop, P. G.; Ikariya, T.; Noyori, R. *Chem. Rev.* **1999**, *99*, 475-493.
- (17) Verreck, G.; Decorte, A.; Heymans, K.; Adriaensen, J.; Cleeren, D.; Jacobs, A.; Liu, D. H.; Tomasko, D.; Arien, A.; Peeters, J.; Rombaut, P.; Van den Mooter, G.; Brewster, M. E. *European Journal of Pharmaceutical Sciences* **2005**, *26*, 349-358.
- (18) Hong, L.; Guo, J. Z.; Gao, Y.; Yuan, W. K. *Industrial & Engineering Chemistry Research* **2000**, *39*, 4882-4887.

- (19) Thakur, R.; Gupta, R. B. *Industrial & Engineering Chemistry Research* **2005**, *44*, 7380-7387.
- (20) Blasig, A.; Shi, C.; Enick, R. M.; Thies, M. C. *Ind. Eng. Chem. Res.* **2002**, *41*, 4976-4983.
- (21) Pai, R. A.; Humayun, R.; Schulberg, M. T.; Sengupta, A.; Sun, J. N.; Watkins, J. J. *Science* **2004**, *303*, 507-510.
- (22) Blackburn, J. M.; Long, D. P.; Cabanas, A.; Watkins, J. J. *Science* **2001**, *294*, 141-145.
- (23) DeSimone, J. M.; Romack, T.; Betts, D. E.; McClain, J. B. *US*, 5,783,082. 1998.
- (24) DeSimone, J. M., Maury, E.E., Menciloglu, Y.Z., McClain, J.B., Romack, T.J., and Combes, J.R. *Science* **1994**, *265*, 356-359.
- (25) Ahmed, T. S.; DeSimone, J. M.; Roberts, G. W. *Macromolecules* **2006**, *39*, 15-18.
- (26) DeSimone, J. M.; Guan, Z.; Elsbernd, C. S. *Science* **1992**, *257*, 945-947.
- (27) Romack, T. J.; Maury, E. E.; Desimone, J. M. *Macromolecules* **1995**, *28*, 912-915.
- (28) Cooper, A. I.; Hems, W. P.; Holmes, A. B. *Macromol. Rapid Commun.* **1998**, *19*, 353-357.
- (29) Cooper, A. I.; Hems, W. P.; Holmes, A. B. *Macromolecules* **1999**, *32*, 2156-2166.
- (30) Cooper, A. I. *Journal of Materials Chemistry* **2000**, *10*, 207-234.
- (31) Hsiao, Y. L.; Maury, E. E.; Desimone, J. M.; Mawson, S.; Johnston, K. P. *Macromolecules* **1995**, *28*, 8159-8166.
- (32) Shaffer, K. A.; Jones, T. A.; Canelas, D. A.; DeSimone, J. M.; Wilkinson, S. P. *Macromolecules* **1996**, *29*, 2704-2706.
- (33) Canelas, D. A.; Betts, D. E.; DeSimone, J. M.; Yates, M. Z.; Johnston, K. P. *Macromolecules* **1998**, *31*, 6794-6805.
- (34) Canelas, D. A.; Betts, D. E.; DeSimone, J. M. *Macromolecules* **1996**, *29*, 2818-2821.
- (35) Adamsky, F. A.; Beckman, D. E. *J. Macromolecules* **1994**, *27*, 312-314.
- (36) Sherrington, D. C. *Chem. Commun.* **1998**, 2275-2286.
- (37) Imhof, A.; Pine, D. J. *Nature* **1997**, *389*, 948-951.
- (38) Cooper, A. I. *Advanced Materials* **2001**, *13*, 1111-1114.
- (39) Cooper, A. I.; Holmes, A. B. *Advanced Materials* **1999**, *11*, 1270-1274.
- (40) Cooper, A. I.; Hebb, A. K. *Abstracts of Papers of the American Chemical Society* **2001**, *221*, U610-U610.
- (41) Butler, R.; Davies, C. M.; Cooper, A. I. *Advanced Materials* **2001**, *13*, 1459-1463.
- (42) Zhang, H.; Cooper, A. I. *Chemistry of Materials* **2002**, *14*, 4017-4020.
- (43) Zhang, H. F.; Cooper, A. I. *Industrial & Engineering Chemistry Research* **2005**, *44*, 8707-8714.
- (44) Watkins, J. J.; McCarthy, T. J. *Macromolecules* **1994**, *27*, 4845-4847.

- (45) Watkins, J. J.; McCarthy, T. J. *Macromolecules* **1995**, *28*, 4067-4074.
- (46) Woods, H. M.; Silva, M. M. C. G.; Nouvel, C.; Shakesheff, K.; Howdle, S. M. *J. Mater. Chem.* **2004**, *14*, 1663-1678.
- (47) Benedetti, L.; Bertucco, A.; Pallado, P. *Biotech. Bioeng.* **1997**, *53*, 232-237.
- (48) Foster, N. R.; Dehghani, F.; Charoenchaitrakool, K. M.; Warwick, B. *AAPS Pharmsci* **2003**, *5*.
- (49) Tom, J. W.; Debenedetti, P. G.; Jerome, R. *Journal of Supercritical Fluids* **1994**, *7*, 9-29.
- (50) Debenedetti, P. G.; Tom, J. W.; Yeo, S. D.; Lim, G. B. *Journal of Controlled Release* **1993**, *24*, 27-44.
- (51) Debenedetti, P. G.; Tom, J. W.; Kwauk, X.; Yeo, S. D. *Fluid Phase Equilibria* **1993**, *82*, 311-321.
- (52) Reverchon, E. *Journal of Supercritical Fluids* **1999**, *15*, 1-21.
- (53) Dixon, D. J.; Johnston, K. P.; Bodmeier, R. P. *AIChE J.* **1993**, *39*, 127-139.
- (54) Yeo, S. D.; Lim, G. B.; Debenedetti, P. G.; Bernstein, H. *Biotech. Bioeng.* **1993**, *41*, 341-346.
- (55) Palakodaty, S.; York, P.; Pritchard, J. *Pharmaceutical Research* **1998**, *15*, 1835-1843.
- (56) Moshashaee, S.; Bisrat, M.; Forbes, R. T.; Nyqvist, H.; York, P. *European Journal of Pharmaceutical Sciences* **2000**, *11*, 239-245.
- (57) Bleich, J.; Muller, B. W. *J. Microencapsulation* **1996**, *13*, 131-139.
- (58) Foster, N.; Mammucari, R.; Dehghani, F.; Barrett, A.; Bezanehtak, K.; Coen, E.; Combes, G.; Meure, L.; Ng, A.; Regtop, H. L.; Tandya, A. *Industrial & Engineering Chemistry Research* **2003**, *42*, 6476-6493.
- (59) Stanton, L. A.; Dehghani, F. B.; Foster, N. R. *Australian Journal of Chemistry* **2002**, *55*, 443-447.
- (60) Young, T. J.; Johnston, K. P.; Mishima, K.; Tanaka, H. *Journal of Pharmaceutical Sciences* **1999**, *88*, 640-650.
- (61) Rehman, M.; Shekunov, B. Y.; York, P.; Lechuga-Ballesteros, D.; Miller, D. P.; Tan, T.; Colthorpe, P. *European Journal of Pharmaceutical Sciences* **2004**, *22*, 1-17.
- (62) Tu, L. S.; Dehghani, F.; Foster, N. R. *Powder Technology* **2002**, *126*, 134-149.
- (63) Elvassore, N.; Bertucco, A.; Caliceti, P. *Journal of Pharmaceutical Sciences* **2001**, *90*, 1628-1636.
- (64) Langer, R.; Vacanti, J. P. *Science* **1993**, *260*, 920-926.
- (65) Murphy, W. L.; Peters, M. C.; Kohn, D. H.; Mooney, D. J. *Biomaterials* **2000**, *21*, 2521-2527.
- (66) Eiselt, P.; Yeh, J.; Latvala, R. K.; Shea, L. D.; Mooney, D. J. *Biomaterials* **2000**, *21*, 1921-1927.

- (67) Mooney, D. J.; Baldwin, D. F.; Suh, N. P.; Vacanti, L. P.; Langer, R. *Biomaterials* **1996**, *17*, 1417-1422.
- (68) Barry, J. J. A.; Gidda, H. S.; Scotchford, C. A.; Howdle, S. M. *Biomaterials* **2004**, *25*, 3559-3568.
- (69) Howdle, S. M.; Watson, M. S.; Whitaker, M. J.; Popov, V. K.; Davies, M. C.; Mandel, F. S.; Wang, J. D.; Shakesheff, K. M. *Chemical Communications* **2001**, 109-110.
- (70) Hile, D. D.; Amirpour, M. L.; Akgerman, A.; Pishko, M. V. *Journal of Controlled Release* **2000**, *66*, 177-185.
- (71) Harris, L. D.; Kim, B. S.; Mooney, D. J. *Journal of Biomedical Materials Research* **1998**, *42*, 396-402.
- (72) Enick, D. R. M.; US DOE FETC: Morgantown, WV, 1998.
- (73) Fenghour, A.; Wakeham, W. A.; Vesovic, V. *Journal of Physical and Chemical Reference Data* **1998**, *27*, 31-44.
- (74) Martin, F. a. H., J. In *90-4*; PRRC, Sept. 1990.
- (75) Martin, F. a. H., J. In *90-34*; PRRC, Sept. 1990.
- (76) Martin, F. a. H., J. In *90-20*; PRRC, June 1990.
- (77) Gullapalli, P. T., J.-S., Heller, J.P. In *the SPE International Symposium on Oilfield Chemistry: the SPE International Symposium on Oilfield Chemistry, 1995*; Vol. SPE 28979.
- (78) Terry, R. E.; Zaid, A.; Angelos, C. In *SPE 16270*, 1987.
- (79) Llave, F., Chung, F., and Burchfield, T.; SPE RE, 1990; pp 47-51.
- (80) Harris, T.; Irani, C.; Pretzer, W. *U.S.* 1990.
- (81) Bae, J.; Irani, C. In *SPE 20467*, Sept. 1990.
- (82) Davis, B. W. *U.S.*, 4,852,651. 1989.
- (83) Wikramanayake, R. T., M. and Enick R. *Fluid Phase Equilibria*, **1991**, *70*, 107-118.
- (84) T.A. Hoefling, D. S., M. Reid, E. Beckman and R.M. Enick. *J. Supercritical Fluids* **1992**, *5*, 237-241.
- (85) Enick, R., Beckman, E., Shi, C. M., and Karmana, E. In *proceedings of the 4th International Symposium on Supercritical Fluids: Sendai, Japan, 1997*; pp 251-254.
- (86) Enick, R., Beckman, E., and Yazdi, A. In *proceedings of the 4th International Symposium on Supercritical Fluids: Sendai, Japan, 1997*; pp 405-408.
- (87) Kilic, S. In *Chemical and Petroleum Engineerin Department*; University of Pittsburgh (Ph.D. Dissertation): Pittsburgh, 2003.
- (88) Guan, G., Samulski, E., DeSimone, J. In *AIChE National Meeting*, 1994.
- (89) McClain, J. B.; Londono, J. D.; Betts, D. E.; Canelas, D. A.; Samulski, E. T.; Wignall, G. D.; DeSimone, J. M. In *Proceedings of the 1996 Spring Meeting of the ACS, Division of*

- Polymeric Materials: Science and Engineering*: New Orleans, LA., 1996; Vol. 74, pp 234-235.
- (90) Shi, C. M.; Huang, Z. H.; Beckman, E. J.; Enick, R. M.; Kim, S. Y.; Curran, D. P. *Industrial & Engineering Chemistry Research* **2001**, *40*, 908-913.
- (91) Huang, Z. H.; Shi, C. M.; Xu, J. H.; Kilic, S.; Enick, R. M.; Beckman, E. J. *Macromolecules* **2000**, *33*, 5437-5442.
- (92) Xu, J. In *Chemical and Petroleum Engineering Department*; University of Pittsburgh (Ph.D. Dissertation): Pittsburgh, 2003.
- (93) Cozzi, F.; Cinquini, M.; Annuziata, R.; Siegel, J. S. *J. Am. Chem. Soc.* **1993**, *115*, 5330-5331.
- (94) Jorgensen, W. L.; Severance, D. L. *J. Am. Chem. Soc.* **1990**, *112*, 4768-4774.
- (95) Muehldorf, A. V.; Engen, D. V.; Warner, J. C.; Hamilton, A. D. *J. Am. Chem. Soc.* **1988**, *110*, 6561-6562.
- (96) Cochran, J. E.; Parrott, T. J.; Whitlock, B. J.; Whitlock, H. W. *J. Am. Chem. Soc.* **1992**, *114*, 2269-2270.
- (97) Xu, J. H.; Wlaschin, A.; Enick, R. M. *Spe Journal* **2003**, *8*, 85-91.
- (98) Xu, J.; Kilic, S.; Michalik, S.; Huang, Z.; Cronin, K.; MacPherson, H.; Bane, S.; Karnikas, C.; Belardi, J.; Enick, R. M.; Beckman, E. J.; Potluri, V.; Hamilton, A.; Shen, Z.; McHugh, M. A.; Department of Energy, 2002.
- (99) Bray, C. L.; Tan, B.; Wood, C. D.; Cooper, A. I. *Journal of Materials Chemistry* **2005**, *15*, 456-459.
- (100) Fan, X.; Potluri, V.; McLeod, M. C.; Wang, Y.; Liu, J.; Enick, R. M.; Hamilton, A. D.; Roberts, C. B.; Johnson, J. K.; Beckman, E. J. *J. Am. Chem. Soc.* **2005**, *127*, 11754-11762.
- (101) Kauffman, J. F. *J. Phys. Chem. A* **2001**, *105*, 3433-3442.
- (102) Nelson, M. R.; Borkman, R. F. *Journal of Physical Chemistry A* **1998**, *102*, 7860-7863.
- (103) Kazarian, S. G.; Vincent, M. F.; Bright, F. V.; Liotta, C. L.; Eckert, C. A. *Journal of the American Chemical Society* **1996**, *118*, 1729-1736.
- (104) Meredith, J. C.; Johnston, K. P.; Seminario, J. M.; Kazarian, S. G.; Eckert, C. A. *J. Phys. Chem.* **1996**, *100*, 10837-10848.
- (105) Raveendran, P.; Wallen, S. L. *J. Am. Chem. Soc.* **2002**, *124*, 12590-12599.
- (106) Tsukahara, T.; Kayaki, Y.; Ikariya, T.; Ikeda, Y. *Angew. Chem. Int. Ed.* **2004**, *43*, 3719-3722.
- (107) Chandrika, B.; Schnackenberg, L. K.; Raveendran, P.; Wallen, S. L. *Chem. Eur. J.* **2005**, *11*, 6266-6271.
- (108) Blatchford, M. A.; Raveendran, P.; Wallen, S. L. *J. Am. Chem. Soc.* **2002**, *124*, 14818-14819.
- (109) Raveendran, P.; Ikushima, Y.; Wallen, S. L. *Acc. Chem. Res.* **2005**, *38*, 478-485.

- (110) Raveendran, P.; Wallen, S. L. *Journal of Physical Chemistry B* **2003**, *107*, 1473-1477.
- (111) Blatchford, M. A.; Raveendran, P.; Wallen, S. L. *Journal of the American Chemical Society* **2002**, *124*, 14818-14819.
- (112) Raveendran, P.; Wallen, S. L. *J. Am. Chem. Soc. Communications* **2002**, *124*, 7274-7275.
- (113) Hong, L.; Thies, M. C.; Enick, R. M. *Journal of Supercritical Fluids* **2005**, *34*, 11-16.
- (114) Prausnitz, J. M. L., R. N.; Azevedo, E. G. *Molecular Thermodynamics of Fluid Phase Equilibria*, 3rd ed.; Prentice Hall: Englewood Cliffs, NJ, 1999.
- (115) Kirby, C. F.; McHugh, M. A. *Chemical Reviews* **1999**, *99*, 565-602.
- (116) DiNoia, T. P.; Kirby, C. F.; van Zanten, J. H.; McHugh, M. A. *Macromolecules* **2000**, *33*, 6321-6329.
- (117) Dinoia, T. P.; Conway, S. E.; Lim, J. S.; McHugh, M. A. *Journal of Polymer Science Part B-Polymer Physics* **2000**, *38*, 2832-2840.
- (118) Rindfleisch, F.; DiNoia, T. P.; McHugh, M. A. *J. Phys. Chem.* **1996**, *100*, 15581-15587.
- (119) Shen, Z.; McHugh, M. A.; Xu, J.; Belardi, J.; Kilic, S.; Mesiano, A.; Bane, S.; Karnikas, C.; Beckman, E. J.; Enick, R. M. *Polymer* **2003**, *44*, 1491-1498.
- (120) Conway, S. E.; Byun, H. S.; McHugh, M. A.; Wang, J. D.; Mandel, F. S. *Journal of Applied Polymer Science* **2001**, *80*, 1155-1161.
- (121) Drohmann, C.; Beckman, E. J. *Journal of Supercritical Fluids* **2002**, *22*, 103-110.
- (122) Hong, L.; Enick, R. M.; Beckman, E. J. **2006**, In Preparation.
- (123) Potluri, V. K.; Hamilton, A. D.; Karanikas, C. F.; Bane, S. E.; Xu, J.; Beckman, E. J.; Enick, R. M. *Fluid Phase Equilibria* **2003**, *211*, 211-217.
- (124) Potluri, V. K.; Xu, J.; Enick, R. M.; Beckman, E. J.; Hamilton, A. D. *Organic Letters* **2002**, *4*, 2333-2335.
- (125) Kilic, S.; Michalik, S.; Wang, Y.; Johnson, J. K.; Enick, R. M.; Beckman, E. J. *Industrial & Engineering Chemistry Research* **2003**, *42*, 6415-6424.
- (126) Fink, R.; Hancu, D.; Valentine, R.; Beckman, E. J. *Journal of Physical Chemistry B* **1999**, *103*, 6441-6444.
- (127) Budd, P. M.; McKeown, N. B.; Fritsch, D. *Journal of Materials Chemistry* **2005**, *15*, 1977-1986.
- (128) McKeown, N. B.; Budd, P. M.; Msayib, K. J.; Ghanem, B. S.; Kingston, H. J.; Tattershall, C. E.; Makhseed, S.; Reynolds, K. J.; Fritsch, D. *Chemistry-A European Journal* **2005**, *11*, 2610-2620.
- (129) Eastoe, J.; Paul, A.; Nave, S.; Steytler, D. C.; Robinson, B. H.; Rumsey, E.; Thorpe, M.; Heenan, R. K. *J. Am. Chem. Soc.* **2001**, *123*, 988-989.
- (130) Eastoe, J.; Dupont, A.; Steytler, D. C.; Thorpe, M.; Gurgel, A.; Heenan, R. K. *Journal of Colloid and Interface Science* **2003**, *258*, 367-373.

- (131) O'Neill, M. L.; Cao, Q.; Fang, M.; Johnston, K. P.; Wilkinson, S. P.; Smith, C. D.; Kerschner, J. L.; Jureller, S. H. *Ind. Eng. Chem. Res.* **1998**, *37*, 3067-3079.
- (132) Baradie, B.; Shoichet, M. S.; Shen, Z. H.; McHugh, M. A.; Hong, L.; Wang, Y.; Johnson, J. K.; Beckman, E. J.; Enick, R. M. *Macromolecules* **2004**, *37*, 7799-7807.
- (133) Enick, R. M.; Beckman, E. J.; Yazdi, A.; Krukonis, V. J.; Schonemann, H.; Howell, J. *Journal of Supercritical Fluids* **1998**, *13*, 121-126.
- (134) Span, R.; Wagner, W. *J. Phys. Chem. Ref. Data* **1996**, *25*, 1509-1596.
- (135) Barrage, T. C. In *Chemical and Petroleum Engineering Department*; University of Pittsburgh (M.S. Thesis): Pittsburgh, 1987.
- (136) Shi, C. In *Chemical and Petroleum Engineering Department*; University of Pittsburgh (Ph.D. Dissertation): Pittsburgh, 2000.
- (137) Wang, Y. In *Chemical and Petroleum Engineering Department*; University of Pittsburgh (Ph.D. Candidate Proposal): Pittsburgh, 2004.
- (138) Michalik, S. J. In *Chemical and Petroleum Engineering Department*; University of Pittsburgh (Master Thesis): Pittsburgh, 2003.
- (139) Wang, Y. In *Department of Chemical Engineering*; University of Pittsburgh: Pittsburgh, 2004.
- (140) Baum, K.; Berkowitz, P. T.; Grakauskas, V.; Archibald, T. G. *J. Org. Chem.* **1983**, *48*, 2953-2956.
- (141) Wojtowicz, J. A.; Polak, R. J. *J. Org. Chem.* **1973**, *38*, 2061-2066.
- (142) Wicks, D. A.; Tirrell, D. A. *Polymer Preprints* **1985**, *26*, 155.
- (143) Vandenberg, E. J.; Mullis, J. C.; Juvet, R. S. *J. Journal of polymer science Part A-Polymer Chemistry* **1989**, *27*, 3113-3149.
- (144) Vandenberg, E. J. *Journal of polymer science Part A-Polymer Chemistry* **1969**, *7*, 525-567.
- (145) Linderman, R. J.; Chen, K. Y. *J Org Chem* **1996**, *61*, 2441-2453.
- (146) Ugliengo, P.; Ahmed, J.; Viterbo, D.; Calleri, M.; Ceruti, M. *Gazzetta Chimica Italiana* **1989**, *119*, 487-492.
- (147) Lora, M.; Rindfleisch, F.; McHugh, M. A. *Journal of Applied Polymer Science* **1999**, *73*, 1979-1991.
- (148) Painter, P. C.; Coleman, M. M. *Fundamentals of Polymer Science: An Introductory Text*, 2nd ed.; CRC Press: Boca Raton, 1997.
- (149) Challa, R.; Ahuja, A.; Ali, J.; Khar, R. K. *AAPS PharmSciTech.* **2005**, *6*, E329-E357.
- (150) Loftsson, T.; Brewster, M. E. *J. Pharm. Sci.* **1996**, *85*, 1017-1025.
- (151) Hwang, S. J.; Bellocq, N. C.; Davis, M. E. *Bioconjugate Chem.* **2001**, *12*, 280-290.
- (152) Arndt, P.; Bockholt, K.; Gerdes, R.; Huschens, S.; Pyplo, J.; Redlich, H.; Samm, K. *Cellulose* **2003**, *10*, 75-83.

- (153) Pyplo-Schnieders, D. J., 2005 (Personal Communication).
- (154) Bayraktar, Z.; Kiran, E. *Journal of Applied Polymer Science* **2000**, *75*, 1397-1403.
- (155) Sarbu, T.; Styranec, T.; Beckman, E. J. *Nature* **2000**, *405*, 165-168.
- (156) Beckman, E. J. *Ind. Eng. Chem. Res.* **2003**, *42*, 1598-1602.
- (157) Van Pelt, A.; Peters, C. J.; de Swaan Arons, J. J. *Chem. Phys.* **1991**, *95*, 7569-7575.
- (158) Van Konynenberg, P. H.; Scott, R. L. *Philosophical Transactions of the Royal Society of London, Series A* **1980**, *298*, 495-540.
- (159) Rowlinson, J. S.; Swinton, F. L. *Liquids and Liquid Mixtures*, 3rd Edition ed.; Butterworth: Boston, 1982.
- (160) Donnelly, H. G.; Katz, D. L. *Industrial & Engineering Chemistry* **1954**, *46*, 511-517.
- (161) Brandt, F. S.; Broers, P. M. A.; de Loos, T. W. *International Journal of Thermophysics* **2001**, *22*, 1045-1055.
- (162) Jones, C. W. *United States Patent*, 5,723,556. 1998.
- (163) Feiring, A. E.; Wonchoba, E. R. *Macromolecules* **1998**, *31*, 7103-7104.
- (164) Kogel, H. C.; Vollmar, J. F.; Proschek, P.; Mager, B.; Scharf, G.; Buttell, H. M. In *Prosthetic Substitution of Blood Vessels: actual state and future development*; Kogel, H. C., Ed.; Quintessenz: Munich, 1991; p 143.
- (165) Lousenberg, R. D.; Shoichet, M. S. *Macromolecules* **2000**, *33*, 1682-1685.
- (166) Baradie, B.; Shoichet, M. S. *Macromolecules* **2002**, *35*, 3569-3575.
- (167) Tuminello, W. H.; Brill, D. J.; Walsh, D. J.; Paulaitis, M. E. *Journal of Applied Polymer Science* **1995**, *56*, 495-499.
- (168) Mertdogan, C. A.; Byun, H. S.; McHugh, M. A.; Tuminello, W. H. *Macromolecules* **1996**, *29*, 6548-6555.
- (169) Mertdogan, C. A.; DiNoia, T. P.; McHugh, M. A. *Macromolecules* **1997**, *30*, 7511-7515.
- (170) Baradie, B.; Shoichet, M. S.; Shen, Z.; McHugh, M. A.; Hong, L.; Wang, Y.; Johnson, K. J.; Beckman, E. J.; Enick, R. M. *Macromolecules* **2004**, Submitted.
- (171) Diep, P.; Jordan, K. D.; Johnson, J. K.; Beckman, E. J. *Journal of Physical Chemistry A* **1998**, *102*, 2231-2236.
- (172) Fried, J. R.; Hu, N. *Polymer* **2003**, *44*, 4363-4372.
- (173) Kroschwitz, J. I.; Howe-Grant, M., Eds. *Propylene Oxide Polymers*, 4th ed.; John Wiley & Sons: New York, 1991; Vol. 19.
- (174) Salamone, J. C., Ed. *Polymeric Materials Encyclopedia*; CRC Press, Inc.: Boca Raton, 1996; Vol. 9.
- (175) Beckman, E. J. *Chemical Communications* **2004**, 1885-1888.
- (176) Sanchez-Moreno, C.; Larrauri, J. A.; Saura-Calixto, F. *Food Res. Int.* **1999**, *32*, 407-412.

- (177) Ammawath, W.; Che Man, Y. B.; Baharin, B. S.; Abdul Rahman, R. B. *Journal of Food Lipids* **2005**, *12*, 198-208.
- (178) <http://www.chemicaland21.com/arokorhi/lifescience/foco/BHT.htm>.
- (179) <http://www.bentonite.biz/bentonite/index.htm>.
- (180) Eustaquio-Rincon, R.; Trejo, A. *Fluid Phase Equilibria* **2001**, *185*, 231-239.
- (181) <http://webbook.nist.gov/chemistry/fluid/>.
- (182) Yamada, K.; Yamaoka, K.; Minoda, M.; Miyamoto, T. *Polymer International* **2001**, *50*, 531-537.
- (183) George, M.; Weiss, R. G. *Langmuir* **2002**, *18*, 7124-7135.